

New Trends and Tools in Complex Networks

Proceedings of the 2007 International Conference on
Modelling and Computation on Complex Networks and Related Topics

Net-Works 2007

Aranjuez, September 10-11, 2007

Edited by:

Regino Criado

Javier Pello

Miguel Romance



Conference held in cooperation with
the Society for Industrial and Applied Mathematics



Editors:

R. Criado, Universidad Rey Juan Carlos

J. Pello, Universidad Rey Juan Carlos

M. Romance, Universidad Rey Juan Carlos

Scientific Committee

S. Boccaletti, Istituto Nazionale di Ottica Applicata

R. Criado, Universidad Rey Juan Carlos

M. Dahlem, Institute für Theoretische Physik

J. Kurths, Potsdam University

V. Latora, Università di Catania

E. Schoell, Technische Universität Berlin

H. Mancini, Universidad de Navarra

Y. Moreno, Universidad de Zaragoza

ISBN: 978-84-690-6890-8

N° Reg.: 07/54873

© 2007 Universidad Rey Juan Carlos

This work is subject to copyright. All rights reserved, whether the whole or part of the material is concerned, specifically the rights of translation, reprinting, re-use of illustrations, recitation, broadcasting, reproduction on microfilms or in other ways and storage in data banks. For any kind of use permission of the copyright owner must be obtained.

Printed in Spain in August, 2007

Preface

Nobody can deny the great importance of the interchange of ideas on theoretical and computational tools between scientists and engineers. By sharing stimulating tools and ideas, we are able to obtain new advances in many rapidly growing field of research related to Complex Networks. This is the primary scope of the International Conference **Net-Works 2007**, which this year 2007 is taken place in Aranjuez (Madrid), Spain.

The **Net-Works 2007** conference is organised into several sessions according to the topics presented. It represents an interesting collocation of interdisciplinary groups, which is a real strength in this conference series. We are particularly happy to give young researches the opportunity to present their results.

For these reasons, is a great pleasure for us to present this collection of selected papers. We heartily wish that everyone experience the best of computational scientific research. This set of papers represents the program of the conference in detail.

We have preferred to emphasise the latest applications of complex networks rather than the theoretical aspects. However, we have been careful to preserve the intrinsic rigour of the mathematics in each article.

The **Net-Works 2007** conference is organised into several sessions according to the topics presented. It represents an interesting collocation of interdisciplinary groups, which is a real strength in this conference. All the papers have been under peer-review, and when this proceedings is completed, we expect to produce a special issue in the prestigious journal *International Journal of Bifurcation and Chaos*.

Acknowledgements

Many thanks to Editor-in-Chief and Publishers of “*International Journal of Bifurcation and Chaos*” that accept to publish selected full papers of **Net-Works 2007**. The selection will be based on the international peer review of at least two independent reviewers.

We want also to thank:

- The Chancellor of Rey Juan Carlos University, Pedro González-Trevijano, for his help and his important support.
- The members of Scientific Committee for their help and their important support. Specially to:
 - S. Boccaletti, Istituto Nazionale di Ottica Applicata,
 - R. Criado, Universidad Rey Juan Carlos,
 - M. Dahlem, Institut für Theoretische Physik,
 - J. Kurths, Potsdam University,
 - V. Latora, Università di Catania,
 - E. Schoell, Technische Universität Berlin,
 - H. Mancini, Universidad de Navarra,
 - Y. Moreno, Universidad de Zaragoza.

We must note here that is a great honour for us that the above leaders on Complex Networks have accepted to participate in Scientific Committee of **Net-Works 2007**.

- The invited speakers which have accepted to give keynote lectures on the scope of the conference. Particularly to Leon Chua: It is a great honour for us to have him between the invited speakers of this conference.
- The anonymous referees, as well as various special session organisers and assistants, who have contributed to the success of this conference, earning the gratitude of all participants.
- The Editorial Committee of “*International Journal of Bifurcation and Chaos*”, where selected full papers will be considered after peer review for publication in a special issue.
- The Organising Committee: Javier Pello, Miguel Romance, and María Vela Pérez, for their encourage during the organisation of the conference.

- The administrative officer, María Bautista, for his help and a highly competent piece of work.

We also take this opportunity to thank all members of Rey Juan Carlos University with whom we have shared many efforts and interactions to organise the multiple aspects related with the organisation of this conference, specially to:

- The Vice-Chancellor of Rey Juan Carlos University, David Ortega, for his help and support, and to José Manuel Azcona. Without their help this conference would not have been possible.
- The board team of the Chancellor, specially to Jose María Bethencourt Fontenla, for their support, help and kindness.

This Conference has been supported and financed by Universidad Rey Juan Carlos, and sponsored by Universidad Rey Juan Carlos, Ferrovial S. A. CESPAs, and Addlink Software Científico S. L.

Contents

Preface	1
Acknowledgements	3
Contents	5
Contributions	7
<i>Topological properties of the contact network of granular packing</i>	9
R. Arévalo, I. Zuriguel, D. Maza	
<i>Understanding complex networks through the study of their critical nodes: Efficiency, vulnerability and dynamical importance</i>	23
R. Criado, J. Flores, A. García del Amo, J. Pello, M. Romance, M. Vela-Pérez	
<i>Structural analysis and optimality of vulnerability and efficiency in artificial networks</i>	31
R. Criado, J. Pello, M. Romance, M. Vela-Pérez	
<i>Control of sub-excitable waves in neural networks by nonlocal coupling</i>	39
M.A. Dahlem, F.M. Schneider, A. Panchuk, G. Hiller, E. Schöll	
<i>Dynamical and spectral properties of complex networks</i>	55
A. Díaz-Guilera	
<i>Topology Induced Instabilities in Neural Nets with Activity-Dependent Synapses</i>	59
S. Johnson, J. Marro, and J.J. Torres	
<i>Enhancing network synchronization by sparse repulsive couplings</i>	73
I. Leyva, I. Sendina-Nadal, J.A. Almendral	
<i>Complex Networks with Time-Dependent Connections and Silent Nodes</i>	81
J. Marro, J.J. Torres, J.M. Cortes, S. de Franciscis	
<i>The Structure of Collective Behavior in Complex Topologies</i>	97
Y. Moreno	
<i>Graph Reconstruction using Spectral Energy</i>	107
S. Strunkov and S. Sánchez	

- Prediction of claims and risk factor selection in automobile insurance using Support Vector Machines and Genetic Algorithms* 115
P. Tolmos Rodríguez-Piñero, R. S. Mozos
- Complete Synchronization between Hyperchaotic Space-Time Attractors* 125
G. Vidal and H. Mancini
- Preferential attachment, aging and weights in recommendation systems* 135
M. Zanin, P. Cano and J.M. Buldú

Contributions

Topological properties of the contact network of granular packing

Roberto Arévalo¹, Iker Zuriguel¹ and Diego Maza^{1,2}

¹*Departamento de Física y Matemática Aplicada, Universidad de Navarra, Pamplona, 31008, Spain.*

²*Also at Institute of Physics, Universidad de Navarra, Pamplona, 31008, Spain.*

Abstract

The force networks of different granular ensembles are defined and their topological properties studied using the tools of complex networks. In particular, for each set of grains compressed in a square box, it is introduced a force threshold that determines which contacts conform the network. Hence, the topological characteristics of the network are analyzed as a function of this parameter. The characterization of the structural features thus obtained, may be useful in the understanding of the macroscopic physical behavior exhibited by this class of media.

Keywords: force chains, complex networks, topology.

MSC 2000: 82D30

1. Introduction

Granular materials are being widely studied by the physics community since they exhibit unusual and distinctive properties [1]. These materials are composed of macroscopic particles that interact by a dissipative contact force and can be thought of as displaying gas, liquid and solid phases. A suitable model for the study of granular materials is to consider each grain as a hard sphere, ignoring fragmentation and moving the effect of deformation to the dissipative term. As pointed in [2], the wide applicability of these model to the study of liquids, glasses and colloids implies a paramount importance of the geometrical properties of the packing of hard spheres in determining the physics

emails: raturnes@alumni.unav.es, iker@fisica.unav.es, dmaza@unav.es

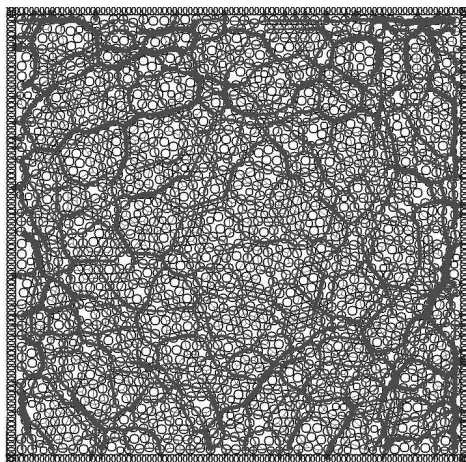


Figure 1: Example of a compressed sample obtained with our simulations showing the force chains. The thickness of the lines represents the magnitude of the normal force originated by the interaction between each pair of particles.

exhibited by the materials analyzed. The geometry of granular packing has been investigated *i.e.* by [2] and [3] using Voronoi-Delaunay partitioning to identify structures in the former and volume distributions in the latter.

In the present work we propose, in the same line of those and other works [4], a structural study of granular packing but using tools specifically developed in the frame of complex networks. As will be explained later we define for each packing a network of contacts, see FIG. 1, which topological properties are studied afterwards.

The contact topology of a granular packing can be studied as a graph where particles are *nodes* and the interacting force pairs *edges*. This approach has important advantages. For one hand, it is a quantitative tool as are not other ideas proposed in the granular community, namely, that of “force chains” [5]; it is an abstract point of view that allows to reach very primitive concepts such as connectivity over which to elaborate more complex definitions; and, finally, the field of complex networks provides us with a great amount of concepts and algorithms among which we can chose the most suitable for our proposes of characterization.

The remainder of this work is structured as follows: in section 2 we explain the numerical method used and the protocol followed to obtain the samples that we study. In section 3 the topological properties analyzed are defined and results presented for several different conditions. Finally, in section 4 we summaries our results and draw some conclusions.

2. Numerical method

We perform soft particle molecular dynamics simulations of discs in two dimensions. The model of contact includes a linear restoring force in the normal direction of the impact and a tangential force providing static friction. The complete details of the simulation protocol are carefully described in [6]. The values used for the parameters of the force model are: the frictional coefficient ($\mu = 0.5$), the elastic constant ($k_n = 10^5$), a dissipative coefficient proportional to the relative normal velocity $\gamma_n = 150$, and the corresponding ones for the tangential component ($k_s = \frac{2}{7}k_n$ and $\gamma_s = 300$) with an integration time step $\delta = 10^{-4}\tau$. The stiffness constants k are measured in units of mg/d , the damping constants γ in $m\sqrt{g/d}$ and time in $\sqrt{d/g}$. Here, m , d and g stand, respectively, for the mass of the discs, the diameter of the discs and the acceleration of gravity.

A typical simulation starts by randomly placing the discs in a wide horizontal area such that no one of them is in contact with any other and the packing fraction is around 0.1. Discs are given random velocities drawn from a gaussian distribution. Four walls made up with the same grains that constitute the bulk compress the system until a certain predefined threshold of force is attained. It is important to note that due to the dissipative nature of the interactions the final kinetic energy is vanishing small. The final configuration obtained is saved in order to be carefully analysed. This configuration is named a “jammed state” by the granular community and essentially corresponds to a metastable equilibrium state compatible with the history of the configuration.

We run simulations under several different conditions to check the variation of the results with the number of grains, polydispersity, friction coefficient, maximum applied pressure and geometry of the compression cell. Let us call sample A that obtained with a bidisperse mixture of discs, 15% with radii d and the rest with radii $7/9d$ and parameter values as given above; sample B has the same properties than A but the disks are monodisperse with radius d ; sample C is bidisperse as A but the friction coefficient is $\mu = 0.25$; sample D is the same as C but the final pressure is increased a 50%; finally, sample E is the same as A but the boundary conditions are circular instead of square. For samples A and B we run simulations with 512, 1024 and 2048 discs, for samples C, D and E only with 2048 since, as will be shown, no significant dependence on system size is found. In order to attain good statistics we perform 20 independent simulations for each sample and average the results.

3. Contact network as a complex network

In the first place we define our network, i.e. a set of nodes connected by edges [8], as follows. Every grain with, at least, one contact constitutes a node and edges are the connections between the grains (nodes) in contact. There is a contact between two grains if the distance between the centre of them is smaller or equal to its diameter. A contact defines a certain amount of normal force F between the grains. Such situation has been deeply studied by many authors using mainly lattices diffusive models [7]. One of the main results of these works is that, independently of the system details, the mean value of the force distribution $\langle F \rangle$ is a typical scale of the problem. Nevertheless, many open questions remain open about the properties of these systems: why the fluctuations in the force distribution are as large as $\langle F \rangle$? Which statistical framework is suitable to explain the experimental results?

In order to study the role of the topology on this problem we will use the tools introduced in the theory of complex network. We introduce a force threshold f such that any contact with a normal force bigger than f is an edge, but contacts with lower values of normal force are not edges and grains with no contact are not nodes. Thus we obtain a network which depends on f , and hence its topological properties can be studied as a function of f . In our definitions we do not consider the grains of the walls. In the remainder of this section we present the results obtained for each of the topological properties studied along with their definitions [8, 9].

3.1. Connectivity

In our case, the connectivity k of a node represents the number of contacts between neighboring particles. Then, the degree distribution $P(k)$ is the distribution function of the number of contacts per particle. In FIG. 2a we show the degree distribution of sample A for three different sample sizes showing that there is no substantial variation. In all the cases the maximum $P(k)$ is found for $k = 3$ and around 95% of the particles present values of k between 2 and 4. The degree distribution for the rest of the samples with $N = 2048$ is shown in FIG. 2b. The overall behavior of the function $P(k)$ remains the same for all samples and only slight deviations are appreciated for samples C and D. In particular, samples C and D display higher number of nodes with higher values of k . This result can be understood if it is considered that samples C and D are the ones with the smaller friction coefficient. This will result in a small amount of arches inside the sample and consequently a reduction of the amount of particles that display just two contacts.

In figure FIG. 3a we show the behavior of the average connectivity $\langle k \rangle$

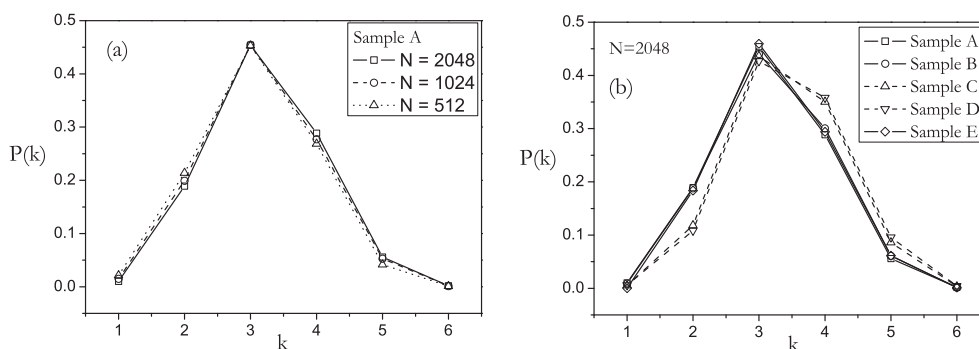


Figure 2: Left panel shows $P(k)$ for sample A using $N = 2048, 1024, 512$ discs. In the right panel we show $P(k)$ with $N = 2048$ for all samples.

as a function of the force threshold $f/\langle F \rangle$ for sample A. Again, this property seems independent of the system size. The figure FIG. 3b shows the results obtained for the different samples. Again, small differences are appreciable for samples C and D without modification of the overall behavior.

The most prominent feature is a fast decay of the connectivity upon increasing the force threshold. It could be said that the small forces are the ones which keep the network connected and the connectivity almost disappears when they are removed.

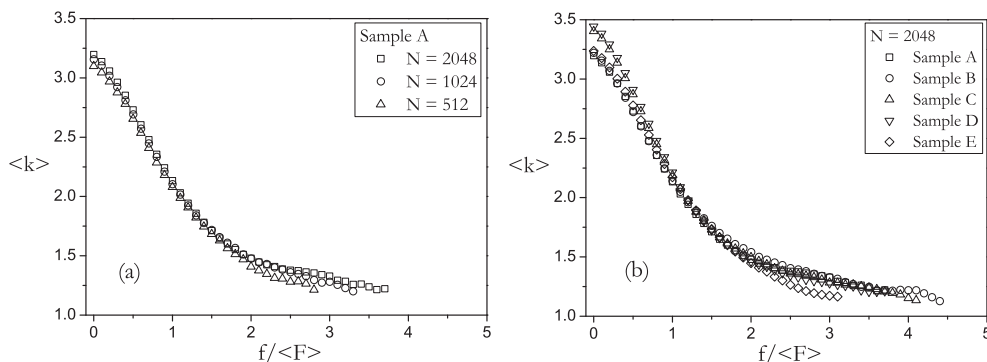


Figure 3: Left panel: average connectivity of sample A. Right panel: average connectivity of all samples.

3.2. Geodesic distance and network diameter

The geodesic distance l between two nodes is the smallest number of edges that separate them. This quantity can be measured by a number of algorithms, we

used the *breadth first search*. The diameter D of the network is the longest of the geodesic distances. In figure FIG. 4 the normalized geodesic distance l^* as a function of $f/\langle F \rangle$ is shown for sample A. The geodesic distance is normalized by $\sqrt{N}/2$ since the geodesic distance increases with the number of particles conforming the sample N . This scaling of l with the network size is what would correspond to a square lattice, so in the limit case of $f/\langle F \rangle \rightarrow 0$ our network seems to be not very different of a square one. The peak near $f/\langle F \rangle = 1$ can be explained in terms of the polygons that appear in the network as will be shown later. In the inset of FIG. 4 it is shown that there is no difference in the behavior of the geodesic distance for the different samples.

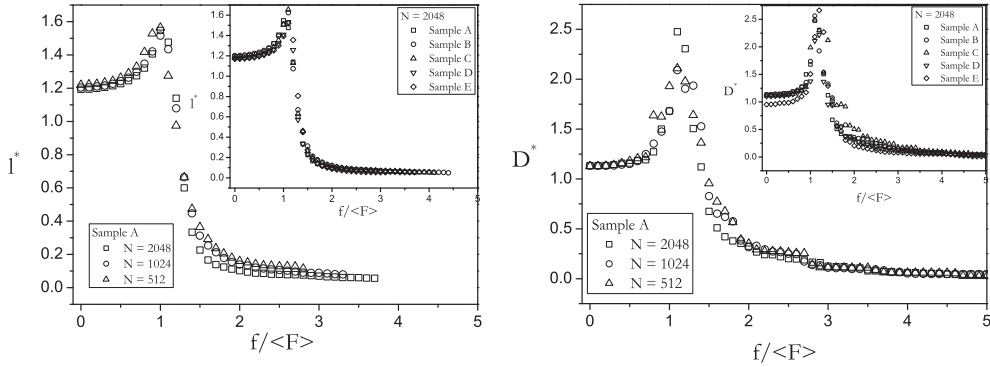


Figure 4: Left panel: l^* is the geodesic distance l normalized by $\sqrt{N}/2$ for sample A. The inset shows l^* for the all the samples with $N = 2048$. Right panel: D^* is the network diameter D normalized by $\sqrt{2N}$ for sample A. The inset shows D^* for all the samples with $N = 2048$.

The right panel of FIG. 4 shows D^* , the network diameter normalized by $\sqrt{2N}$. This normalization factor is applied to show that the diameter of the network scales with the diagonal of the compression cell. The behavior is entirely similar to that of the geodesic distance and only a small deviation is noticeable for sample E which was generated with a circular cell. For this reason we can attribute this minor difference to the scaling factor.

3.3. Number of nodes and maximum cluster size

We define a cluster as a group of nodes mutually connected. The total number of nodes in the network includes nodes from different clusters. In the inset of FIG. 5.a the total number of nodes is presented for sample A normalized by N , in semilogarithmic scale, showing that no variation appears upon increasing the network size. The inset of FIG. 5.b shows the result for the rest of the

samples. The number of nodes in the network decays exponentially, the line in both figures has slope 1.9, as the force threshold $f/\langle F \rangle$ is increased beyond $f/\langle F \rangle = 1$. Before the point $f/\langle F \rangle = 1$ the number of nodes decays only slightly. For $f/\langle F \rangle = 0$ the normalized number of nodes is not 1 implying that there are grains without any contact. This is due to the frictional nature of the medium which is able to create arches surrounding one or more grains.

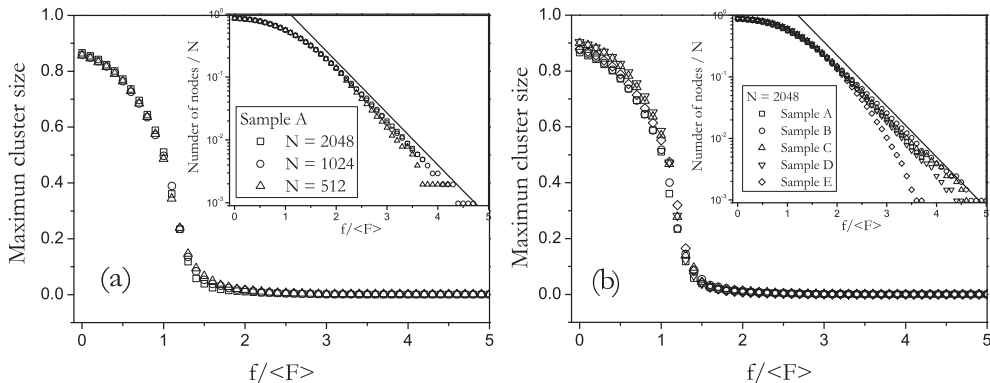


Figure 5: (a) Size, in number of nodes normalized by N , of the largest cluster in the network for sample A. Inset: Total number of nodes in the network normalized by N for sample A with $N = 512, 1024, 2048$. (b) Size, in number of nodes normalized by N for all the samples and $N = 2048$. Inset: total number of nodes for all the samples and $N = 2048$. The line in both graphics has slope 1.9.

As $f/\langle F \rangle$ increases the network disaggreate in clusters that are not connected to each other. In FIG. 5.a the size of the largest cluster, measured in number of grains, is shown for sample A normalized by N while FIG. 5.b shows this quantity for the rest of the samples. The largest cluster size dramatically drops in the vicinity of $f/\langle F \rangle = 1$ and is almost zero beyond $f/\langle F \rangle \simeq 1.5$.

3.4. Properties of clusters

In this section we further analyze the properties of clusters as defined in the previous section. As it is done in percolation theory [4] we remove the largest cluster, which has yet been analyzed, and study the distribution of the sizes s of the remaining clusters for different values of the force threshold: $n(s, f/\langle F \rangle)$. We use the samples with 2048. In figure FIG. 6 $n(s, 1.2)$, the cluster size distribution for $f/\langle F \rangle = 1.2$, is shown for all samples. In logarithmic scale it can be fitted by a line whose slope, in this case is around 1.9. We have enough statistics only for values of $f/\langle F \rangle$ between 1 and 3 and in this range we find

that the distribution of sizes behaves like $n(s, f/\langle F \rangle) \propto s^\alpha$ with α varying with $f/\langle F \rangle$.

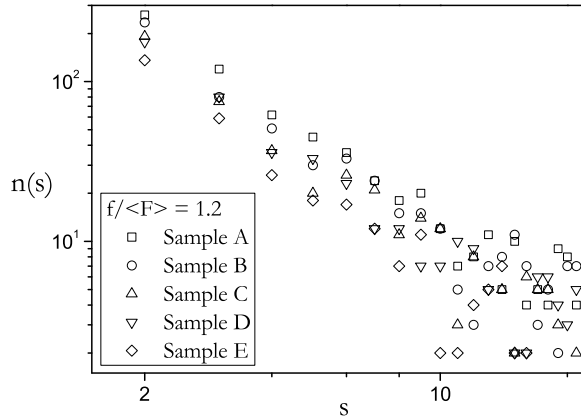


Figure 6: The distribution of cluster sizes s for all samples at $f/\langle F \rangle = 1.2$ showing that it is a power function.

In FIG. 7 we show the average cluster size $\langle s \rangle$ as a function of $f/\langle F \rangle$ with an inset showing the behavior of α . If we had retained the largest cluster to compute the sizes distribution, FIG. 7 would display a monotonically increasing function upon decreasing $f/\langle F \rangle$. Instead, it reveals a characteristic feature, a peak around $f/\langle F \rangle \simeq 1.2$ which is accompanied by a minimum in $\alpha(f/\langle F \rangle)$ around $f/\langle F \rangle = 1.5$.

3.5. Fractal dimension

In the theory of critical phenomena the value of the fractal dimension determines the universality of a system, and thus, a set of properties. In this section we compute the fractal dimension as a function of $f/\langle F \rangle$. Two such fractal dimensions can be defined [10]: the mass fractal dimension and the box counting fractal dimension. The former is computed choosing a node and tracing circumferences of increasing radius R around it. The mass M , in number of nodes, inside each circumference is computed and if it behaves like $M \propto R^{d_M}$ then d_M is the mass fractal dimension. This procedure is repeated changing the initial node and averaging the results. The boxcounting fractal dimension is computed analyzing how the minimum N_B number of boxes necessary to cover the network changes with the box size L . If this verifies $N_B \propto L^{d_B}$

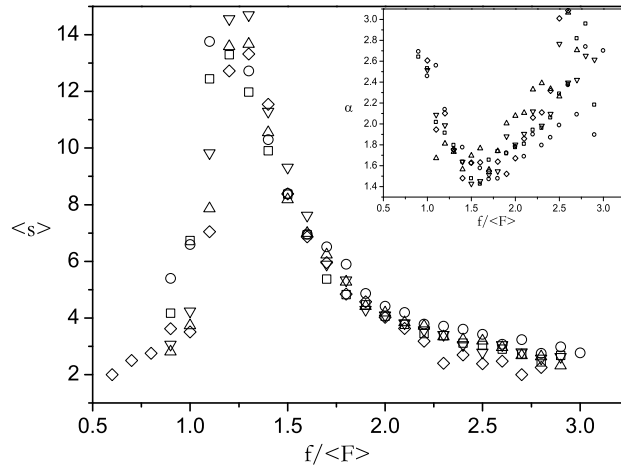


Figure 7: Average cluster size, removing the largest one, as a function of the force threshold $f/\langle F \rangle$. The inset shows the power α of the cluster size distribution $n(s, f/\langle F \rangle)$ as a function of $f/\langle F \rangle$.

then d_B is the box counting fractal dimension. The process of minimization involved in the last calculation renders it non immediate and we followed the methods exposed in [11]. The results obtained for both, the mass fractal dimension and the box counting fractal dimension, are shown in FIG. 8 as a function of the force threshold $f/\langle F \rangle$.

Both dimensions are fairly equal to 1.8 for values of $f/\langle F \rangle$, roughly, lower than 1. A slight increase can be perceived from $f/\langle F \rangle = 0$ until $f/\langle F \rangle \simeq 1$ where a marked drop takes place. This fall of the fractal dimension is sharper and deeper for the mass dimension but clearly present in both cases. The calculation of the fractal dimensions cannot be carried out beyond the limit shown since the network rapidly disaggregates. Thus we find a change of behavior of the contact network in the vicinity of $f/\langle F \rangle = 1$ that could be assigned to a change in the universality class that describes the network as a function of the force threshold.

3.6. Third order loops of contacts

A third order loop is defined as a three-step walk whose first and last nodes are the same. Third order loops are thus contacts arranged in a triangular

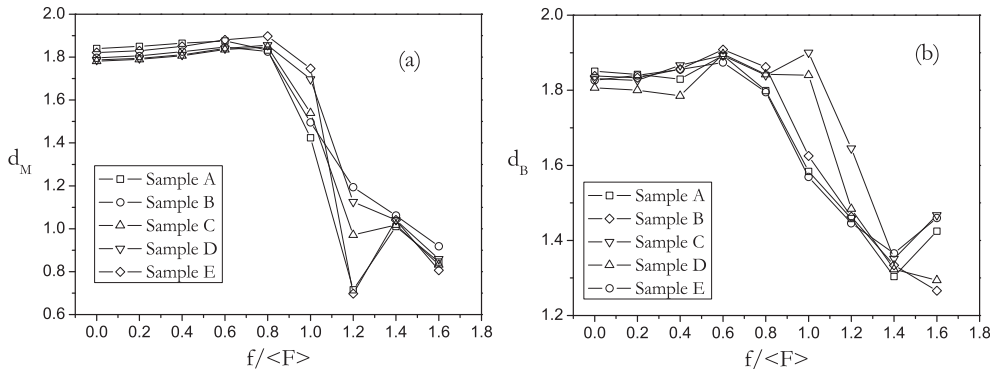


Figure 8: Left panel: the mass fractal dimension as a function of $f/\langle F \rangle$ for all samples with $N = 2048$. Right panel: the box counting fractal dimension as a function of $f/\langle F \rangle$ for all samples with $N = 2048$.

fashion whose number can be computed by the clustering coefficient [8, 9] or the third moment of the adjacency matrix [12]. In rigidity theory [13] these are, in two dimensions, the simplest rigid structures. Indeed if we think in a triangle whose edges are rigid and joined by freely rotational hinges it remains undeformed upon external perturbations. On the contrary a square made of rigid hinges and freely rotational hinges is easily deformed by shear in parallel sides. It is important to note that it is a sufficient, but not necessary, condition for a polygon to be rigid that all its faces are composed of triangles. Thus, triangles may be important for the rigidity displayed by granular packing in two dimensions.

In FIG. 9 the number of triangles is reported for all samples. There are no triangles beyond $f/\langle F \rangle \geq 1.5$ and they concentrate in the edges carrying a small amount of normal force, increasing exponentially when decreasing the force threshold. We believe that the apparition of third order loops of contacts is at the heart of the behavior found for some of the topological properties presented in this paper as the geodesic distance and the network diameter. For force values above $f/\langle F \rangle = 1.5$ a decrease in the force threshold provokes the connection of different clusters of the network and then, both the geodesic distance and the network diameter grow. However, a further decrease in the force threshold below $f/\langle F \rangle = 1.5$ implies the apparition of third order loops which will reduce the geodesic distance between the nodes that belong to them, and hence the diameter of the network. The way in which a third order loop reduces the geodesic distance between nodes can be easily understood. If we imagine three nodes (a,b,c) where the connections are a-b and b-c, the mean geodesic distance in the cluster will be 1.33 as a-b and b-c are separated by

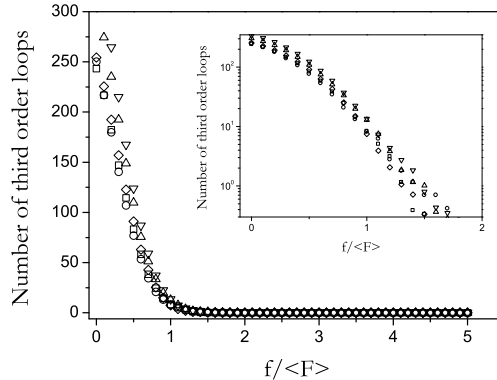


Figure 9: Number of third order loops as a function of $f/\langle F \rangle$ for all samples with $N = 2048$. The inset shows the same data in semilogarithmic scale.

one edge but a-c are separated by two edges. In the same way the diameter of this small network will be 2 as it is the maximum geodesic distance between the nodes. If now the nodes a and c are also connected giving rise to a third order loop, both the mean geodesic distance and the diameter of the network will be reduced to 1.

4. Discussion

In this work we report on some topological properties of the force interactions of granular packing by means of ideas specifically introduced for complex networks. Our aim is to characterize the heterogeneity of these systems without using definitions that may change from one author to another, like usually occurs in the case of force chains.

The set of properties analyzed is insensitive to the size of the system and shows only slight variations of behavior when the friction coefficient or the applied pressure are changed. Thus, they constitute a robust and useful description of an heterogeneous material like the packing studied. It is noteworthy that all the properties that have been analyzed as a function of the force threshold $f/\langle F \rangle$, that determines if an edge is present in the network or not, display some distinctive feature or sharp variation in the vicinity of $f/\langle F \rangle \simeq 1$. This behavior is indicative of a change in the structural properties of the network in this point. As has been pointed out by Radjai *et al.* there seems to be two subnetworks in the network of contacts, one “weak” network

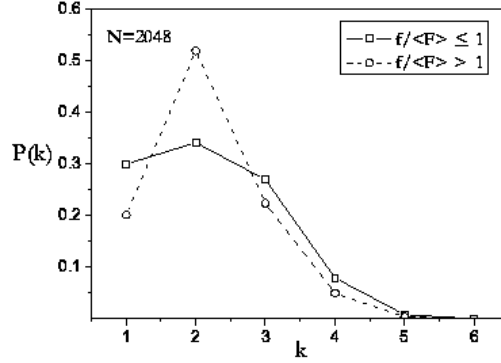


Figure 10: Connectivities distribution for sample A where the nodes connected by a force $f/\langle F \rangle > 1$ and $f/\langle F \rangle \leq 1$ have been treated separately. The subnetworks thus obtained exhibit well differentiated behaviors in the region of low connectivity.

composed of small forces and containing around 60% of grains, and a “strong” network constituted for edges carrying a force above the average.

Our findings seem to support the existence of these two subnetworks. As the force threshold is increased we remove the weak network and retain only the strong one, leading to dramatic changes that signal the change of behavior expected if both subnetworks exist and are intrinsically different. In FIG. 10 we show the connectivities distribution for both subnetworks. It can be checked that they are quite similar for high connectivities while differ significantly around $k = 2$.

A natural extension of this work is to consider the intensity of the force in every edge of the network and define weighted networks. This point of view could be a more suitable tool in order to relate structural features of the network with the physical properties of the packing; in particular, it could shed light into the question of the change of behavior at $f/\langle F \rangle \simeq 1$.

Acknowledgements

This work has been supported by project FIS2005-03881 (MEC, Spain), and PIUNA (University of Navarra). R. A. thanks Friends of the University of Navarra for a scholarship.

References

- [1] J. Duran, *Sands, powders and grains*, Springer-Verlag, New York, 1999.
- [2] A. V. Anikeenko and N. N. Medvedev, Phys. Rev. Lett. **98**, 235504 (1997).
- [3] T. Aste, M. Saadatfar and T. J. Senden, Phys. Rev. R **71** 061302 (2005).
- [4] S. Ostojic, E. Somfai and B. Nienhuis, Nature 439, 828 - 830 (2006).
- [5] J. F. Peters, M. Muthuswamy, J. Wibowo and A. Tordesillas, Phys. Rev. E **72**, 041307 (2005).
- [6] R. Arévalo, D. Maza and L.A. Pugnaloni, Phys. Rev. E **74**, 021303 (2006).
- [7] *Jamming and Rheology. Constrained Dynamics on Microscopic and Macroscopic Scales* A.J. Liu & S. Nagel Eds. Taylor & Francis. London and New York, 2001.
- [8] M. E. J. Newman, SIAM review **45**, 167 (2003).
- [9] L. F. Costa, F. A. Rodrigues and G. Travieso, Arxiv cond-mat/0505185 (2005).
- [10] C. Song, S. Havlin and H. A. Makse, Nature 433, 392-395 (2005).
- [11] C. Song, L. A. Gallos, S. Havlin and H. A. Makse, Arxiv cond-mat/0701216 (2007).
- [12] K.I. Goh, B. Kahng, and D. Kim Phys. Rev. E **64**, 051903 (2001).
- [13] H. Crapo, Structural Topology **1** (1979), 26-45; T. S. Tay and W. Whiteley, Structural Topology **11** (1985), 21-69.
- [14] F. Radjai, M. Jean, J-J. Moreau and S. Roux, Phys. Rev. Lett. **77**, 274 - 277 (1996).

Understanding complex networks through the study of their critical nodes: Efficiency, vulnerability and dynamical importance

R. Criado¹, J. Flores¹, A. García del Amo¹, J. Pello¹,
M. Romance¹ and M. Vela-Pérez¹

¹*Department of Applied Mathematics, Universidad Rey Juan Carlos, Madrid
(Spain)*

Abstract

The spectral radius of the adjacency matrix of a network has recently emerged as an important parameter related to many important properties of different network processes. We analyze some relationships between the spectral radius and the vulnerability of a network, and we give some estimations for the fall of efficiency and dynamical importance.

Keywords: efficiency, dynamical importance, vulnerability, network topology

MSC 2000: AMS 05C75, 05C90, 94C15, 94C30

1. Introduction

From metabolic pathways to computer systems, a huge variety of real systems of interest in science and technology may be described in terms of complex networks. The study of the structural properties of the underlying network can be crucial in the understanding of the functions of a complex system as well as its response to external factors such as the spreading of a perturbation over the network.

In this paper we study several parameters associated to a complex network as well as the correlation between some of them; we also examine the evolution of those parameters under removal of critical nodes.

emails: regino.criado@urjc.es, julio.flores@urjc.es,
alejandro.garciadelamo@urjc.es, javier.pello@urjc.es, miguel.romance@urjc.es,
maria.vela@urjc.es

The first parameter considered is the efficiency of a network G of n vertices which is defined as ([1],[2],[4])

$$E^+(G) = \frac{1}{n(n-1)} \sum_{\substack{i,j \in G \\ i \neq j}} \frac{1}{d_{ij}},$$

where d_{ij} is the distance on a graph between two vertices i and j , i.e., the length of the shortest path in G between i and j (if no such path exists, then we define d_{ij} to be infinite). Note that this magnitude embodies the idea of how the information flows through the network and turns out to be essential in the understanding of the response of a complex network to external factors as the spreading of a perturbation over the network. Metabolic pathways, genetic regulatory networks, protein folding, communication networks, trophic webs, blood vessel networks, disease transmissions and sexual contacts, . . . are natural examples on which this parameter proves useful. Several alternative definitions of this concept have been introduced in the literature, but all of them share the same spirit ([2],[4]).

The vulnerability of a network is a parameter that measures how the performance of a network under attack or random breakdown decreases. An attack is a *targeted* removal of the most “important” nodes (the nodes with highest degree). There are many approaches to this idea in the literature. For instance, Latora and Marchiori define the importance of local vulnerability of a vertex i in a network G as

$$v_{loc}(i) = E(G) - E(G \setminus \{i\}),$$

where $G \setminus \{i\}$ is obtained from G by deleting the node $\{i\}$. As an average of this expression, there have been obtained two global versions of the concept of vulnerability of complex networks, one related to random attacks or breakdowns given by

$$v_1(G) = \frac{1}{n} \sum_{i \in G} |E(G) - E(G - i)|,$$

while for intentional attacks we get

$$v_2(G) = \max\{|E(G) - E(G - i)| : i \in G\}.$$

Following this approach, both networks in Figure 1 below have vulnerability 0, but our intuition suggests that the complete graph K_4 is more robust than the cycle C_4 .

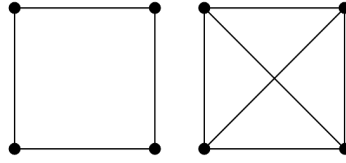


Figure 1: Two networks with the same $v_1(\cdot)$ and $v_2(\cdot)$

As an alternative approach, in [3] the vulnerability is considered as an (a priori) efficiency-independent magnitude, which can be defined as follows:

$$\hat{V}_D(G) = \exp\left(\frac{M - m + 1}{n} + n - a - 2\right),$$

$$\hat{V}_\sigma(G) = \exp\left(\frac{\sigma + 1}{n} + n - a - 2\right),$$

where σ is the standard deviation of the degree sequence, a is the number of edges and M and m are the values of the maximum and minimum degree of the vertices.

Many examples support the definition of $\hat{V}_D(G)$ and $\hat{V}_\sigma(G)$. However, the fact that only the vertices of maximum and minimum degree are considered in $\hat{V}_D(G)$ makes it not as sharp as desirable. For example, in figure 2, we find two networks that have the same $\hat{V}_D(\cdot)$ but different $\hat{V}_\sigma(\cdot)$.

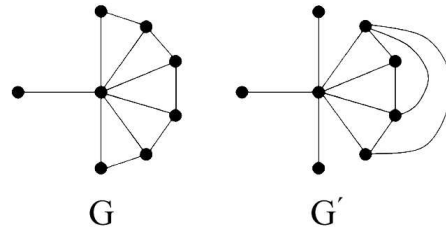


Figure 2: Two networks with the same $\hat{V}_D(\cdot)$ but different $\hat{V}_\sigma(\cdot)$

On the other hand, the largest eigenvalue of the network adjacency matrix (denoted by λ) has recently emerged as the key quantity determining many important properties for the study of a variety of different dynamical network processes ([7],[9],[10]). Recently, in order to characterize the dynamical importance of network, it was defined ([12]) the dynamical importance of node k

in terms of the amount $-\Delta\lambda_k$ by which λ decreases upon removal of the node k (or equivalently removal of all edges that are incident with k):

$$I_k = \frac{-\Delta\lambda_k}{\lambda}.$$

2. Estimations for the efficiency, vulnerability and dynamical importance of a network

In this section we establish some estimations involving the parameters considered above. Despite the fact that a vulnerability function should be independent of the efficiency of the network, if G is a connected network, we have that

$$\begin{aligned} \hat{p}(n) + q(n) \left(\frac{1}{n-2} - \frac{n-1}{n-2} E^+(G) \right) &\leq \log(\hat{V}_D(G)) \\ &\leq \hat{p}(n) + q(n) \left(1 - 2E^+(G) \right) + \frac{n-2}{n}, \end{aligned}$$

where $\hat{p}(n) = n - 2 + \frac{1}{n}$ and $q(n) = \frac{n(n-1)}{2}$.

Also we can obtain an inequality for the efficiency $E^+(\cdot)$ in terms of the networks maximum degree M ([4],[5]) getting that

$$E^+(G) \geq \frac{2m(n-M)}{n(n-1)(n+1-M)} + \frac{1}{n+1-M}.$$

As said above, the largest eigenvalue of the network adjacency matrix λ is a key quantity determining several important dynamical processes on complex networks. For instance:

- The critical coupling strength for the emergence of coherence is proportional to $\frac{1}{\lambda}$.
- The critical disease contagion probability for the onset of an epidemic scales as $\frac{1}{\lambda}$.
- In percolation, the condition for the emergence of a giant component also involves λ .

By using the well known inequality $\sqrt{M} \leq \lambda \leq M$, we can obtain several relationships between $\hat{V}_D(G)$, $\hat{V}_\sigma(G)$ and λ since

$$\lambda - m - 1 + \frac{2}{n} \leq \log(\hat{V}_D(G)) \leq \frac{\lambda^2 - 1}{n} + n - m + \frac{2}{n}$$

and

$$\frac{\sqrt{n\lambda^2 - 4m^2n}}{n^2} + n - m - 2 + \frac{2}{n} \leq \log(\hat{V}_\sigma(G)) \leq \frac{1}{n} \sqrt{\lambda^4 - \left(\frac{2m}{n}\right)^2} + n - m + \frac{2}{n}.$$

3. Estimations for the fall of efficiency and dynamical importance

The estimates obtained for the efficiency can be used to estimate the fall of efficiency upon removal of a node or an edge. In fact since

$$\frac{2m}{n(n-1)} \leq E^+(G) \leq \frac{m}{n(n-1)} + \frac{1}{2},$$

we get that

$$\Delta E = \frac{E^+(G) - E^+(G')}{E^+(G)} \leq \frac{(n+4)(n-1)}{4m} - \frac{1}{2},$$

where we denote by G' the graph G after the removal of a node $i \in G$.

Similar results can be obtained for the fall of dynamical importance, but we need some tools from the spectral analysis network theory. The inequality $\lambda(A) \geq 2m/n$ is due to Collatz and Sinogovitz ([6]), where m is the number of edges, n the number of nodes and $\lambda(A)$ the spectral radius of the graphs adjacency matrix A . From Weyl theorem ([8]) we get for two Hermitian matrices A and E

$$|\lambda(A) - \lambda(A + E)| \leq \|E\|$$

By combining these results, the following estimation is derived

$$0 \leq \Delta I = \frac{\lambda(A) - \lambda(A')}{\lambda(A)} \leq \frac{\sqrt{2}}{2} \frac{n\sqrt{n-1}}{m},$$

where we denote by A' the adjacency matrix of the graph G' obtained after the removal of a node.

4. Correlation between the fall of efficiency and of the fall of dynamical importance

We briefly provide in this section a numerical illustration regarding the correlations between the fall of efficiency and the fall of the dynamical importance

defined in the previous section. We will now present examples of the dynamical importance of nodes in simulated and real networks. The two graphs below show different situations.

In the first case, Figure 3, a random Erdős-Renji network G with 75 nodes is generated. Once we have constructed this network, we choose at random a node i and we compute the fall of efficiency $\Delta E^+(G)$ (plotted in blue in the figure) and the fall of dynamical importance ΔI (in red in the figure) if the node i is eliminated. We continue deactivating nodes at random until we get the empty network. The result shows the existence of very significant correlations between the fall of the efficiency and the fall of dynamical importance.

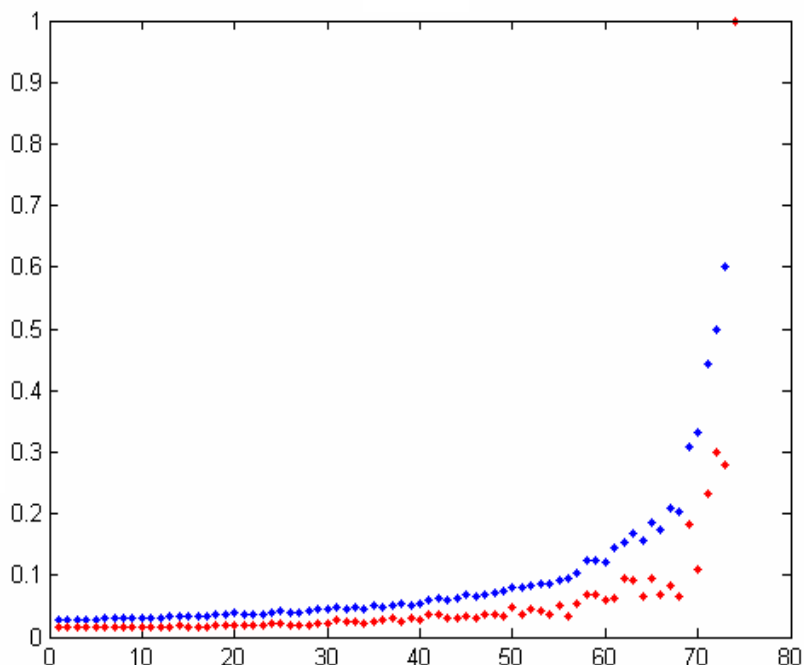


Figure 3: A random testing of the correlation between $\Delta E^+(G)$ and ΔI for a Erdős-Renji network with 75 nodes.

On the other hand, if we simulate the same random node elimination procedure for for the yeast protein interaction network of more that 500 nodes (obtained from [13]) and we compute the fall of efficiency $\Delta E^+(G)$ (plotted in blue in the figure) and the fall of dynamical importance ΔI (in red in the

picture), Figure 4 shows that, in this case the fall of the dynamical importance is practically void, while there are huge variations in the fall of the efficiency.

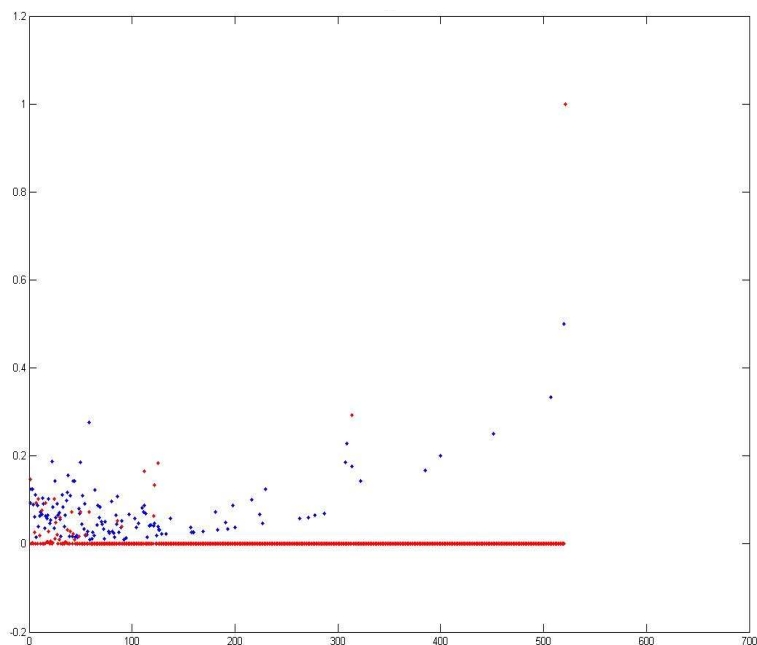


Figure 4: $\Delta E^+(G)$ and ΔI for the yeast protein interaction network of more than 500 nodes.

References

- [1] R. ALBERT, H. JEONG A.L. BARABASI, “Error and attack tolerance in complex networks”, *Nature* 406 (2000), 378-386.
- [2] S. BOCCALETTI, V. LATORA, Y. MORENO, M. CHAVEZ, D.U. HWANG, “Complex Networks: Structure and dynamics”, *PHYSIC REPORTS* 424 (2006), 175-308.
- [3] R. CRIADO, J. FLORES, B. HERNÁNDEZ-BERMEJO, J. PELLO, M. ROMANCE, “Effective measurement of network vulnerability under random and intentional attacks”, *J.Math.Mod.Algorith.* 4 (2005), 307-316.

- [4] R. CRIADO, A. GARCÍA DEL AMO, B. HERNÁNDEZ-BERMEJO, M. ROMANCE, “New results in computable efficiency and its stability for complex networks”, *J.Comp.Appl.Math.* 192 (2006), 59-74.
- [5] R. CRIADO, B. HERNÁNDEZ-BERMEJO, J. MARCO-BLANCO, M. ROMANCE, “Asymptotic estimates for efficiency, vulnerability and cost for random networks”, *To appear in J.Comp.Appl.Math*
- [6] L. COLLATZ, U. SINOGOWITZ, “Spektren endlicher Grafen, Abh. Math.”, *Sem. Univ. Hamburg* 21 (1957), 63-77.
- [7] D. CVETKOVIC AND P. ROWLINSON, *Linear Multilinear Algebra* 28, 3 (1990).
- [8] G. H. GOLUB AND C. F. VAN LOAN *Matrix Computations*, The Johns Hopkins University Press, Baltimore, third ed., 1996.
- [9] C.R. MACCLUER, *SIAM Rev.* 42 487 (2000).
- [10] R. M. MAY, “Will a large complex system be stable?”, *Nature* 238 413-414 (1972); J. FENG, V. K. JIRSA, M. DING, “Synchronization in Networks with Random Interactions: Theory and Applications”, *Chaos* 16 015109 (2006); M. BREDE AND S. SINHA, “Assortative mixing by degree makes a network more unstable”, *cond-mat/0507710* (2005).
- [11] M.E.J. NEWMAN, “The structure and function of complex networks”, *SIAM Review* 45 (2003), 167-256.
- [12] J.G. RESTREPO, EDWARD OTT, AND BRIAN R. HUNT, “Characterizing the dynamical importance of network nodes and links”, *Phys. Rev.Lett.* 97 094102 (2006)
- [13] <http://www.weizmann.ac.il/mcb/UriAlon/Papers/networkMotifs/sma.html>.

Structural analysis and optimality of vulnerability and efficiency in artificial networks

R. Criado¹, J. Pello¹, M. Romance¹ and M. Vela-Pérez¹

¹*Departamento de Matemática Aplicada, ESCET, Universidad Rey Juan Carlos,
C/ Tulipán s/n, 28933, Móstoles, Madrid, Spain*

Abstract

It is important, in many applications, to design an optimal artificial network. We analyse some structural properties such as vulnerability and efficiency, and we also present some characterisation of the extremal networks for those parameters giving improvements of those properties when adding a new link.

Keywords: Optimal networks, robustness, efficiency, vulnerability, network topology, network design.

MSC 2000: 05C75, 05C90, 94C15, 94C30

1. Introduction

Networks have been used in order to describe the complex structure of many real and artificial systems. Many authors have been interested in describe both real and artificial systems using many and different complex systems [1, 2, 3, 4, 7, 11, 12]. From biology and chemistry to Internet and financial markets or social relationships, the structural properties of those complex networks have been studied.

In order to understand the structure of those complex systems, it is necessary to analyse some properties such as the robustness and the performance. For the robustness, we will employ the *vulnerability* (as the opposite concept to robustness) which is related with the ability of a network to avoid malfunctioning when a fraction of its constituents is damaged due to random failures

emails: regino.criado@urjc.es, javier.pello@urjc.es, miguel.romance@urjc.es, maria.vela@urjc.es

or intentional attacks [6, 9]. There are several different approaches in the literature to measure the vulnerability of a complex network [5, 6] but, in general, they can be divided in two types. On the one hand we find the *static vulnerability* which analyses the response of the structural properties of the networks when some of its nodes or links are removed, while, on the other hand, the *dynamical vulnerability* is considered to measure the redistribution of flow in the network when a failure or attack occurs.

We will consider static vulnerability, related to structural properties of the complex network that allows us to spot its critical components in order to improve the security. In [6], an axiomatic description of the robustness is presented and some candidates for vulnerability functions are proposed based on the network regularity. Roughly speaking, a *vulnerability function* is a normalised function $v(G)$ intrinsic to the topology of G that increases if we remove some components of the network. In [6] it is considered that the vulnerability is related to the node regularity and the number of alternative links that can balance a random or intentional attack. The basic idea is that the *more similar* the nodes are, the more robust the network is, assumed that we have fixed the number of links and nodes in the network. Hence, in addition to the number of nodes and links, the dispersion of the degree distribution also should play a central role in the vulnerability of the network. Following this approach the vulnerability function of a network $G = (V, E)$ with n nodes and m links $V_1(G)$ was introduced as

$$V_1(G) = \exp\left(\frac{M - a}{n} + n - m - 2 + \frac{2}{n}\right), \quad (1)$$

where $M = \max\{gr(v_i); i \in V\}$, $a = \min\{gr(v_i); i \in V\}$ and $gr(v_i)$ is the degree of node $i \in V$. This definition can be computed easily and gives a good estimation of the robustness of a complex network but the fact that only the nodes of extremal degrees are considered makes it not as sharp as desirable from a statistical point of view. To avoid this problem, a sharper estimator of the regularity of the degree distribution must be considered, leading to the vulnerability function $V_2(G)$ given by

$$V_2(G) = \exp\left(\frac{\sigma}{n} + n - m - 2 + \frac{2}{n}\right), \quad (2)$$

where n is the number of nodes of G , m stands for the number of links and σ denotes the standard deviation of the degree distribution, i.e.

$$\sigma = \left(\frac{1}{n} \sum_{i \in V} \left(gr(v_i) - \frac{2m}{n}\right)^2\right)^{1/2}. \quad (3)$$

The *performance* of a complex network $G = (V, E)$ with n nodes and m links, is a single function $\Phi(G) > 0$ that measures the behaviour of G . Some examples of the performance of a network G are the characteristic path length of the network $L(G)$, the mean flow-rate information over G , but we will use the efficiency $E^+(G)$, defined (see [8, 9]) as

$$E^+(G) = \frac{1}{n(n-1)} \sum_{i \neq j \in V} \frac{1}{d_{ij}}, \quad (4)$$

where d_{ij} stands for the shortest distance between the nodes i and j . This concept plays the role of measuring its ability for the exchange of information and its response for the spread of perturbations in diverse applications [3, 5].

We are interested in analyse those parameters and try to improve our complex network. To do so, we study two different problems. The first one is how to improve the network vulnerability or efficiency in order to get the best possible result by adding just one link (for real cases could be a railroad track, a new subway station or a new fly connection between two cities). The second one is related to the design of an optimal network given the number of nodes n and links m . We show have to construct the optimal network for the efficiency or the vulnerability. The approaches for optimising vulnerability and efficiency are rather different since the problems have different nature. While we get a complete characterisation of the extremal network for the vulnerability function, the case of efficiency function is much deeper and we present some approximation algorithms.

2. Extreme networks for vulnerability and efficiency

In this section we consider the set of all connected networks G with n nodes and m links and we find the extreme graphs for vulnerability and efficiency. That is, we find those networks with maximal vulnerability, with minimal vulnerability and with maximal efficiency for a given number of nodes n and links m .

When dealing with a vulnerability function we work with definition $V_2(\cdot)$, since for definition $V_1(\cdot)$ the results are straightforward. On the other hand, for efficiency, we use the additive definition $E^+(\cdot)$ given by Latora and Marchiori (see [8, 9]), but note that since there is a relationship between the different definitions for the efficiency, we can transfer the results from one to the other.

Our first result is about vulnerability and its extreme values. To prove it we will use the inequality:

$$\sum_{i=1}^n gr(v_i)^2 = \|gr\|^2 \geq \frac{4m^2}{n}, \quad (5)$$

which is valid for every network $G = (V, E)$ with $n > 1$ nodes and m links and $gr = (gr(v_1), \dots, gr(v_n))$ its degree vector.

Note that we have the equality in (5) for the K -regular graphs, simply by the equality case in Cauchy-Schwartz inequality.

By using this result, we can characterise the networks $G = (V, E)$, with a given number of nodes and links and degree vector $gr = (gr(v_1), \dots, gr(v_n))$, having minimal and maximal vulnerability. We find that the minimum vulnerability is obtained for those networks having its degree factor of the form $(a, \dots, a, a + 1, \dots, a + 1)$, $a, a + 1 \leq n - 1$, with

$$\sum_{i=1}^n gr(v_i) = 2m;$$

i.e. for those networks G which are the *closest* ones to the K -regular graph with m links.

When dealing with extremal networks for the efficiency function, a first analysis should include the local structure of the graph. By using this approach, the degree vector is the natural tool, and we show that for the networks having a node with maximum degree (i.e. $gr(v_i) = n - 1$) there is a simple formula for the efficiency function:

$$E^+(G) = \frac{m}{n(n-1)} + \frac{1}{2}.$$

As a consequence, we deduce that, for a network G (with $n > 1$ nodes) to have maximum efficiency it is enough that G has the n -Star as a subgraph or another K -complete bipartite subgraph.

We find also the following inequality for efficiency in terms of the maximum degree of the network (not necessarily equal to $n - 1$):

$$E^+(G) \geq \frac{2m(n-a)}{n(n-1)(n+1-a)} + \frac{1}{n+1-a},$$

where we apply the inequality $d_{ij} \leq n - a + 1$ for the distances between nodes and $v_k \in V$ is the node with maximum degree in the network (not necessarily equal to $n - 1$), that we denote $gr(v_k) = a$.

3. Optimal improvement of complex network

A major problem in network design is spotting the critical element to be added to a given (real-life) complex network that gets the best possible network for some parameters. By cost restrictions, the elements to be added to the network (nodes or links) are usually limited and hence the problem of finding the optimal improvement of the network is related to a discrete and conditioned critical points problem which is hard to solve by direct methods. In this section we will consider such problems when we want to get an optimal improvement of the network that maximises its robustness (i.e. minimises some vulnerability function) or maximises its performance (i.e. the efficiency function) and we will give some computationally effective criteria to determine these conditioned critical points.

If we consider a complex network G and we want to add a single link ℓ such that we get a network $G' = G \cup \{\ell\}$ with minimal vulnerability or maximal efficiency, a first naive approach leads us to compute all possible improvements of type $G \cup \{\ell\}$ and spot the optimal, but in real networks this can be computationally non-effective. Note, for example, that if we want to locate the improvement of a complex network with n nodes which has maximal efficiency, an exhaustive analysis of all possible candidates uses an algorithm of computational complexity of order n^7 , which is far from being effective when dealing with real networks with thousand (or million) of nodes. Therefore it is necessary to develop new strategies of design that reduce the complexity of locating the critical component to be added in order to get effective tools for the network optimisation.

Locating the critical single link ℓ that gets the most robust improvement $G \cup \{\ell\}$ of a network G is related to the degree of the nodes to be linked. If we want to minimise the vulnerability function $V_1(G \cup \{\ell\})$, it is straightforward that the optimal design strategy is to decrease the range of the degree distribution of G by adding a link joining the node of minimal degree with other node which has no maximal degree. If we consider the vulnerability function $V_2(\cdot)$, we could think that the same idea should work, but since this vulnerability function uses the whole degree distribution, it can be checked that this is not the optimal strategy for network improvement. Despite this fact, the optimal computationally effective strategy is also related to the minimal degree of the nodes since, for a given network $G = (V, E)$, with $\ell_0 = \{v_{i_0}, v_{j_0}\}$ such that $v_{i_0}, v_{j_0} \in V$ and $\ell_0 \notin E$, it is equivalent that $G' = G \cup \{\ell_0\}$ has minimal vulnerability $V_2(\cdot)$ among all improvements $G \cup \{\ell\}$ and that $\gamma(v_{i_0}, v_{j_0}) = \min \{\gamma(v_i, v_j); \{v_i, v_j\} \notin E\}$, where $\gamma(v_i, v_j) = gr(v_i) + gr(v_j)$.

Note that the computational complexity to find the minimum of $\gamma(v_i, v_j)$

directly is of order n^4 , while the exhaustive computation of the optimal improvement of type $G \cup \{\ell\}$ has complexity n^5 .

Locating the maximal efficiency improvement of type $G \cup \{\ell\}$ is, by far, a much more complicated problem. In this case, it is clear that the addition of a single link ℓ to a network G can produce deep changes in its geodesic structure. We could naively expect that the optimal improvement occurs when we link the most distant nodes, but it is easy to find simple example where this idea fails. Actually, it seems that there is no other clear-enough criterium for locating the improvement of the network with maximal efficiency. As an alternative approach, we propose to give other computationally effective method that gives an approximation of the optimal improvement. If we want to get a near-optimal improvement of type $G \cup \{\ell\}$ we have to mix two different facts:

- (i) Nodes to be mixed have to be far in order to produce a significant increase in the efficiency.
- (ii) The new link should produce the biggest change in the geodesic structure of the network. Note that this geodesic sensitivity is related again to the degree of the nodes involved.

However, these conditions do not, by themselves, guarantee that a certain edge will provide the greatest, or close to the greatest, efficiency increase. It can be seen that linking nodes already close always has a small impact on efficiency, while picking distant nodes may have a larger effect, but it may as well not be the case.

So, while choosing the two most connected nodes does not always bring the highest efficiency, at least we know we have to take two of the most connected, and preferably distant, nodes. There is a bound to how much the efficiency can increase when adding a single edge, based on their initial distance and their degrees. Therefore, a suitable course of action to find the best edge would be to sort the possible edges to be added according to distance and node degree and run through them in decreasing order, testing the change in efficiency and stopping when the bound ensures that we have already come across the best choice. The graphs above suggest that this best choice will actually be one of the first pairs to be tested.

References

- [1] R. ALBERT AND A. L. BARABÁSI, “Statistical mechanics of complex networks”, *Rev. Mod. Phys.* **74** (2002), 47–97.

- [2] Y. BAR-YAM, *Dynamics of Complex Systems*, Addison-Wesley, 1997.
- [3] S. BOCCALETTI, V. LATORA, Y. MORENO, M. CHAVEZ, D.-U. HWANG, “Complex networks: Structure and dynamics”, *Physics Reports* **424** (2006), 175–308.
- [4] S. BORNHOLDT, H. G. SCHUSTERS (EDS), “Handbook of graphs and networks”, *Wiley-VCH* (2002)
- [5] R. CRIADO, A. GARCÍA DEL AMO, B. HERNÁNDEZ-BERMEJO, M. ROMANCE, “New results on computable efficiency and its stability for complex networks”, *Journal of Computational and Applied Mathematics* **192**, 59 (2006).
- [6] R. CRIADO, J. FLORES, B. HERNÁNDEZ-BERMEJO, J. PELLO, M. ROMANCE, “Effective measurement of network vulnerability under random and intentional attacks”, *Journal of Mathematical Modelling and Algorithms* Vol 4, No 3 (2005), 307–316.
- [7] S. N. DOROGOVTSSEV AND J. F. F. MENDES, “Evolution of networks (from Biological nets to the Internet and www)”, *Oxford University Press* (2002).
- [8] V. LATORA AND M. MARCHIORI, “Efficient behaviour of small-world networks”, *Phys. Rev. Lett.* **87** (2001), art. no. 198701.
- [9] V. LATORA AND M. MARCHIORI, “How the science of complex networks can help developing strategies against terrorism”, *Chaos, Solitons and Fractals* **20** (2004), 69–75.
- [10] V. LATORA, M. MARCHIORI, “Vulnerability and protection of infrastructure networks”, *Phys. Rev.* **E71**(2005), art. no. 015103
- [11] M. E. J. NEWMAN, “The structure and function of complex networks”, *SIAM Review* **45** (2003), 167–256.
- [12] S. H. STROGATZ, “Exploring complex networks”, *Nature* **410** (2001), 268–276.

Control of sub-excitable waves in neural networks by nonlocal coupling

M.A. Dahlem^{1,2}, F.M. Schneider¹, A. Panchuk^{1,3}, G. Hiller¹ and
E. Schöll¹

¹*Institut für Theoretische Physik, Technische Universität Berlin, Germany*

²*Klinik für Neurologie II, Otto-von-Guericke-Universität Magdeburg, Germany*

³*Institute of Mathematics, National Academy of Sciences of Ukraine*

Abstract

Transient wave forms in neural networks with diffusive and nonlocal coupling have attracted particular interest because they may mediate recruitment of healthy cortical tissue into a pathological state during migraine. To investigate this process, we use a reaction-diffusion system of inhibitor-activator type as a generic model of pathological wave propagation and set it close to bifurcation in the sub-excitable regime. We report the influence of various nonlocal connectivity schemes on wave propagation. Wave propagation can be suppressed with cross coupling inhibitor and activator for both positive and negative coupling strength K , depending on the connection length δ . The area in the parameter plane (δ, K) where this control goal is achieved resembles a Mexican-hat-type network connectivity. Our results suggest that nonlocal synaptic transmission can control wave propagation, which may be of therapeutic value.

Keywords: nonlinear dynamical systems, excitability, control, nonlocal and time delay coupling

emails: dahlem@physik.tu-berlin.de, schneider@itp.physik.tu-berlin.de,
nastyap@imath.kiev.ua, hiller@itp.tu-berlin.de, schoell@physik.tu-berlin.de

1. Introduction

During migraine attacks, localized pathological excitation can spread through cortical tissue and invade large areas before it abates. This activity causes migraine aura, that is, neurological symptoms preceding the headache phase [1]. The underlying process is a phenomenon called cortical spreading depression (SD). It is assumed to be a reaction-diffusion process in the cortex, although reactions and diffusion processes that provide the mechanism of propagation are still under debate [2, 3]. However, the generic dynamics of reaction-diffusion systems are largely independent of the interaction details and shared among various biological systems [4]. Therefore, to describe the spatio-temporal patterns of SD, the cortex can be approximated as a continuous excitable media supporting reaction diffusion waves [5, 6, 7].

Psychophysical studies on visual processing in migraine patients suggest that changes in their networks of cortical neurons lead to an interictal state of changed excitability, i. e., an anomalous cortical state in the interval between migraine attacks [8, 9]. This motivates efforts to understand how the spread of reaction diffusion waves is controlled by nonlocal network connectivity. To include this, we investigate in this work the hypothesis that the emergence of SD waves can be attributed to these network changes as well. Previously, we have investigated how to change parameters of an excitable medium so as to efficiently protect cortical tissue surrounding a stimulus against recruitment [10]. Our current results suggest that failures in synaptic transmission result in increased susceptibility of cortical tissue to SD. Such a modulation of excitability becomes of crucial importance when the cortical state is close to the bifurcation of the onset of wave propagation. The clinically relevant conclusion to be drawn from this is that therapy might target network connectivity that modulates cortical tissue excitability, even though a specific network connectivity is not required for the initiation or propagation of SD in a regime far from the bifurcation.

2. Neural network with diffusive and nonlocal coupling

A variety of neural network models for SD have been proposed, though there is not yet consent on the mechanism. Roughly speaking, two classes of models exist. One taking a bottom up approach based on biophysical laws including several ionic currents, ion pumps, membrane potentials, and osmotic forces [13, 14, 15, 16]. The other approach is top down trying to incorporate the system properties without detailing any first-level subsystems. Hodgkin proposed the first simplified reaction-diffusion approach to SD. The model was

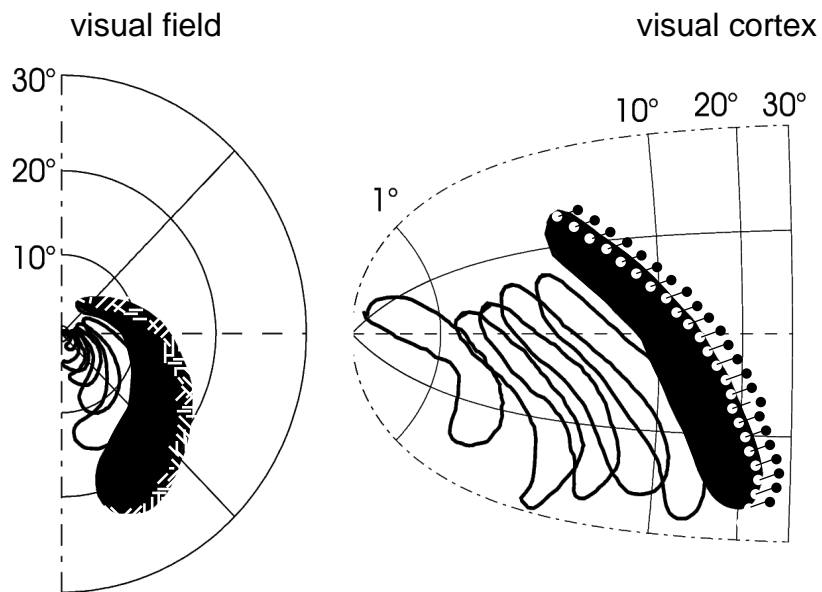


Figure 1: (left) Visual migraine aura symptom in the shape of a jagged crescent pattern moving through the visual field (modified from [11]). (right) Translation of the visual field disturbance by inverse retinotopic mapping. The crescent patterns translates into a wave segment resembling a “critical finger” [12]. Such patterns are unbounded wave segments observed close to the excitability boundary, i. e., a bifurcation of the systems described by Eqs. (1-2).

never published, but communicated to Grafstein [17, 18]. According to this references, Hodgkin suggested to consider a balance equation for potassium with a cubic source function and diffusion. The three roots of the cubic function being the resting state, a threshold, and a potassium ceiling level, respectively. Based on methods introduced by Huxley, solving the equation led to the approximate speed of SD. However, the diffusion coefficient used was four times higher than that of potassium in aqueous solution. This may either indicate the anomalous nature of potassium migration in the cortex [19], or the leading role of a faster transcellular reaction-diffusion mechanism [20].

Another model [5] followed Grafstein's potassium hypothesis with two extensions. We shortly summarize this work, because we follow a similar approach but with a different interpretation and aim. Firstly, the model included a second dynamic variable describing a refractory phase of SD. The source term in the balance equation of potassium is replaced by a quartic polynomial as the major nonlinearity of this activator-inhibitor system. Secondly, the reaction-diffusion model was connected to a neural network building together a hybrid model. The neural network was originally used to study cortical dynamics and sensory map reorganization. In the hybrid model it was used to explain visual field defects occurring during migraine with aura. We also use a reaction-diffusion system combined with a nonlocal interaction coming from a neural network. Our goal is to investigate which neural network connectivity can prevent SD, as suggested and studied using cellular automata in [21].

We use the spatially extended FitzHugh-Nagumo (FHN) system [22, 23], which has a cubic nonlinearity, as a generic model of SD waves

$$\begin{aligned} \frac{\partial u}{\partial t} &= u - \frac{1}{3}u^3 - v + D\frac{\partial^2 u}{\partial x^2} \\ &\quad + \text{nonlocal coupling} \end{aligned} \tag{1}$$

$$\begin{aligned} \frac{\partial v}{\partial t} &= \epsilon(u + \beta - \gamma v) \\ &\quad + \text{nonlocal coupling} . \end{aligned} \tag{2}$$

The model approximates the cerebral cortex as a two-dimensional surface with the ability to support sustained SD wave propagation. As a generic model this system does not make an explicit distinction between the various species involved in SD. In effect it lumps together sodium inward currents and extracellular potassium concentration $[K^+]_o$ into a single activator variable u and their combined kinetics into the cubic source term. Likewise, a single inhibitor variable v is related to recovery processes, such as effective regulation of $[K^+]_o$ by Na^+-K^+ ion pumps and the glia-endothelial system [20, 14, 15]. Whether a transcellular or extracellular route is taken, is at this level not specified. The main reason we use the FHN mechanism as the reaction-diffusion part of the

model is that it has been shown to successfully reproduce the two-dimensional spatio-temporal pattern of SD [7, 24]. Our study is essentially based on these pattern formation properties of SD waves and less on its detailed biophysical mechanism.

We extend the FHN system to encompass cortical lateral interactions, i. e., connections running parallel to the cortical surface. They are accounted for in the form of nonlocal coupling terms

$$K [s(x + \delta) - 2s(x) + s(x - \delta)]. \quad (3)$$

The signal s can either be the activator u or inhibitor v . A connection in the cortex can extend over several millimeters and it either mediates competitive or cooperative interactions. The parameter δ describes the connection length and the coupling strength K of the interaction.

Lateral connections in the cortex can form clusters at regular intervals [25]. Their structure and how they might interact with SD waves will be further considered in Sec. 4. Until then, we consider only one nonlocal coupling term occurring either in the activator (1) or inhibitor (2) balance equation, with fixed values for δ and K . This leads to four different coupling schemes: two of cross coupling (CC) activator and inhibitor, and two in which each dynamic variable is coupled via Eq. (3) into its own balance equation (NCC).

3. Suppression of waves by nonlocal interaction

The investigations were done in a one-dimensional spatial FHN system. We chose the parameter of the FHN system such that it is without the nonlocal coupling term in Eqs. (1-2) above but near to the excitability boundary of a one-dimensional system. This boundary was obtained by transforming the system into a co-moving frame and searching for homoclinic orbits. These orbits correspond to pulse solutions in the original coordinates. The excitability boundary (∂P) is defined by a saddle-node bifurcation at which the stable and unstable homoclinic orbit disappear [26]. The parameter values of β , ϵ , and γ at which homoclinic orbits disappear constitute a boundary of codimension one. In other words, ∂P separates the parameter plane into a regime where local stimulations is transmitted without damping and a regime where such sustained 1D reaction-diffusion waves do not exist (Fig. 2).

We chose a FHN system near ∂P because the transient nature of the observed symptomatic and electrophysiological events during migraine suggest such a regime [11, 27]. In the regime below but close to ∂P transient wave forms exist in a one-dimensional system [10]. Above ∂P transient wave forms exist in two-dimensional systems until excitability reaches a boundary called

∂R . There, sustained wave segments, called “critical fingers”, propagate without reentering tissue (c.f. Fig. 1). The regime between ∂P and ∂R is therefore called sub-excitable. The regime in which this transition takes place is also well investigated in chemical model systems in experiment and theory, for a review see [28].

To investigate the influence of various nonlocal connectivity schemes on wave propagation in the regime of sub-excitability, we start by setting a super-threshold stimulation in the one-dimensional system, choosing a particular FHN system with parameter values $\beta = 0.8$, $\epsilon = 0.1$, $\gamma = 0.5$, and $D = 1$. Once a stable one-dimensional wave profile is obtained, the nonlocal lateral network is switched on. Different networks for various parameter values K and δ are classified by their effect on the wave. We distinguish two cases. Either the wave is suppressed. This indicates that the excitability boundary ∂P of the combined system is shifted to higher excitability values (upwards in Fig. 2) into a regime where without the nonlocal coupling pulse solutions would exist. Or the wave continues to spread, though its profile and speed might change. From a clinical point of view, the wave suppression is a desirable control goal for the network achieved within the solid black regions in the (K, δ) -planes in Fig. 3.

We find that wave propagation can be suppressed with a NCC (non-cross-

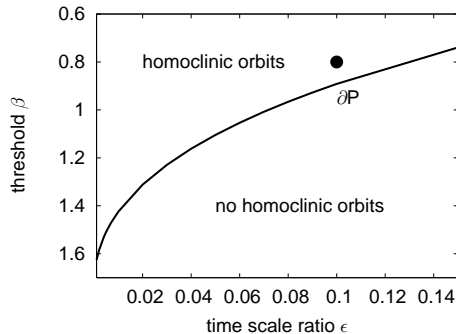


Figure 2: Parameter space of the FHN system at the section $\gamma = 0.5$. ∂P is the propagation boundary. Below ∂P any confined perturbation of arbitrary profile decays eventually. Above ∂P some wave profiles are stable and propagate with constant speed. They correspond to homoclinic orbits in a co-moving frame. The simulations have been done with a FHN system at $\beta = 0.8$ and $\epsilon = 0.1$ (solid black circle). A successful suppression of reaction-diffusion waves by nonlocal coupling indicates a shift of ∂P of the combined system beyond the point at $\beta = 0.8$ and $\epsilon = 0.1$.

coupled) setup only with positive coupling strength K . When the NCC term appears in the activator balance equation, the desired control goal is achieved largely independent of the connection length δ (Fig. 3 a), as long as δ is in the range of the wave width, including its refractory tail. When the nonlocal coupling term appears in the inhibitor balance equation, a similar picture arises, though waves are suppressed for connection lengths ranging into the refractory tail of the wave ($\delta > 40$) only for a narrow regime of K . Suppression completely fails for $\delta > 70$ (Fig. 3 b).

Cross coupling of inhibitor and activator achieves the desired control goal for both positive and negative coupling strengths K , depending on the connection length δ (Fig. 3 c-d). The area in the parameter plane (δ, K) where this control goal is achieved resembles a Mexican-hat-type network connectivity. This is readily seen in Fig. 4. When the nonlocal term appears in the inhibitor balance equation (2) the regimes of successful control in the K direction is much wider (Fig. 3 d) than the regime for cross coupling in the activator balance equation (1, Fig. 3 c).

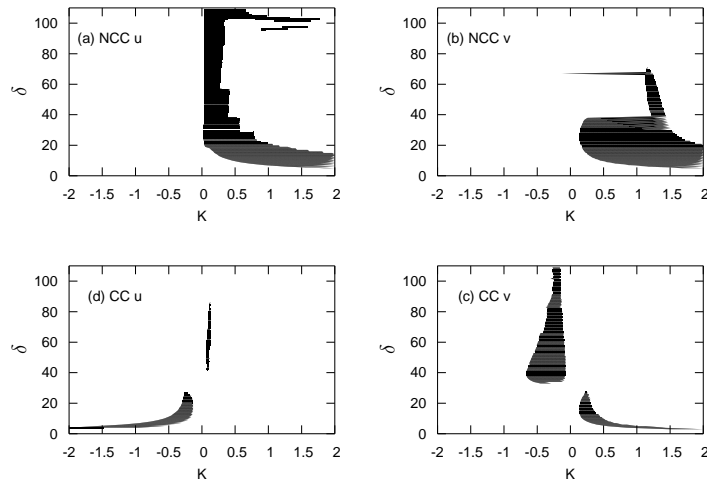


Figure 3: Parameter plane (K, δ) of the nonlocal control term. Black areas indicate successful suppression of wave propagation. (a) Non-cross coupling (NCC) in the activator equation (1). (b) NCC in the inhibitor equation (2). (c) Cross coupling (CC) in the activator equation (1). (d) CC in the inhibitor equation (2).

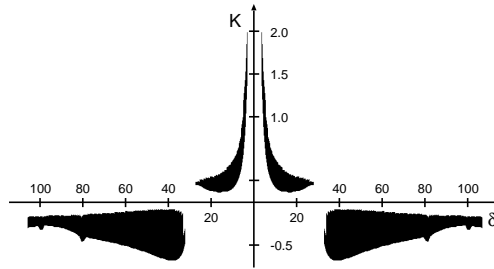


Figure 4: The "Mexican hat" connectivity profile of successful wave suppression for cross coupling (CC) is clearly visible when the control plane is rotated and the space coordinate δ is plotted as the distance ranging from negative to positive values. Shown is the successful control area (black) for the CC term appearing in the inhibitor equation (2). When the CC term is in the activator equation (1) the profile of the Mexican-hat connectivity is inverted.

4. On the nature of nonlocal coupling in migraine

In the previous section, we have shown which network failures lead to the emergence of reaction-diffusion waves. From this alone it is not deducible whether some of these network failures can also explain the anomalous cortical state in the interval between migraine attacks. It would be a plausible hypothesis, however, that the same network changes that cause the ictal migraine events, i. e., SD waves, lead to the anomalous interictal state. Changes causing the latter have been attributed to abnormal aspects in early visual processing in the cortex [9]. Various, seemingly contradictory explanations have been given, such as lack of both intra-cortical inhibition and excitation. They are also referred to as cortical hypo- or hyperexcitability (see [29] and references therein).

There is substantial work on the functional role of lateral connectivity for cortical processing, but little is known how the mechanism of SD is coupled to it. Evidence supporting a coupling comes from two independent sources. On the one hand, there is the structure of the hallucinatory aura patterns, in particular the typical zigzags (see Fig. 1). Such patterns were suggested to reflect the cortical network organization [30, 31]. The main idea is that the approaching wave initially affects cortical cells which possess the highest spontaneous activity and are clustered in patches. Within these patches the neuronal response properties remain relatively constant. Their feature distribution corresponds to the organization of the receptive field structure in the cortex. For example, the connection pattern in the visual cortex is unspecific in the immediate vicinity of each neuron, while long-range connections primar-

ily run between so-called iso-orientation columns [25]. Cells in an orientation column have the same oriented receptive field structure, thus they are responsive to edges with the same orientation. These edges are literally seen during a migraine attack as the building blocks of the hallucinatory zigzag pattern. Therefore, it is reasonable to assume that the SD wave interacts with this neural network structure in form of a synchronization process that occurs at the front of the SD wave and extends over the typical spatial length scale of iso-orientation columns.

The other line of evidence comes from *in vivo* studies in animal research on SD. In [20] Herreras et al. showed that a synchronization of the firing pattern is possible up to the order of millimeters ahead of the SD wave. The peculiarity of this activity is that it is resistant to synaptic transmission blockade. This led to the hypothesis of direct neuron-to-neuron communication by previously closed gap junctions. They suggested that SD propagates through transcellular pathways using a reaction-diffusion mechanism. Computer simulations of Shapiro support this scheme [16]. A complete description of SD, however, must additionally include the full network connectivity of synaptic transmission when SD occurs close to a bifurcation. Such a description of SD is beyond the scope of the present study. The time and space scales of these dynamics differ by several orders of magnitude such that a separate treatment is justified. Therefore we investigate the stability of the suggested neuron-to-neuron communication by gap junctions separately. We assume that the way this transcellular pathway interacts with synaptic transmission is in principle described in the previous section.

5. Time-delayed diffusive electrical coupling

In a previous study [32] we used the FHN system modeling two individual neurons with a diffusive coupling in the activator variable. We showed that two FHN-neurons, each oscillating under its own source of noise, can synchronize. The application of time-delayed feedback to only one of two subsystems was shown to change coherence and time scales globally. Time delayed feedback is also able to induce stochastic synchronization under certain conditions. This motivates the approach pursued here to examine a time-delayed coupling between two identical neurons. Since the time-delay can introduce rich dynamics we study the case without random fluctuations.

To distinguish this system of two neurons from the spatially extended FHN reaction diffusion system describing the cortical tissue in Eqs. (1-2), we use the variables x and y with a subscript 1 and 2 identifying the two neurons. The variables represent the membrane potential and the gating, respectively.

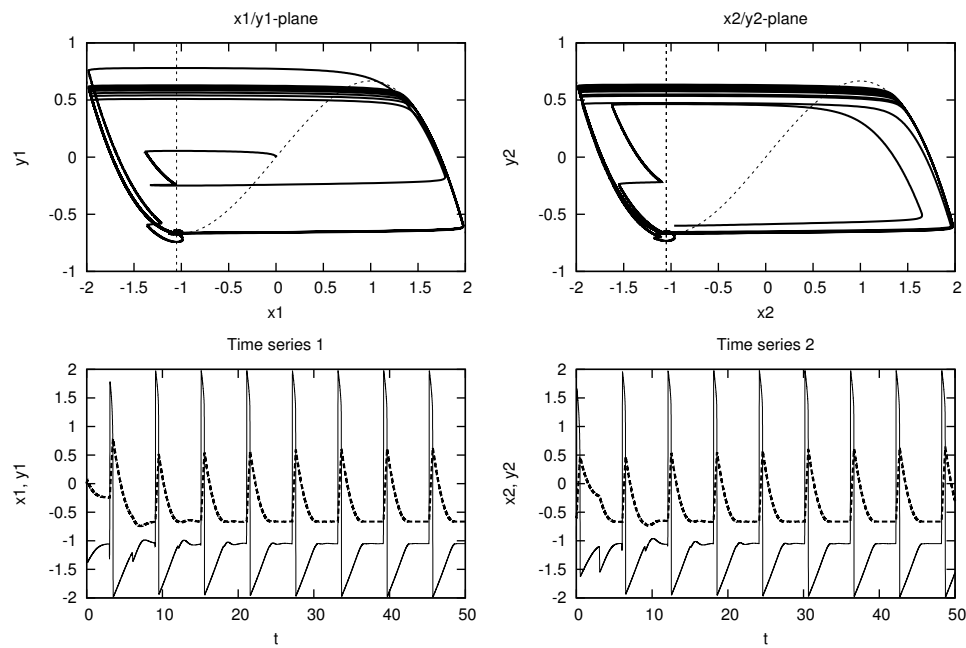


Figure 5: Simulation for two symmetrically coupled identical FHN-subsystems. Parameter values are $\epsilon = 0.01$, $a = 1.05$, $\tau = 3$, $C = 0.4$. Shown are phase space sections corresponding to the individual subsystems and their associated time series. After a short transient effect the combined system settles into a stable firing oscillation. The initial history functions used for this simulation are solutions to the uncoupled subsystems.

The diffusive coupling occurs in the membrane potential. This is a discrete model of a gap junction-mediated electrical coupling, because ionic currents through gap-junctions give rise to strong electrical coupling of the neurons. Gating mechanisms of neuronal gap junctions have not been described as yet. Therefore, we do not consider any gating. But we include a time delay τ because if the spread in the transcellular pathway is diffusion limited, as the slow propagation speed of SD clearly suggests, the transmission time can be in the order of the excitation cycle.

$$\begin{aligned} \frac{\partial x_1}{\partial t} &= x_1 - \frac{1}{3}x_1^3 - y_1 + C(x_2(t - \tau) - x_1) \\ \frac{\partial y_1}{\partial t} &= \epsilon(x_1 + a) \\ \frac{\partial x_2}{\partial t} &= x_2 - \frac{1}{3}x_2^3 - y_2 + C(x_1(t - \tau) - x_2) \\ \frac{\partial y_2}{\partial t} &= \epsilon(x_2 + a) \end{aligned}$$

Individual neurons have only one stable fixed point (for $a > 1$). It is readily shown that when $\tau = 0$, the coupled system also has only one stable fixed point. With a non-vanishing delay time the phase space is infinite dimensional. Then, the fixed point is given by the four coordinates above as well as their respective history functions of length τ , which need to be constant. Along the lines of [33], it can be shown that this fixed point is stable. We find that for adequate parameter values C , ϵ and τ , the system is multi-stable. It can avoid the stable fixed point and instead exhibit a mutual resonance phenomenon. In the 4D phase space section at time t , this results in a stable firing oscillation of period 2τ between the two sub-systems (see Fig.5). Thus, for two FHN-Neurons in the excitable regime, a non-vanishing delay enables a synchronous operation of the two subsystems.

6. Discussion

We showed that certain control schemes of an inhibitor-activator type system shift the emergence of wave propagation towards higher values of excitability. The control we investigated is of the form of a nonlocal coupling given in Eq. (3). This nonlocal transaction was added to the reaction-diffusion mechanism either in the inhibitor or the activator balance equation. The sum of all individual cross coupling terms that achieve a clinically desirable control goal takes the shape of an upright or inverted Mexican hat, respectively. This supports our assumption that the nonlocal coupling results from intrinsic lateral cortical connections.

Dichotomic lateral interaction is an architecture widely used in models of topographic feature maps. The prototypical example of such maps is the orientation preference in primary visual cortex, which is activated by the SD wave. The link between SD and the neuronal network architecture is still missing. One possibility is that gap-junction-mediated oscillatory patterns trigger SD. If so, these oscillatory patterns are likely to be modulated by lateral synaptic connections, although their existence is in general resistant to synaptic transmission blockade [20]. However, when SD is close to the bifurcation of the onset of wave propagation, as suggested by the spatio-temporal patterns (e.g. in Fig. 1), therapy might target network connectivity as to prevent spread.

Although we are still far from modeling the full mechanism of migraine with aura, neural network models have become sophisticated enough to constrain and validate possible underlying cortical circuitry of involved subsystems. To understand the origin of the gap-junction-mediated oscillatory patterns better, we performed simulations in a system of two gap-junction-coupled neurons. We showed that a time-delay is sufficient to produce sustained oscillations in an otherwise merely excitable ensemble. Thus, opening gap junctions between neurons, which are closed in a healthy state, can explain a localized pathological synchrony in the cortex when there exists a time delay.

To summarize, in modeling migraine a major objective is to understand cortical susceptibility to focal neurological symptoms in terms of neural circuitry [10, 21, 5]. This could open up to us new strategies for therapy using methods of controlling complex dynamics. Control of complex dynamics has evolved during the last decade as one of the central issues in applied nonlinear science [34]. Progress toward clinical implementation of nonlinear methods has been done so far in neurology in particular in Parkinson's disease, a neurological disease also characterized by pathological brain synchrony. There, techniques based on control of complex dynamics [35] are now tested in clinical studies and fundamentally novel therapy methods are being evolved [36]. It is hoped that this success can be expanded.

Acknowledgments

This work has been partially supported by the DFG within the framework of Sfb 555 and the Sachbeihilfe DA-602/1-1.

References

- [1] M. Lauritzen: *Pathophysiology of the migraine aura. the spreading depression theory [see comments]*, *Brain* **117**, 199 (1994).

- [2] A. J. Strong: *Dr. Bernice Grafstein's paper on the mechanism of spreading depression*, J Neurophysiol **94**, 5 (2005).
- [3] O. Herreras: *Electrical prodromals of spreading depression void Grafstein's potassium hypothesis*, J Neurophysiol **94**, 3656 (2005).
- [4] B. Hess: *Periodic patterns in biology*, Naturwissenschaften **87**, 199 (2000).
- [5] J. A. Reggia and D. Montgomery: *Modeling cortical spreading depression*, Proc. Annu. Symp. Comput. Appl. Med. Care pp. 873–877 (1994).
- [6] M. A. Dahlem and S. C. Müller: *Migraine aura dynamics after reverse retinotopic mapping of weak excitation waves in the primary visual cortex*, Biol Cybern **88**, 419 (2003).
- [7] M. A. Dahlem and S. C. Müller: *Reaction-diffusion waves in neuronal tissue and the window of cortical excitability*, Ann. Phys. **13**, 442 (2004).
- [8] K. M. Welch, G. D'Andrea, N. Tepley, G. Barkley, and N. M. Ramadan: *The concept of migraine as a state of central neuronal hyperexcitability*, Neurol Clin **8**, 817 (1990).
- [9] A. J. Shepherd: *Increased visual after-effects following pattern adaptation in migraine: a lack of intracortical excitation?*, Brain **124**, 2310 (2001).
- [10] M. A. Dahlem, F. M. Schneider, and E. Schöll: *Efficient control of transient wave forms to prevent spreading depolarizations*, submitted to J. Theo. Biol. (2007).
- [11] K. Lashley: *Patterns of cerebral integration indicated by scotomas of migraine*, Arch. Neurol. Psychiatry **46**, 331 (1941).
- [12] V. Hakim and A. Karma: *Theory of spiral wave dynamics in weakly excitable media: asymptotic reduction to a kinematic model and applications*, Phys. Rev. E **60**, 5073 (1999).
- [13] H. C. Tuckwell and M. R. M.: *A mathematical model for spreading cortical depression*, Biophysical J. **23**, 257 (1978).
- [14] H. Kager, W. J. Wadman, and G. G. Somjen: *Simulated seizures and spreading depression in a neuron model incorporating interstitial space and ion concentrations*, J. Neurophysiol. **84**, 495 (2000).
- [15] G. G. Somjen: *Mechanisms of spreading depression and hypoxic spreading depression-like depolarization*, Physiol. Rev. **81**, 1065 (2001).

- [16] B. E. Shapiro: *Osmotic forces and gap junctions in spreading depression: a computational model*, J. Comput. Neurosci. **10**, 99 (2001).
- [17] B. Grafstein: *Neural release of potassium during spreading depression.*, in *Brain Function. Cortical Excitability and Steady Potentials.*, edited by M. A. B. Brazier (University of California Press, Berkeley, 1963), pp. 87–124.
- [18] J. Bureš, O. Burešová, and J. Krivánek: *The mechanism and applications of Leão's Spreading Depression* (Academia, New York, 1974).
- [19] C. Nicholson and J. M. Phillips: *Ion diffusion modified by tortuosity and volume fraction in the extracellular microenvironment of the rat cerebellum*, J Physiol **321**, 225 (1981).
- [20] O. Herreras, C. Largo, J. M. Ibarz, G. G. Somjen, and R. Martín del Río: *Role of neuronal synchronizing mechanisms in the propagation of spreading depression in the in vivo hippocampus*, J Neurosci **14**, 7087 (1994).
- [21] L. H. A. Monteiro, D. C. Paiva, and J. R. C. Piqueira: *Spreading depression in mainly locally connected cellular automaton*, J. of Biol. Systems **14**, 617 (2006).
- [22] R. FitzHugh: *Impulses and physiological states in theoretical models of nerve membrane*, Biophys. J. **1**, 445 (1961).
- [23] J. Nagumo, S. Arimoto, and S. Yoshizawa.: *An active pulse transmission line simulating nerve axon.*, Proc. IRE **50**, 2061 (1962).
- [24] M. A. Dahlem and S. C. Müller: *Self-induced splitting of spiral-shaped spreading depression waves in chicken retina*, Exp. Brain Res. **115**, 319 (1997).
- [25] C. D. Gilbert and T. N. Wiesel: *Columnar specificity of intrinsic horizontal and corticocortical connections in cat visual cortex*, J Neurosci **9**, 2432 (1989).
- [26] Y. A. Kuznetsov: *Elements of Applied Bifurcation Theory* (Springer, New York, 1995).
- [27] N. Hadjikhani, M. Sanchez Del. Rio., O. Wu, D. Schwartz, D. Bakker, B. Fischl, K. K. Kwong, F. M. Cutrer, B. R. Rosen, R. B. Tootell, A. G. Sorensen, and M. A. Moskowitz: *Mechanisms of migraine aura revealed by functional MRI in human visual cortex*, Proc. Natl. Acad. Sci. USA **98**, 4687 (2001).

- [28] A. S. Mikhailov and K. Showalter: *Control of waves, patterns and turbulence in chemical systems*, Phys. Rep. **425**, 79 (2006).
- [29] M. A. Dahlem and E. P. Chronicle: *A computational perspective on migraine aura*, Prog. Neurobiol. **74**, 351 (2004).
- [30] E. L. Schwartz: *A quantitative model of the functional architecture of human striate cortex with application to visual illusion and cortical texture analysis*, Biol Cybern **37**, 63 (1980).
- [31] M. A. Dahlem, R. Engelmann, S. Löwel, and S. C. Müller: *Does the migraine aura reflect cortical organization*, Eur J Neurosci **12**, 767 (2000).
- [32] B. Hauschildt, N. B. Janson, A. G. Balanov, and E. Schöll: *Noise-induced cooperative dynamics and its control in coupled neuron models*, Phys. Rev. E **74**, 051906 (2006).
- [33] N. B. Janson, A. G. Balanov, and E. Schöll: *Delayed feedback as a means of control of noise-induced motion*, Phys. Rev. Lett. **93**, 010601 (2004).
- [34] E. Schöll and H. G. Schuster (Editors): *Handbook of Chaos Control* (Wiley-VCH, Weinheim, 2007).
- [35] P. A. Tass, J. Klosterkötter, F. Schneider, D. Lenartz, A. Koulousakis, and V. Sturm: *Obsessive-compulsive disorder: development of demand-controlled deep brain stimulation with methods from stochastic phase resetting*, Neuropsychopharmacology **28 Suppl 1**, 27 (2003).
- [36] C. Hauptmann and P. A. Tass: *Therapeutic rewiring by means of desynchronizing brain stimulation*, Biosystems **89**, 173 (2007).

Dynamical and spectral properties of complex networks

Albert Díaz-Guilera¹

¹*Departament de Física Fonamental, Universitat de Barcelona*

Abstract

We will review some results about the relation between dynamical and spectral properties of complex networks. From the dynamical point of view we will focus on the time the whole population needs to be completely synchronized and how partial synchronization of more tightly connected clusters (communities or modules) appears. This properties can be related with the eigenvalues of the the Laplacian matrix of the network.

Keywords: networks, synchronization
MSC 2000: AMS codes

In 1998 Watts and Strogatz presented a simple model of network's structure that was the seed of the modern theory of complex networks [1]. Beginning with a regular lattice, they showed that the addition of a small number of random links reduces the diameter drastically. This effect, know has small-world effect, was already detected in natural and artificial networks. The research was in part originally inspired by Watts' efforts to understand the synchronization of cricket chirps, which show a high degree of coordination over long distances as though the insects where "invisibly" connected. Since then complex networks are being subject of attention of the physicists' community [2, 3, 4, 5].

Complex networks are found in fields as diverse as the Internet, the World-Wide-Web, food-webs, and many forms of biological and social organizations (see [6] and references therein). The description of these networks, as it occurs in many physical systems, can be performed at different scales. The lower level of description, the "microscale", is represented by single nodes. From the static point of view the key point is to determine certain properties of

emails: `albert.diaz@ub.edu`

individual nodes (degree, centrality, clustering, etc.), while from the dynamics perspective the goal is to know about the dynamical process each node is performing. This level of description is unfortunately very precise and does not allow a generic analysis of the global properties of the system. At the other extreme, we have the higher level of description, the “macroscale”, represented by the statistical properties of the network as a whole. This description has been the realm of statistical physics in complex networks and has provided great insight in the universality of certain features of many real world systems.

In the middle of these descriptions still remains a huge space for different scales of descriptions that we like to name as “mesoscales”, or intermediate scales. These scales are understood as substructures (eventually subgraphs) that have topological entity compared to the whole network, e.g. motifs [7, 8], cliques [9], cores [10], loops [11] or, generally speaking, communities [12, 13]. In particular, the community detection problem concerning the determination of mesoscopic structures that have functional, relational or even social entity is still controversial, starting from the “a priori” definition of what a community is [14]. The correct determination of the mesoscale in complex networks is a major challenge. Under the name of the community detection problem, consisting in finding a ‘good’ partition of the network in sub-graphs that represent communities according to a given definition, physicists have provided different methods that confront this challenge[15]. However, in many complex networks the organization of nodes is not completely represented by a unique partition but by a set of nested communities that appear at different topological scales. This evidence comes from indirect experimental data revealing functionalities in complex networks that involve different subsets of nodes at different hierarchical levels [16, 17].

In a completely different scenario, physicists have largely studied the dynamics of complex biological systems, and in particular the paradigmatic analysis of large populations of coupled oscillators [18, 19, 20]. The connection between the study of synchronization processes and complex networks is interesting by itself. Indeed, the original inspiration of Watts and Strogatz in the development of the Small-World network structure was, as mentioned before, to understand the synchronization of cricket chirps. This synchronization phenomena as many others e.g. asian fireflies flashing at unison, pacemaker cells in the heart oscillating in harmony, etc. have been mainly described under the mean field hypothesis that assumes that all oscillators behave identically and interact with the rest of the population. Recently, the emergence of synchronization phenomena in complex networks has been shown to be closely related to the underlying topology of interactions [21] beyond the macroscopic description.

In this talk we review some of the results concerning the dynamics towards synchronization of phase oscillators in complex networks at the mesoscale description [22, 23, 24, 25].

Acknowledgments

This work has been supported by DGES of the Spanish Government Grants No. BFM-2003-08258 and FIS2006-13321.

References

- [1] D. J. Watts, S. H. Strogatz, *Nature* **393**, 440 (1998).
- [2] S. Strogatz, *Nature* **410**, 268 (2001).
- [3] R. Albert and A.-L. Barabasi, *Rev. Mod. Phys.* **74**, 47 (2002).
- [4] M. E. J. Newman, *SIAM Review* **45**, 167 (2003).
- [5] S. Boccaletti, V. Latora, Y. Moreno, M. Chavez, and D.-U. Hwang, *Phys. Rep.* **424**, 175 (2006).
- [6] M. Buchanan, *Nexus* (W.W. Norton NewYork - London, 2002).
- [7] R. Milo, S. Shen-Orr, S. Itzkovitz, N. Kashtan, D. Chklovskii and U. Alon, *Science* **298**, 824 (2002).
- [8] N. Kashtan and U. Alon, *PNAS* **102**, 13773 (2005).
- [9] G. Palla, I. Derenyi, I. Farkas and V. Tamas, *Nature* **435**, 814 (2005)
- [10] S. Wuchty and E. Almaas, *BMC Evol. Biol.* **5**, 24 (2005).
- [11] G. Bianconi and A. Capocci, *Phys. Rev. Lett.* **90**, 078701 (2003)
- [12] M. E. J. Newman, *Eur. Phys. J. B* **38**, 321 (2004).
- [13] L. Danon, A. Diaz-Guilera, J. Duch, and A. Arenas, in *Large Scale Structure and Dynamics of Complex Networks: From Information Technology to Finance and Natural Science*, ed. By G. Caldarelli and A. Vespignani, World Scientific, Singapore, 2007.
- [14] F. Radicchi, C. Castellano, F. Cecconi, V. Loreto, and D. Parisi, *PNAS* **10**, 2658 (2004).

- [15] L. Danon, A. Diaz-Guilera, J. Duch, and A. Arenas, J. Stat. Mech. P09008 (2005).
- [16] E. Ravasz, A. L. Somera, D. A. Mongru, Z. N. Oltvai, A.-L. Barabasi, Science **297**, 1551 (2002).
- [17] A. W. Rives and T. Galitski, PNAS **100**, 1128 (2003).
- [18] A. T. Winfree, *The geometry of biological time* (2nd ed. Springer-Verlag, 2001).
- [19] S. H. Strogatz, *Sync: The Emerging Science of Spontaneous Order* (New York: Hyperion, 2003).
- [20] Y. Kuramoto, *Chemical oscillations, waves, and turbulence* (2nd ed. Mineola NY, Dover Publications, 2003).
- [21] F. M. Atay, T. Biyikoglu, and J. Jost. IEEE Trans. Circuits and Systems **53**, 92 (2006).
- [22] A. Arenas, A. Diaz-Guilera and C.J. Perez-Vicente, Phys. Rev. Lett. **96**, 114102, (2006).
- [23] A. Arenas, A. Diaz-Guilera and C.J. Perez-Vicente, Physica D **224**, 27h, (2006).
- [24] A. Arenas and A. Diaz-Guilera, Euro. Phys. J ST **143**, 19 (2007).
- [25] J.A. Almendral and A. Díaz-Guilera, New J. Phys. **9**, 187, (2007).

Topology Induced Instabilities in Neural Nets with Activity-Dependent Synapses

S. Johnson¹, J. Marro¹ and J.J. Torres¹

¹*Department of Electromagnetism and Physics of Matter, and Carlos I Institute
for Theoretical and Computational Physics, University of Granada, Spain.*

Abstract

We study the effect of topology in an attractor neural network in which a noise parameter meant to mimic synaptic depression causes instabilities of the memory patterns leading to complex behaviour, including the possibility of chaos. Investigation of the system shows that three distinct phases can emerge: a ferromagnetic (memory) phase, a phase of chaotic hopping among the attractors, and a phase of periodic pattern-antipattern switching. In a mean-field approach and for a single pattern, the dynamics of the network is well approximated by a two-dimensional discrete map in which the exponent of the power-law degree distribution is a relevant parameter. Analysis of this map reveals that there is an optimal exponent, around 2, which minimises the amount of depression needed to destabilise the memories. Our study shows that there are particular topologies that are most convenient for storage and retrieval of memories, whereas others allow for a better performance in tasks such as pattern recognition and class identification and categorisation. We go on to suggest a mechanism by which a network could switch from stable to unstable behaviour by means only of a slight rewiring. Monte Carlo simulations agree both qualitatively and quantitatively with mean-field results.

Keywords: Topology, scale-free, synaptic depression, dynamic synapses, chaos

MSC 2000: AMS codes

1. Introduction

It is widely believed that synapses are responsible for information storage in the animal brain [1]. Neural network models can be constructed in which nodes represent neurons and links play the role of synapses [2]. A set of patterns can then be stored by allocating synaptic weights according to the Hebb rule [3]. In this way, the phase space of network dynamics acquires attractors which coincide with the patterns stored, thereby conferring to the system a mechanism for retrieval known as *associative memory*. However, it is clear that a real neural system must be capable of much more if it is to do anything except recall the same memory pattern forever: some destabilising mechanism must exist. In fact, certain experimental evidence suggests that chaotic activity may be necessary for some high level brain tasks [4,5]. In relation to this, there has recently been much interest in so-called *dynamic synapses* [9,10,11], fluctuations of the synaptic weights that occur on time scales of milliseconds - as opposed to the time scale of static learning that can be of anything from minutes to years [1]. Biologically, these fluctuations fall into two categories: synaptic depression (a decrease in conductance due to a depletion in available neurotransmitters) and synaptic facilitation (increased conductance thanks to residual calcium within the membrane) [12,13]. Both are thought to appear as a result of a high frequency of spikes arriving at the presynaptic neuron ¹. In this study we extend a general dynamic synapse model that has been shown to exhibit chaotic (dynamic memory) as well as ferromagnetic (static memory) behaviour to the case of networks endowed with a topology [6,7,8]. To the best of our knowledge, this is the first work to investigate the effect of topology on this type of neural automata, and we have found that the nature of the behaviour exhibited does indeed depend strongly on the precise wiring of the network.

2. The model

We consider a set of N binary neurons with possible states $s_i = \{-1, +1\}$ situated at the nodes of a network [2,14]. This network has a topology given by the adjacency matrix $\epsilon_{ij} = \{1, 0\}$, signifying the existence or inexistence of a link that represents synaptic interaction. A set of M patterns $\xi_i^\nu = \{-1, +1\}$ (which we will generate randomly) can be stored by giving each link a *synaptic weight* ω_{ij} according to the Hebb rule [3]: $\bar{\omega}_{ij} = M^{-1} \sum_{\nu=1}^M \xi_i^\nu \xi_j^\nu$ and consider

¹Most neurons will of course be simultaneously both pre- and postsynaptic, but we will use these terms in reference to the particular synapse whose fluctuations are being considered at the time.

the synaptic weights ω_{ij} as the result of $\bar{\omega}_{ij}$ being altered by fast presynaptic noise in the form of the stochastic variable x_j , $\omega_{ij} = \bar{\omega}_{ij}x_j$. At the limit where the time scale of x_j is infinitely smaller than that of neuron dynamics, we will take it to follow a bimodal distribution

$$P(x_j|S) \equiv q\delta(x_j - \bar{\Phi}_j) + (1 - q)\delta(x_j - 1), \quad (1)$$

implying that at each time step every synapse has a probability q of altering its weight by a factor $\bar{\Phi}_j$, where $\bar{\Phi}_j$ is a function of the local network activity to be determined. This distribution differs from the one used in references [6,7,8] in that they consider an activity-dependent probability ($q = q(m)$) and a fixed depression factor ($\bar{\Phi}_j = \Phi = \text{constant}$). The fact that, as we shall see, for appropriate choices of parameters the same *effective local fields* - and therefore the same behaviour - can be obtained from either model suggests a greater generality of the bimodal noise distribution than might be expected. The main extension made in this study is to consider a dependency on *local* activity since we wish to apply the model to systems with topologies other than that of the fully-connected network.

We assume the factorisation $P^{st}(X|S) = \prod_j P(x_j|S)$ and express the transition rate for postsynaptic neuron i in terms of an effective local field $h_i^{eff}(S)$ (see [15] for details). Effective synaptic weights ω_{ij}^{eff} such that $h_i^{eff}(S) = \sum_j \omega_{ij}^{eff} s_j \epsilon_{ij}$ can then be obtained analytically:

$$\omega_{ij}^{eff} = [1 + q(\bar{\Phi}_j - 1)]\bar{\omega}_{ij}. \quad (2)$$

These effective synaptic weights can be used for numerical simulations for a given function $\bar{\Phi}_j$. In this study we will consider only parallel updating, though the model could perhaps be extended to sequential updating, or anything in between.

As well as the standard macroscopic overlap vector $\vec{m} = (m^1, \dots, m^M)$, where $m^\nu \equiv N^{-1} \sum_i \xi_i^\nu s_i$, which tells us which attractor (if any) the system finds itself in at a given time, we can define an analogous local overlap for each pattern as $m_j^\nu \equiv N^{-1} \sum_l \xi_l^\nu s_l \epsilon_{jl}$. Through these we define the function

$$\zeta(\vec{m}_j) \equiv \frac{\kappa}{1 + \alpha} \sum_\nu (m_j^\nu)^2, \quad (3)$$

where $\alpha \equiv M/N$ is the load parameter and κ is a constant that we will set at $\kappa = (N/\langle k \rangle)^2$ so as to make $\zeta(\vec{m}_j) \simeq |\vec{m}|$ for a ‘‘typical’’ presynaptic neuron j of average degree $k_j \simeq \langle k \rangle$. This function $\zeta_j = \zeta(\vec{m}_j)$ (or in fact

any other monotonously increasing function of m_j^{\prime}) can be seen as a measure of the electrical activity felt by neuron j . Since we would like $\bar{\Phi}_j$ to depend on the current arriving at presynaptic neuron j , a possible definition is $\bar{\Phi}_j \equiv 1 + q_0^{-1} \zeta(\bar{m}_j)(\Phi - 1)$. In this way we can recover the behaviour observed in [6,7,8] at the fully-connected network limit for any choice of $q = q_0$. We will set $q_0 = 1/2$ for the sake of comparison ². The parameter Φ is proportional to the extent of synaptic variation, its sign signifying either of the two regimes: *facilitation* if $\Phi > 1$ or *depression* if $\Phi < 1$. Simulations are carried out by inserting (3) into (2) for the synaptic weights and simply computing ζ_j for each neuron at every MCS.

3. Mean field

Particularising for a single pattern ($M=1$) the effective local fields reduce to

$$h_i^{eff} = \frac{1}{N} \sum_j [1 + (\Phi - 1)m_j^2] \xi_i \xi_j s_j \epsilon_{ij}. \quad (4)$$

Defining $\eta_i \equiv \xi_i s_i$, we have $m_j = \langle \eta_i \epsilon_{ij} \rangle_i$. Because previous studies [16] have shown that, in general, $\langle k\eta \rangle \neq \langle k \rangle \langle \eta \rangle$, we define a new set of overlap parameters, $\mu_n \equiv \langle k_i^n \eta_i \rangle_i / \langle k^n \rangle$ (note that $\mu_0 = m$), and their associated local versions $\mu_{n,j} \equiv \langle k_i^n \eta_i \epsilon_{ij} \rangle_i / \langle k^n \rangle$.

We also need the mean value (a quenched average over realisations of the network) of the adjacency matrix ϵ_{ij} . For this we will imagine that each neuron i has been allocated k_i *half-links* according to some distribution $p(k)$, the total number of half-links in the net being $\langle k \rangle N$. We now proceed to chose a neuron at random and join one of its half links to one belonging to another random neuron ³. The probability of choosing one of a given neuron j 's half-links is $k_j / (\langle k \rangle N)$. After as many realisations as are necessary to link up all the neurons, the expected value of the number of links joining neurons i and j will be $k_i k_j / (\langle k \rangle N)$. If we impose the restriction that there can be at most one link between any two neurons ($\epsilon_{ij} = \{0, 1\}$), then the value will be slightly smaller. However, it is easy to prove that this value is a good approximation

²i.e., the results obtained in the references will coincide with those yielded by our model if we take $q = 1/2$ in the noise distribution (1).

³Although it is well known that the degree distribution of a network does not determine all its statistical properties, this kind of algorithm is probably the most general way of generating a topology with a given $p(k)$, and is indeed the mechanism used here.

in this case also, at least if $k_i, k_j \ll N$, and so we will use ⁴

$$[\epsilon_{ij}] = \frac{k_i k_j}{\langle k \rangle N}. \quad (5)$$

The value given in (5), which is general for any graph, coincides - for a power-law distribution with $\gamma = 3$ - with the one obtained by G. Bianconi for a Barabási-Albert evolving network [17,18].

Standard mean-field analysis (see [15] for details) yields

$$\mu_{n(t+1)} = \frac{1}{\langle k^n \rangle} \sum_k p(k) k^n \tanh \left\{ \frac{k}{TN} \left[\mu_{1(t)} + (\Phi - 1) \frac{\langle k^3 \rangle}{N^2 \langle k \rangle} \mu_{1(t)}^2 \mu_{3(t)} \right] \right\}, \quad (6)$$

which, applied recursively to μ_1 and μ_3 , constitutes a two-dimensional map, valid in principle for any topology with a known distribution $p(k)$. Although it is not a variable of the map's dynamics, we can also use (6) to calculate $\mu_0 = m$, which is after all the macroscopic magnitude of interest. At the thermodynamic limit ($N \rightarrow \infty$), the sum over degrees becomes an integral, which can be solved analytically only for certain distributions $p(k)$.

4. Criticality

Near the critical temperature we expect stable solutions $\mu_n \neq 0$ such that $\mu_{n(t+1)} = \mu_{n(t)}$ to occur (for any n). Since $\mu_{n(T \simeq T_c)} \simeq 0$, we can expand the hyperbolic tangent in (6) around the origin and keep only terms up to order three. If we also make the approximation $\mu_3 \simeq \mu_1$, then we have

$$\mu_{1(T \simeq T_c)} = \frac{1}{\sqrt{T_c \theta_3}} \left[\frac{T_c - T}{\Phi_c - \Phi} \right]^{\frac{1}{2}}, \quad (7)$$

where $\theta_n \equiv \frac{\langle k^n \rangle}{\langle k \rangle N^{n-1}}$, $\Phi_c = \frac{\theta_4}{3\theta_3 \theta_2 T^2}$, and the critical temperature ⁵ is

$$T_c = \theta_2 = \frac{\langle k^2 \rangle}{\langle k \rangle N}. \quad (8)$$

Equation (7) tells us that even if $T \geq T_c$ the behaviour of the overlap will become ferromagnetic at $\Phi = \Phi_c > 0$ due to the high degree of facilitation.

⁴It is interesting, however, that in the case of more than one link permitted, which may in fact be biologically more realistic, the result is exact.

⁵This expression for the critical temperature, which is general in our mean-field approximation for any topology given by the adjacency matrix ϵ_{ij} , means that we can define a matrix $\tau_{ij} \equiv k_i k_j / (\langle k \rangle N)$ such that $[\epsilon_{ij}] = \tau_{ij}$ and $T_c = \text{Tr}(\tau_{ij}) N^{-1}$.

However, more interesting to us is the value of Φ at which the overlap becomes unstable. Proceeding as before but setting the condition $\mu_{n(t+1)} = -\mu_{n(t)}$, we find that (at high temperatures) we will have bistability (periodic hopping) if $\Phi > \Phi_{bi}$, where

$$\Phi_{bi} = \Phi_c - \frac{1}{\theta_3} \left(1 + \frac{T}{T_c} \right). \quad (9)$$

At low temperatures, simulations show the existence of three distinct phases: ferromagnetic, chaotic and periodic, depending on the noise parameter. The value of Φ at which the behaviour of m becomes chaotic, Φ_{chaos} , cannot be calculated analytically since this only occurs at relatively low temperatures, which undermines our expansion of the hyperbolic tangent. However, it is possible to study the stability of the single-pattern system for a given topology by analysing the Lyapunov exponents associated with (6). This is contrasted with results obtained from Monte Carlo simulations for different scale-free topologies in Fig.2.

5. Scale-free networks

Up until now, everything that has been said is general for any topology following a distribution $p(k)$, the equations only requiring various moments of k . Motivated by many recent findings relating to the emergence in nature of scale-free networks [18,19,20] and the interesting properties these topologies exhibit [21], we will now concentrate on distributions of this type, such that

$$p(k) \sim k^{-\gamma}. \quad (10)$$

As their name indicates, these distributions do not have a characteristic size, the probability being spread in theory over all values of k . However, since in a real network values of k can only take whole numbers, we will assume the limits to be given by k_o and $k_m \leq (k_o N^{\frac{1}{\gamma-1}}, N)$. Much of the analysis done on scale-free networks tends to set $\gamma = 3$, the exponent that arises naturally in a Barabási-Albert evolving network [18]. Nevertheless - and as these authors point out - in nature we find networks with values of γ ranging at least from slightly larger than 1 to more than 4, depending probably on the precise mechanism involved in their realisation. For this reason, we make γ a control parameter and study its influence on the behaviour of nets with given mean degree $\langle k \rangle$ and number of neurons N (this imposition, together with normalisation of $p(k)$, is enough to define the limits k_o and k_m).

In Fig.1 we see the critical temperature plotted against the exponent γ for different fixed mean degrees as given by equation (8). High values of γ result in a distribution $p(k) \simeq \delta(\langle k \rangle)$, and so $T_c \rightarrow \langle k \rangle / N$. At γ slightly larger than 2, the tail of the distribution is truncated by the net size (hubs with $k = N - 1$ will exist) and the slope of T_c becomes suddenly smaller. Then there comes a point for even lower exponents at which no neuron can have a degree larger than a certain $k_{max} < N$ without resulting in a higher $\langle k \rangle$ than is imposed, and so T_c drops. This relation between the critical temperature and the maximum degree allowed agrees qualitatively with one of the main results reported in [16] - namely, that hubs continue to store information even at relatively high temperatures.

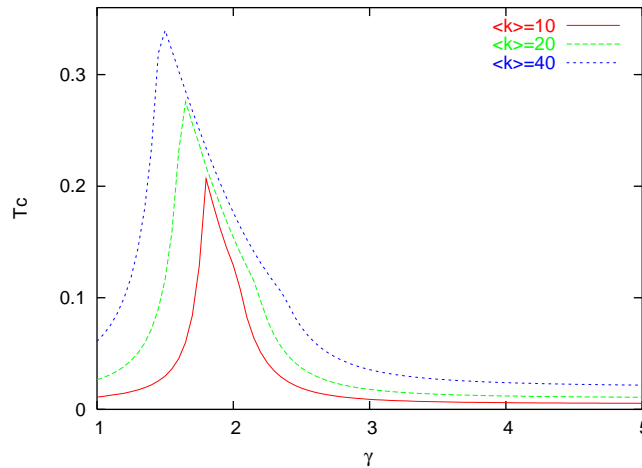


Figure 1:

Critical temperature against exponent γ for different mean degrees ($N=1600$) as given by (8).

Φ_{chaos} is also found to depend strongly on the slope of the degree distribution. Fig.2. shows this critical value plotted against γ as obtained from Monte Carlos simulations and from mean-field analysis. There is good agreement for all but very low values of γ - which may be due to the fact that, as mentioned above, the mean adjacency matrix (5) used is in fact for a net in which multiple connections are allowed, an effect that we would expect to be most noticeable in nets containing hubs with $k \rightarrow N$; indeed, these might well then tend to destabilise the system at higher levels of Φ as the map predicts.

Most interesting is the existence of a plateau, around $\gamma \simeq 2$, at which very little depression ($\Phi \simeq 1$) is required to make the attractors unstable.

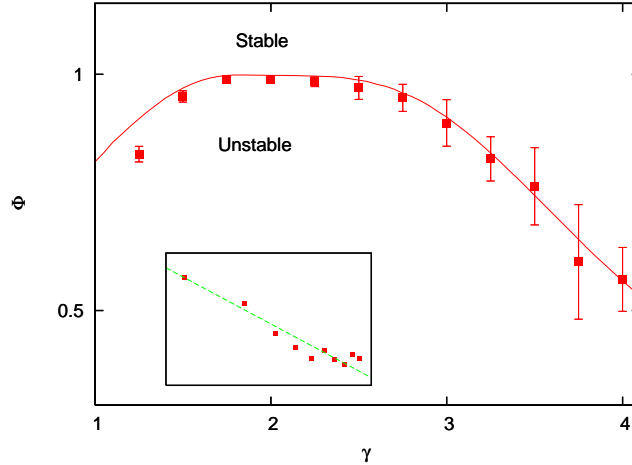


Figure 2:

Depression coefficient at which behaviour becomes chaotic, Φ_{chaos} , from map (lines) compared to MC simulations (bars). (Data correspond to averages over 10 nets, with $\langle k \rangle = 20$, $N = 1600$, $T = 1/800$). Inset shows standard deviation σ of Φ_{chaos} against net size for fixed $\langle k \rangle/N = 1/100$. As expected, $\sigma \sim 1/\sqrt{N}$ (dotted line). (Data obtained from MC simulations of 10 different realizations of the network for each N , with $\gamma = 3$ and iterated at $T = 1/800$.)

The map also allows us to plot bifurcation diagrams of the overlap m against the exponent γ . These are shown in Fig.3, along with associated Lyapunov exponents, for two different values of Φ . The top two panels correspond to very slight depression. This results in the opening of an unstable window, periodic in the middle and chaotic at the borders, around $\gamma \simeq 2$. (Note that the chaotic region on the left has a smaller amplitude in m than that on the right: this is presumably because T_c varies with γ while we are keeping T constant.) If we gradually reduce Φ , this window of instability widens, as well as the chaotic regions themselves, until the chaotic border on the left disappears from our diagram (it would occur at $\gamma < 1$). The two lower panels are for a higher value of depression, at which only much steeper degree distributions ($\gamma \uparrow$) present stable (ferromagnetic) behaviour.

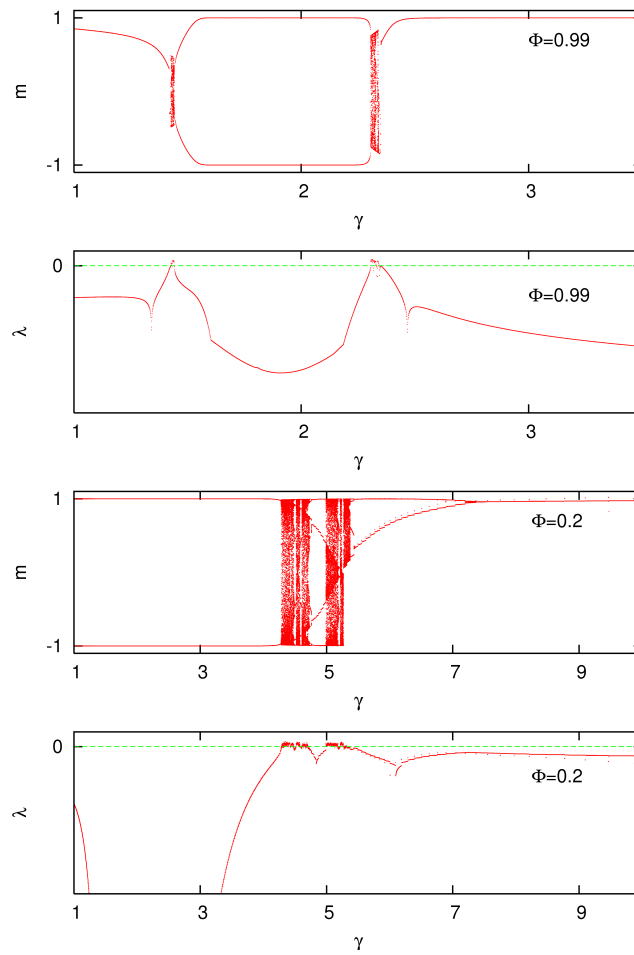


Figure 3:
Bifurcation diagrams and associated Lyapunov exponents for two different values of depression ($\langle k \rangle = 20$, $N = 1600$, $T = 1/800$)

6. Dynamic topologies

This sensitivity that network behaviour exhibits to topology can be illustrated with a simple *dynamic topology* model. The algorithm used generates an initial scale-free topology with an exponent γ_1 and a final (virtual) topology according to a given γ_2 such that it is the result of multiplying the degree of each node by an appropriate factor. Then, at each time step of the simulation, a given number of nodes, chosen with a probability proportional to $k_1 - k_2$, have one link removed, to be re-connected to another node chosen with probability $k_2 - k_1$. In this way the degree distribution goes smoothly from γ_1 to γ_2 without altering the total number of links (and so $\langle k \rangle$). (Because this implies varying k_o , the intervening stages are not all strictly-scale free, but do have distributions with long power-law tails.)

Fig.4. shows how the behaviour of a network which finds itself representing a given pattern (red) can, simply through small rewiring actions of the type described above, become unstable (chaotic phase) and end up representing a different - uncorrelated - pattern (green). In the final state, the phase is periodic hopping, which as we can see is another way of representing a given pattern - e.g. if this were, say, an image, it would be switching continuously between the recorded pattern and its negative.)

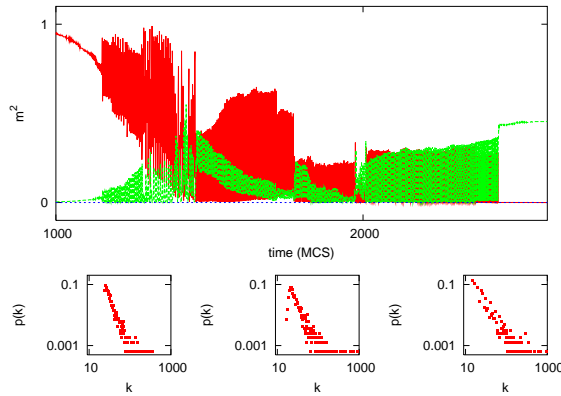


Figure 4:

Evolution from $\gamma_1 = 3$ to $\gamma_2 = 2$, with 10 links re-connected at each MCS ($\Phi = 0.98, \langle k \rangle = 40, N = 1600, TN = 0.001$).

7. Discussion

We have extended the dynamic synapse model of an attractor neural network presented and studied by Torres *et al.* [6,7,8] so as to take into account the local effects that are to be expected in a network with topology. Mean-field analysis, though only exact for the case of a fully connected network, proves nonetheless to be remarkably accurate at predicting certain critical phenomena even for nets with low mean degrees. Applying the model to scale-free networks reveals a strong dependency of the emergent complex behaviour on the exponent γ of the degree distribution. In particular, phase diagrams obtained both from mean-field analysis and Monte Carlo simulations show a plateau, around $\gamma \simeq 2$, at which the behaviour of the network becomes unstable for very slight depression. This may point to the existence of a topology that is optimal for certain dynamic memory tasks, such as pattern recognition and class identification and categorisation. As an example application we present a simple dynamic topology model in which a few synapses are rewired at each MCS without altering any other parameters, with the result that the network can pass suddenly from one type of behaviour (or phase) to another.

Acknowledgements

This work has been supported by the Junta de Andalucía project P06-FQM-01505.

References

- [1] R. C. MALENKA AND R. A. NICOLL, “Long-term potentiation - a decade of progress?”, *Science*, **285**(5435) (1999) 1870–1874.
- [2] J. J. HOPFIELD, “Neural networks and physical systems with emergent collective computational abilities”, *Proc. Natl. Acad. Sci. USA*, **79** (1982) 2554–2558.
- [3] D. O. HEBB, “The organization of behavior”, *Wiley, New York* (1949).
- [4] J. M. BARRIE, W. J. FREEMAN, AND M. LENHART, “MOdulation by discriminative training of spatial patterns of gamma EEG amplitude and phase in neocortex of rabbits”, *J. Neurophysiol.*, **76** (1996) 520–539.
- [5] H. KORN AND P. FAURE, “Is there chaos in the brain? ii. experimental evidence and related models”, *C. R. Biol.*, **326** (2003) 787–840.

- [6] J. J. TORRES, J. M. CORTÉS, AND J. MARRO, “Instability of attractors in auto-associative networks with bio-inspired fast synaptic noise”, *LNCS*, **3561** (2005) 161–167.
- [7] J. M. CORTÉS, J. J. TORRES, J. MARRO, P. L. GARRIDO, AND H. J. KAPPEN, “Effects of fast presynaptic noise in attractor neural networks”, *Neural Computation*, **18** (2006) 614–633.
- [8] J. MARRO, J. J. TORRES, AND J. M. CORTÉS, “Chaotic hopping between attractors in neural networks”, *Neural Networks*, **20(2)** (2007) 230–235.
- [9] L. F. ABBOTT, J. A. VARELA, K. SEN, AND S. B. NELSON, “Synaptic depression and cortical gain control”, *Science*, **275(5297)** (1997) 220–224.
- [10] L. PANTIC, J. J. TORRES, H. J. KAPPEN, AND S. C. A. M. GIELEN, “Associative memory with dynamic synapses”, *Neural Comp.*, **14(12)** (2002) 2903–2923.
- [11] D. HOLCMAN AND M. TSODYKYS, “The emergence of up and down states in cortical networks”, *PLoS Comput. Biol.* **2(S)**, **2(3)** (2006) 174–181.
- [12] J. J. TORRES, J. CORTÉS, J. MARRO, AND H. J. KAPPEN, “Competition between synaptic depression and facilitation in attractor neural networks”, *Neural Comp.* (2007) In press, q-bio.NC/0604019.
- [13] J. F. MEJÍAS AND J. J. TORRES, “The role of synaptic facilitation in spike coincidence detection”, *J. Comp. Neurosci.* (2007) In press.
- [14] L. F. ABBOTT AND T. B. KEPLER, “From Hodgkin-Huxley to Hopfield”, *Statistical mechanics of neural networks*, Springer-Verlag, Berlin (1990) 5–8.
- [15] S. JOHNSON, J. MARRO, AND J. J. TORRES, *To be published*.
- [16] J. J. TORRES, M. A. MUÑOZ, J. MARRO, AND P. L. GARRIDO, “Influence of topology on a neural network performance”, *Neurocomputing*, **58-60** (2004) 229–234.
- [17] G. BIANCONI, “Mean field solution of the Ising model on a Barabási-Albert network”, *Phys. Lett., A* **303** (2002) 116.
- [18] A.-L. BARABÁSI AND R. ALBERT, “Emergence of scaling in random networks”, *Science*, **286** (1999) 509–512.

- [19] V. M. EGUÍLUZ, D. R. CHIALVO, G. A. CECCHI, M. BALIKI, AND A. V. APKARIAN, “Scale-free brain functional networks”, *Physical Review Letters*, **95**, 018102 (2005).
- [20] L. DE ARCANGELIS, C. PERRONE-CAPANO, AND H. J. HERRMANN, “Self-organized criticality model for brain plasticity”, *Phys. Rev. Lett.*, **96**(2) (2006) 028107.
- [21] D. J. WATTS AND S. H. STROGATZ, “Collective dynamics of ‘small-world’ networks”, *Nature, London*, **395** (1998) 440–442.

Enhancing network synchronization by sparse repulsive couplings

I. Leyva¹, I. Sendina-Nadal¹ and J. A. Almendral¹

¹*Department of Physics, Universidad Rey Juan Carlos*

Abstract

In a small-world network of mainly attractively coupled non-identical neurons, we show that a small fraction of phase-repulsive couplings is able to strongly improve synchronization for certain values of link and repulsivity probabilities. By a spectral analysis we link the observed dynamical behaviour with the structural properties of the network.

Keywords: phase repulsive, synchronization

1. Introduction

One of the most important mechanisms for transmit and code information, in large oscillator ensembles is synchronization, specially in biological networks. Different experiments have pointed out this fact in the neural tissue, finding a relationship between the behaviour of the system and the net structure [1, 2].

The importance of the synchronous behaviour in real collectives has rise the question of how to optimize the network topology for synchronization. Several strategies have been developed with the aim of finding the best way to achieve synchronization in complex networks, mainly focused in the role of weighted links in heterogeneous networks [3]. Most of the works are devoted to obtain synchronization between attractively coupled identical units, but heterogeneity of dynamical unit is naturally present in real networks, biological or social. Also, in real systems, heterogeneity in connections is also a common feature; it is known that biological networks combine different kinds of connections to improve synchronization and transmission performance, as in the case of the coexistence of excitatory and inhibitory synapses in the brain [4].

emails: inmaculada.leyva@urjc.es, irene.sendina@urjc.es,
juan.almendral@urjc.es

In this work we explore both the heterogeneity of units and couplings, and the connexion with the topological structure [5]. We show that a small percentage of repulsive links in a small-world structure can induce the emergence of a coherent oscillation dynamics in cases where the equivalent network composed of only attractive connections is not able to synchronize or even to activate the ensemble.

2. Model and numerical results

We want to study the rising of synchronous behaviour in a population of heterogeneous excitable units, where initially part of the group stay in oscillant and the rest in silent state. For this purpose, we study of the dynamics of an ensemble of non-identical locally coupled Hodgkin-Huxley (HH) neurons considered as spatially isopotential cells:

$$\begin{aligned} C\dot{V}_i &= I_i - I_i^{ion}(V_i, x_i) + d \sum_j \hat{L}_{ij} V_j \\ \dot{x}_i &= \alpha_x(1 - x_i) - \beta_x x_i \end{aligned} \quad (1)$$

The variables and parameters are the standards in literature [4]. The connectivity matrix is $\hat{L}_{ij} = L_{ij}/k_i$, where k_i normalize the connection strength by the number of connections to node i , and L_{ij} is a zero-row sum adjacency matrix. The coefficient d stands for the coupling strength.

The heterogeneity in the population is introduced by means of the external bias current I_i , which is uniformly distributed within the interval $I_0 \pm \Delta I$, being $I_0 = 9 \mu\text{A}/\text{cm}^2$ near a Hopf bifurcation, in such a way that for the chosen $\Delta I = 0.2$, about 70% of the neurons stay around the silent state while the rest will fire periodically.

In order to observe how units heterogeneity and phase repulsive couplings affects to coherent behavior, initially we consider just a regular lattice topology with identical (all positive or negative) connexions for an ensemble of N neurons. As expected, the system reaches a phase synchronization state for a certain $d = d_+ = 0.12$ and equivalently, for $d = d_- = -0.02$ it reaches an antiphase coherent state. Being $|d_-| < |d_+|$, phase-repulsive coupling results to be more effective to globally activate and entrain the whole network. This result is common in excitable systems due to the asymmetry of the attractor in the phase space.

However, our main interest is to explore the influence of a complex topology in the activation and synchronization of the network. Taking into account the previous result, we consider the possibility of being repulsive at least part of the long-range connections. Then, we fix $d = 0.1$ for the coupling

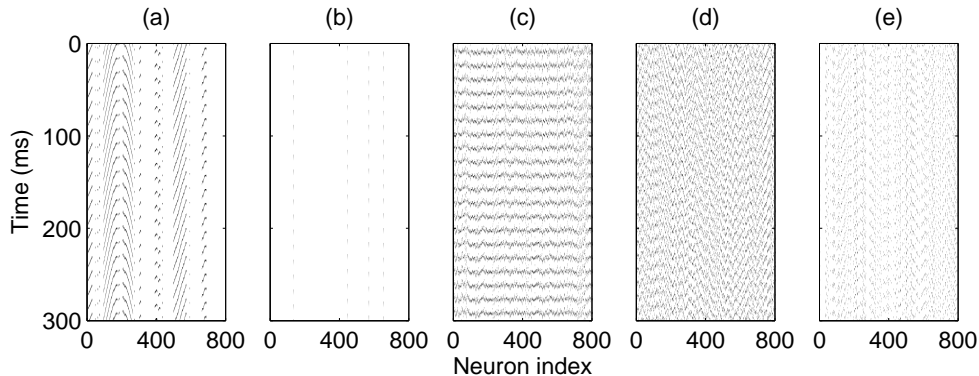


Figure 1: Space-time plots of the neuron voltage for a $N = 800$ HH units network, with $\Delta I = 0.2$, $d = 0.1$, and different coupling connectivities: (a) Local coupling with $q = 0$; (b) network with long range couplings, $p = p_c = 0.0055$, and $q = 0$; (c) same as (b) but $q = 0.3$; (d) same as (c) but $q = 0.45$; (e) same as (c) but $p = 0.015$.

strength, that is, within the unsynchronized regime, and L is modeled now by keeping the regular short-range connections positive $L_{i,i\pm 1} = +1$, and by randomly adding (rather than rewiring) a fraction p of long-range couplings $L_{ij} = L_{ji} = \pm 1$ with a probability q of being negative.

Figure 1 shows space-time plots of the voltage variable through the whole array for different probabilities p and q . As expected, in the absence of long-range connection, for chosen coupling strength d only around the initial 30% of the neurons is firing and the array is not activated or synchronized, as shown in Fig. 1(a). When long-range links are included, the first observations is that for any p , a minimum fraction of the new added links needs to be repulsive in order to increase the activity of the network, as becomes evident when comparing Fig. 1(b) with Figs. 1(c)-(e). In Fig. 1(b) the activity generated by the initially active neurons is reduced or even annihilated when all the long-range connections are attractive ($q = 0$). However, the scenario completely changes when, for the same p , some of the shortcuts are repulsive ($q > 0$) like in Figs. 1(c)-(e) where self-sustained electrical activity emerges for nonzero q .

In addition, we observe the existence of optimal values for p (let us call $p = p_c$ to this value) and q for which the collective oscillation becomes maximally phase-coherent. This fact can be observed by comparing Fig. 1(c) where $p = p_c$ and Fig. 1(d) for the same q but slightly higher p .

We now quantitatively study how the dynamics is affected by p and q , by measuring the mean firing rate (MF) of the network and the standard de-

viation of the global electrical voltage $V(t) = \sum_{i=1}^N V_i(t)$ obtained as $\sigma_V = \sqrt{\langle V^2(t) \rangle - \langle V(t) \rangle^2}$. While the MF measures the network activation, a high σ_V indicates that this activity is coherent. When the network is fully activated the MF approaches to 70 Hz.

The effect of the topology in the dynamics as a function of p and q can be seen in the contour plots in the p - q space shown in Fig. 2. We first observe that there is a change in the behaviour of both the activity and coherence as a function of p . The effect of the activity (measured by means of the MF rate) is shown in the left panel, and the coherence is measured in the right panel through σ_V . While for the MF there is a transition towards a fully activated system at certain p , the σ_V reaches a maximum at this point. In the right panel of Fig. 2 it is clear the signature of a resonance both in p and q , as observed in Fig. 1.

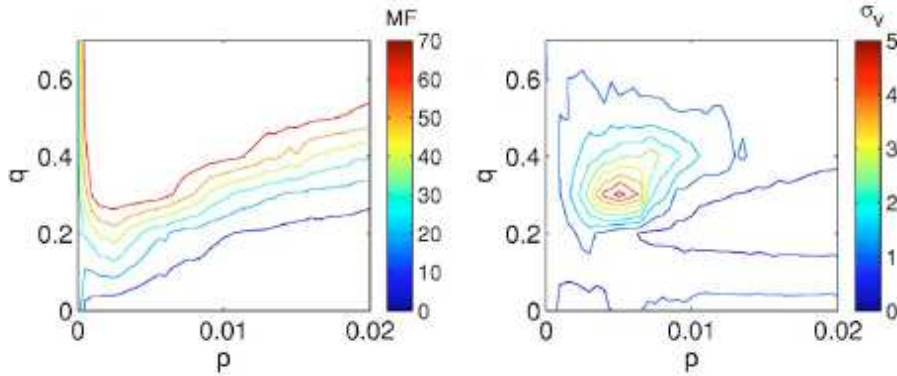


Figure 2: Contour plots in the p - q plane of the (left) mean frequency (MF) and (right) network coherence σ_V as a function of p and q in a $N=800$ network. It becomes evident in the right panel the resonance in p and q . Each point is averaged over 100 simulations, 1 s. long.

In Fig 2 we can also observe the importance of q in the behaviour. First it is clear that a value $q \neq 0$ is needed to activate the network, which is related with the larger capacity of negative perturbations to get the system out of the stable point (silent state). The q value of maximal activity depends slightly on p . Additionally, this activity will be coherent for a p - q pair of values that shift to higher p as q increases.

3. Structural analysis

When we explore the influence of the topology on the dynamics pointed on by these observations becomes evident when we observe that the critical link probability p_c depends strongly in the ensemble size as $\simeq \ln(N)/N$, that is, coincides with the birth of the giant connected component (GCC) of the Poisson random graph with N elements, which is precisely the network we have when only the randomly added long-range connections are considered (i. e. when we neglected the local couplings).

Therefore, we want to analyze whether the network structure has some bearing on the dynamics. Recently, the method of the master stability function has been successfully used for this goal in several situations [3]. However, this method requires the dynamics unit to be identical in order to consider the stability of the perfectly synchronous state, which is not our case. Then, to perform our analysis we use a purely structural analysis, based in the properties of \mathbf{L} , ignoring the dynamics imposed on it, that is, we consider

$$\dot{\mathbf{V}} = d\mathbf{L}\mathbf{V} \quad (2)$$

where $\mathbf{V} = (V_1, \dots, V_N)$. Then, there is a basis in which $V_i \approx \exp(d\lambda_i t)$, where λ_i are the eigenvalues of \mathbf{L} .

It is well known that all the eigenvalues of the Laplacian associated to a network with only attractive couplings are negative. However, when we add some repulsive connections, \mathbf{L} has positive and negative eigenvalues. We find that any set of initial states rapidly evolves into the subspace S^+ , associated to the positive eigenvalues, within a time smaller than the characteristic temporal scale of the system dynamics ($\tau \approx 15ms$).

To quantify the effect of S^+ , we note that, for a given positive λ_i , $e^{d\lambda_i t}$ is a measure of how much the system spreads into the subspace defined by the corresponding eigenvector. Then, the ratio

$$\frac{e^{d\lambda_i t}}{e^{d\lambda_{max} t}} = e^{d(\lambda_i - \lambda_{max})t} \quad (3)$$

measures how different is the evolution in that subspace with respect to the one where the system develops faster. By defining the geometric average

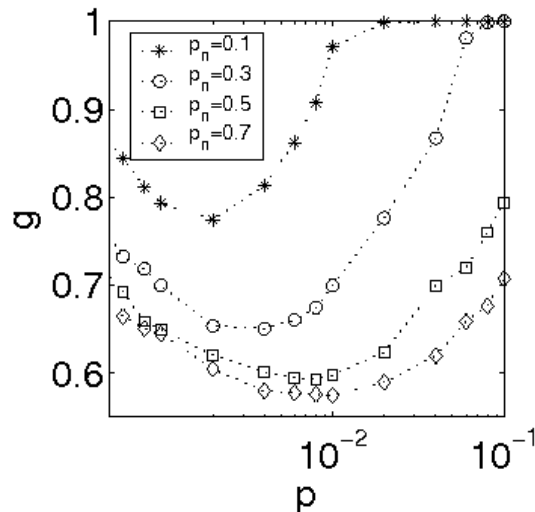
$$g(t) = e^{d(\langle \lambda_i \rangle - \lambda_{max})t} \quad (4)$$

we can estimate the homogeneity of the evolution in S^+ with a number in $(0, 1]$. Then, $g \rightarrow 1$ means similar evolution in all dimension in S^+ , whereas $g < 1$ implies that the behaviour is determined by those vector with the largest associated eigenvalues.

We are now interested in the behaviour of $g(t)$ as a function of p and q . As the shape of $g(t)$ with p is not very sensitive to time, we fix $t = d^{-1} \sim \tau$ to focus our study within the time scale of our dynamical unit. In figure 3, we observe that $g \equiv g(\tau)$ presents a minimum at p_c which is lower for higher values of q , and whose position shifts to higher p as q increases, as in the numerical simulations of the networks. In this last case, the system becomes more heterogeneous due to the connectivity, and therefore, the intrinsic dynamics is minimally constrained by the structure that arises around p_c due to the repulsive shortcuts.

The results reflect the fact that at p_c there is a transition from a 2-k lattice to a lattice with an exponential degree distribution, indicating the presence of hubs. In this state, where the eigenvalues dispersion is large, the activity is enhanced, as observed in the numerical simulations, and the network is compatible with the diversity of the dynamical units, which are allowed to reach a partially coherent state. On the other hand, far from p_c the nodes are indistinguishable from a topology point of view and the dynamical units are constrained to evolve alike, when they have different intrinsic dynamics, failing in obtaining a coherent behavior.

In summary, we have shown numerically how a small fraction of phase-repulsive links can enhance activity and coherence in a complex network of non-identical dynamical units, initially in different dynamical states. A spectral analysis allows us to obtain information about how the topology influences the dynamics.



References

- [1] R.SERGEV, M.BENVENISTE, E.HULATA, N.COHEN, A.PALEVSKI, E.KAPON, Y.SHAPIRA, E.BEN-JACOB, “Long Term Behavior of Lithographically Prepared In Vitro Neuronal Networks”, *Phys. Rev. Lett.* **88** (2002) 118102.
- [2] V. M. EGUILUZ, D. R. CHIALVO, G. A. CECCHI, M.BALIKI, A. V. APKARIAN, “Scale-Free Brain Functional Networks”, *Phys. Rev. Lett.***94** (2005) 018102.
- [3] S. BOCCALETTI, V. LATORA, Y. MORENO M. CHAVEZF, D.-U. HWANGA , “Complex networks: Structure and dynamics”, *Phys. Rep.* **424** (2006) 175-308.
- [4] MIKHAIL I. RABINOVICH AND PABLO VARONA AND ALLEN I. SELVERSTON AND HENRY D. I. ABARBANEL, “Dynamical principles in neuroscience”, *Rev. Mod. Phys.* **78** (2006) 1213.
- [5] I. LEYVA, I. SENDINA-NADAL, J. A. ALMENDRAL, M. A. F. SANJUÁN, “Sparse repulsive couplings enhances synchronization in complex networks”, *Phys. Rev. E* **74** (2006) 056112.

Complex Networks with Time–Dependent Connections and Silent Nodes

J. Marro¹, J.J. Torres¹, J.M. Cortes² and S. de Franciscis¹

¹*Institute Carlos I for Theoretical and Computational Physics, and
Departamento de Electromagnetismo y Física de la Materia, University of
Granada, Facultad de Ciencias, 18071 Granada, Spain*

²*Institute for Adaptive and Neural Computation,, University of Edinburgh, EH1
2QL, UK.*

Abstract

We present a model of an attractor neural network with complex, time–dependent connections in which some of the nodes remain silent at each time step. The network has a heterogenous distribution of connection weights and, depending on the current degree of order, some connections are reinforced/weakened with strength Φ on short–time scales. We also consider that only a fraction ρ of nodes are simultaneously updated. The resulting dynamics has attractors which, for a certain range of relevant parameters Φ and ρ , become unstable, and results in a chaotic itineracy among them which highly depends on ρ . For intermediate values of ρ , we observe that the number of attractors visited increases with ρ , and the trajectory may change from regular to chaotic and vice versa as ρ is modified. Finally, a statistical analysis of time series show a power–law spectra under conditions in which the attractors’ space is most efficiently explored. We argue on the possible qualitative relevance of this phenomenology to networks in several natural contexts.

PACS: 05.45.Pq; 05.50.+q; 87.18.Sn; 87.23.Ge; 89.40.-a; 89.65.-s; 89.75.-k

1. Introduction

In the last decade, there has been a great interest in the study of complex networks —that is a large set of nodes connected in pairs by edges— in physics [1, 2]. Most of these studies have focused on the *wiring* topology of the network

emails: jmarro@ugr.es, jtorres@ugr.es, ,

which, for example, has led to the discovery of *scale-free* and *small-world* networks in natural and man-made systems. However, real networks exhibit a number of relevant qualities besides interesting topological structure [2, 3, 4, 5]. In this work, we are concerned with two features which could affect the network performance. First, we consider a network with *weighted and time-dependent connections*, as it occurs, for instance, in trophic webs, social and communication (e.g., cell phone) networks, or transport connections. In these examples, connection weights usually vary on a long-time scale. One, however, can consider that weights may change on a short-time scale to improve actual functioning as it happens, for instance, in neural media. As a matter of fact, the human brain is the paradigm of a weighted network [6], and it is also clear-cut that high-level functions in the brain rely on fast synaptic changes during operation [7]. Then, in the rest of the paper, we shall often use the language and refer to observations on neural and, eventually, computational networks. In any case, our study is rather general and we believe that the main behaviour described in this paper should apply to networks in different contexts (see, for instance, Refs. [3, 4]). Secondly, in our study we consider *partial activation of nodes* which can also induce *fast fluctuations* in the network. One may argue that the cost for the network to maintain all nodes synchronized and fully informed of the activity of *all* the others can be very high, because it will require a lot of energy. Moreover, there are some indications that certain nodes are more active than others, and that only a fraction of nodes is actually engaged at each time in some cooperative tasks. For example, this is a characteristic of nodes in excitable media which include a finite refractory period after each excitation [8]. The possibility of having reticent nodes is also a recent concern in computer science in relation with parallelism [9, 10], in mathematical-physics [11], and in neuroscience, where it has been associated with working memories [12, 13], variability of neuron thresholds [14] and silent neurons [15, 16]. In principle, this is a different phenomenon but one may argue that some of the observed partial synchronization processes, in which some elements do not attend to the others' mode, could be associated with the existence of silent and/or excitable units, the case of interest here.

The investigation of time-dependent connections in physics has only recently been initiated; see, for instance, Refs.[3, 4, 5]. However, studying the consequences of fast connection changes in biologically inspired models has already a two-decades history —see [17] and references therein. For example, it has recently been shown that the susceptibility of a network to outside influence increases dramatically for excitable nodes [18] and, more specifically, under a competition of processes which tend to increase and decrease, respectively, the efficiency of synaptic connections at short times [19]. On the

other hand, the investigation of the effect of the *partial activation of nodes* is rarer [20, 11, 10, 21], in spite of the fact that there is some —e.g., the above mentioned— specific motivation for it in several fields. In this paper we have investigated the combined effect of these two features, in an attractor neural network. We show that varying the fraction of nodes that are simultaneously active induces a variety of qualitatively different behaviours in situations of great susceptibility, but not in more general conditions. The susceptibility needed to observe the most interesting behaviour is shown to occur under appropriate tuning of the connection weights with the network activity. As a first application of our study, we describe here how a model exhibits unstable dynamics, which leads to itinerancy and chaotic behaviour in a way that mimics both general expectations and some recent biological observations.

2. The model

We consider a network with N nodes with $\mathbf{s} \equiv \{s_i\}$ and $\mathbf{w} \equiv \{w_{ij} \in \mathbb{R}\}$ ($i, j = 1, \dots, N$) representing, respectively, the node states or *activities* and the connection weights. From these we define a local field on each node due to the weighted action of the others, namely, $h_i(\mathbf{s}, \mathbf{w}) \equiv \sum_{j \neq i} w_{ij} s_j$. At each time unit, the activity of n nodes is updated according to the probabilistic master equation:

$$P_{t+1}(\mathbf{s}) = \sum_{\mathbf{s}'} \mathbf{T}(\mathbf{s}' \rightarrow \mathbf{s}) P_t(\mathbf{s}'), \quad (1)$$

with transition probability

$$\mathbf{T}(\mathbf{s} \rightarrow \mathbf{s}') = \sum_{\mathbf{x}} p_n(\mathbf{x}) \prod_{\{i|x_i=1\}} \tau_n(s_i \rightarrow s'_i) \prod_{\{i|x_i=0\}} \delta_{s_i, s'_i}. \quad (2)$$

Here, \mathbf{x} is an operational set of binary indexes —fixed to 1 at n sites chosen at each time according to distribution $p_n(\mathbf{x})$, and fixed to zero at the other $N - n$ sites. The choice (2) simply states that one (only) updates simultaneously the selected n nodes. The corresponding elementary rate is

$$\tau_n(s_i \rightarrow s'_i) = \sigma(s_i \rightarrow s'_i) \left[1 + \left(\delta_{s'_i, -s_i} - 1 \right) \delta_{n,1} \right], \quad (3)$$

where $\sigma = \sigma(\mathbf{s}, \beta)$ is a function to be determined, with β an inverse temperature parameter, whose particular form is chosen for reference purposes. In fact, the above describes *parallel updating*, as in cellular automata, for $n = N$ or, macroscopically, $\rho \equiv n/N \rightarrow 1$. However, the model describes *sequential updating*, as in kinetic magnetic models, for $n = 1$ or $\rho \rightarrow 0$. We are interested in changes with $\rho \in (0, 1)$ which allow for a sensible generalization of familiar cellular automata and represent more real situations, as indicated in the

introduction. For example, assuming a neural network, ρ may stand for the fraction of neurons that are stimulated each cycle. There is no input on the other $1 - \rho$, so that information from the previous state is maintained. This induces persistent activity which has been argued to be a basis for working memory [12, 13]. Varying ρ may also be relevant to simulate the observed variability of the neurons' threshold [14] and the possible existence of *silent neurons* [15] or *dark neuro-matter* [16], for instance.

The equations above may be simulated in a computer for different choices of p_n and transition details. In order to obtain analytical results, we consider the simplest case in which the node activities are binary, $s_i = \pm 1$, the n nodes to be updated are chosen at random, so that one has $p_n(\mathbf{x}) = \binom{N}{n}^{-1} \delta(\sum_i x_i - n)$, and σ is an arbitrary function of (only) $\beta s_i h_i$ which satisfies detailed balance. In spite of the latter, detailed balance is not fulfilled by the superposition \mathbf{T} for $n > 1$, so that resulting steady states are generally out of equilibrium, which is known to be realistic [22]. We also assume that fields are $h(\mathbf{s}, \mathbf{w}) = h[\pi(\mathbf{s}), \xi_i]$. Here, $\xi_i \equiv \{\xi_i^\mu = \pm 1; \mu = 1, \dots, M\}$ stands for M given realizations of the set of activities, or *patterns*, and

$$\pi \equiv \{\pi^\mu(\mathbf{s})\}, \quad \pi^\mu(\mathbf{s}) = N^{-1} \sum_i \xi_i^\mu s_i, \quad (4)$$

measures the *overlap* between the current state and pattern μ . For $N \rightarrow \infty$ and finite M , i.e., in the limit $\alpha \equiv M/N \rightarrow 0$, the time equation

$$\pi_{t+1}^\mu(\mathbf{s}) = \rho N^{-1} \sum_i \xi_i^\mu \tanh\{\beta h_i[\pi_t(\mathbf{s}), \xi_i]\} + (1 - \rho) \pi_t^\mu(\mathbf{s}) \quad (5)$$

follows for any μ . Actual applications concern finite values for both M and N , so that the limit $\alpha \rightarrow 0$ is not very interesting in practice. This and other restrictions are not essential to the model, however; in fact, our simulations below concern more general situations, as pointed out when necessary.

The model allows for different relations between the fields h_i and the other network properties. The simplest case at hand for specific relations of such kind is Hopfield's [23] which follows here for $\rho \rightarrow 0$ and weights fixed according to the Hebb prescription, i.e., $w_{ij} = N^{-1} \sum_\mu \xi_i^\mu \xi_j^\mu$. The symmetry $w_{ij} = w_{ji}$ then assures $P_{t \rightarrow \infty}(\mathbf{s}) \propto \exp(\beta \sum_i h_i s_i)$. This (equilibrium) case exhibits *associative memory* property. That is, for high enough β , the patterns $\{\xi_i\}$ are attractors of dynamics [24], as if they would have been *stored* in the connections and recalled in the course of the system relaxation with time.

Equilibrium is generally impeded for $\rho > 0$ [25], and the asymptotic state then strongly depends on dynamic details [22, 26]. We checked that, in agreement with some indications [20], the Hopfield-Hebb network also exhibits

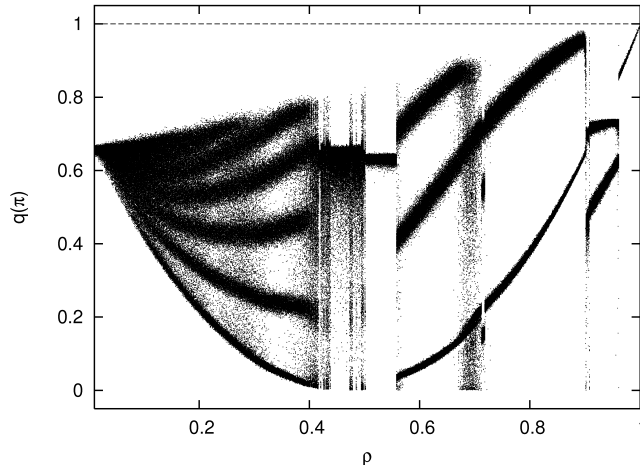


Figure 1: Evidence of chaos. Bifurcation diagram showing the stationary order parameter $q(\pi)$, as defined in the main text, versus the synchronization parameter ρ for $M = 5$ random patterns, $N = 1600$ nodes, $\beta = 100$ and $\Phi = -1/2$. This behaviour is characteristic of any $\Phi \neq 1$, and it follows indistinctly from the analytical solution and from Monte Carlo simulations. The dashed line corresponds to the Hopfield equilibrium case.

associative memory for $\rho > 0$. However, no new physics emerges as ρ is varied in this case, and it is likely this occurs rather generally concerning dynamics for simple weighted networks.

Our model may exhibit a complex dependence on ρ assuming activity dependent weights. This is expected to occur in many excitable media [8]. However, as far as we know, the only situation with time-dependent connections which is well documented in the literature concerns the brain. In this case, transmission of information and computations have repeatedly been reported to be correlated with activity-induced fast fluctuations of synapses, i.e., our w_{ij} 's [27, 7]. For example, it has been observed that the efficacy of synaptic transmission can undergo short-time increasing (sometimes called *facilitation*) [28, 29] or decreasing (*depression*) [30, 31], and that these effects depend on the activity of the presynaptic neuron. It has already been demonstrated that such processes may importantly affect a network performance [17, 19, 33, 32, 34]. Likewise, it seems sensible to assume that similar short-time variations may occur in other networks —e.g., reaction-diffusion systems and the cardiac tissue [8]— associated with some efficacy lost after heavy work or with excitations, for instance.

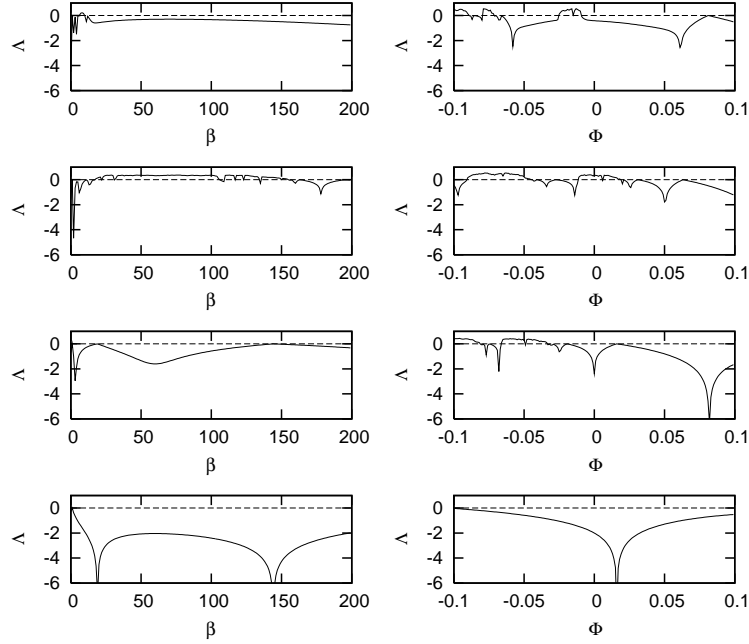


Figure 2: The Lyapunov exponent Λ as a function of the β and Φ for several values of $\rho = 0.25, 0.5, 0.8, 0.99$, from bottom to top, respectively. $\Lambda > 0$ correspond to an irregular or chaotic dynamics. Left graphs correspond to $\Phi = 0.01$ and Λ as a function of β , and right panels correspond to $\beta = 25$ and Λ as a function of Φ . Note that there is a small chaotic region ($\Lambda > 0$) for $\rho \lesssim 1$ and low β and $\Phi = 0.01$.

Motivated by all these facts, and also trying to maintain a well-defined reference frame, we shall assume that the connection weights are

$$w_{ij} = \varepsilon_{ij} \bar{w}_{ij} = \varepsilon_j \bar{w}_{ij}, \quad (6)$$

where the second equality is introduced for simplicity. Here, \bar{w}_{ij} stands for some reference value and ε_j for a random variable. That is, we are assuming some “noise” on top of a previous preparation of the connections designed so that the network can perform some specific function. This also suggests us to assume that the random variable in (6) is fluctuating very rapidly so that, on the time scale for the activity changes, it behaves as stationary with distribution given, for example, by

$$p^{\text{st}}(\mathbf{s}, \varepsilon_j) = q \delta(\varepsilon_j - \Phi) + (1 - q) \delta(\varepsilon_j - 1). \quad (7)$$

We shall further assume that q depends on the degree of *order* in the system at time t , namely, that $q = q(\pi_t)$. For the sake of concreteness, our choices here will be that $q(\pi) = (1 + \alpha)^{-1} \sum_{\mu} \pi^{\mu}(\mathbf{s})^2$ and that \bar{w}_{ij} is given by the Hebb prescription. The result is that each node is acted on by an effective field

$$h_i^{\text{eff}}(\mathbf{s}, \mathbf{w}) = \sum_{j \neq i} w_{ij}^{\text{eff}} s_j \quad (8)$$

with

$$w_{ij}^{\text{eff}} = [1 - (1 - \Phi) q(\pi)] \bar{w}_{ij}. \quad (9)$$

This amounts to assume short-term variations affecting the intensity of connections by an amount, either positive or negative, Φ on the average. More specifically, one has a decreasing effect for any $\Phi < 1$, and enhancement for $\Phi > 1$, as far as $\Phi > 0$, while $\Phi < 0$ allows for the possibility of a change in the nature of the weights. For the indicated choices of fields and reference weights, our framework reduces to the familiar Hopfield-Hebb case for $\Phi = 1$. It should not be difficult to implement the model for choices other than (6) and (7).

3. Results

Assuming (8) and (9), it readily ensues from (5) for $M = 1$ that $\pi_{\infty} = F(\pi_{\infty}; \rho, \Phi)$. Local stability requires that $|\partial F / \partial \pi| < 1$, where

$$F(\pi; \rho, \Phi) \equiv \rho \tanh \{ \beta \pi [1 - (1 - \Phi) \pi^2] \} + (1 - \rho) \pi. \quad (10)$$

Therefore, fixed points are independent of ρ for any Φ , but stability demands that $\rho < \rho_c$ with $\rho_c = 2 \{ 3\beta\pi_{\infty}^2 [(\frac{4}{3} - \Phi) - (1 - \Phi) \pi_{\infty}^2] - \beta + 1 \}^{-1}$. The resulting situation for any $\Phi \neq 1$ is illustrated in Fig. 1, where one observes regular behaviour, bifurcations and chaotic windows. This picture cannot occur for fixed weights, e.g., in the Hopfield case (dashed line). In order to deepen on the possibility of chaos, we computed the Lyapunov exponents for different values of ρ as a function of the relevant parameters, namely Φ and β , and from the analytical solution for $M = 1$. This is shown in Fig. 2. The figure clearly reveals the existence of chaos above some degree of synchronization, more specifically, for $\rho > \rho_c(\beta, \Phi)$ which marks the onset of period doubling before irregular behaviour. For example, the left graphs show that, for a small positive value of Φ , which corresponds to some slight depression of connections which occurs more likely the higher the current system order is, there is a region for large β (relatively small temperature, say $T \approx 0.02$ in our arbitrary units) and $1 > \rho \gtrsim 0.8$ for which dynamics may eventually become chaotic.

In the same graph one may notice a tiny chaotic window for $\rho \approx 1$ and $\beta \approx 7$; this is the case identified previously by us [35]. The right graphs, on the other hand, illustrates that chaos is typically an exception for positive values of Φ ; it may only occur then for a rather large fraction of synchronized nodes (large ρ) near $\Phi \lesssim 0$. On the contrary, for negative Φ , i.e., when the order tends to induce changes in the nature of the connection intensities, it is more likely that the system will behave chaotically. It is also to be remarked that, inside the chaotic region in each graph, there is a complex pattern of transitions from regular to irregular behaviour as one changes, even very slightly the values of ρ , Φ and β . The next question is whether such complex behaviour may have some constructive role in natural and man-made networks.

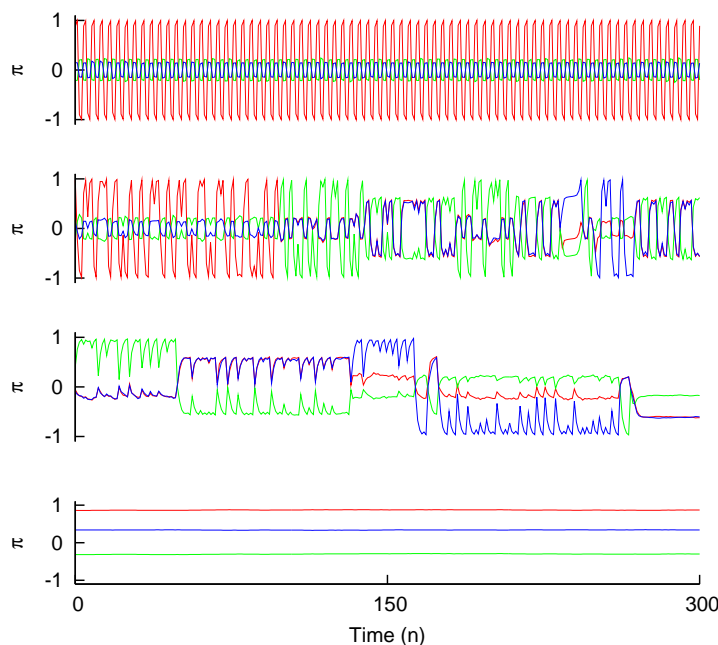


Figure 3: Typical Monte Carlo runs. This shows the overlap as a function of time (in units of n MC trials), during the stationary regime after equilibration, for $N = 1600$ nodes, $\beta = 50$, $\Phi = 0.0035$ and, from bottom to top, $\rho = 0, 0.59, 0.89$, and 0.95 , respectively. In this case, $\rho_c \simeq 0.5$. This is for $M = 3$ correlated patterns (identified here with different colours). That is, we generated three patterns completely at random, and then replaced 20% of the digits in the second and third patterns with the same number of digits, and flipped digits, respectively, taken from the first pattern.

Different types of behaviour the system may exhibit are illustrated by the

stationary Monte Carlo runs in Fig. 3. This involves three partially correlated patterns, as explained in the figure caption, and illustrates, from bottom to top: (a) for $\rho < \rho_c$, convergence towards one of the attractors, namely, fixed points corresponding to the patterns provided, which is revealed by the fact that one of the overlaps (the red one) is large, close to 1, while the others two are closer to zero; (b) irregular behaviour with positive Lyapunov exponent for a larger value of ρ where that dynamics is now unstable and the system activity is visiting the different attractors, including the negative of some of them or *antipatterns*; (c) a different type of irregular behaviour in which, in addition to visiting different attractors on a large time scale, there are much more rapid irregular transitions between one pattern and its antipattern; and finally (d) regular oscillation between one attractor and its negative, which is more rapid as $\rho \rightarrow 1$ (that is, when all the nodes are active).

The cases (b) and (c) above are examples of instability-induced switching phenomena, namely, the system seems to describe in these cases kind of heteroclinic paths among the attractors, and remains different time intervals in the neighbourhood of each of them, as it was previously observed in a related case [35].

An interesting fact concerning the nature of temporal itineracy among the stored patterns as ρ is varied is illustrated in Fig. 4. This shows time evolution of the mean firing rate defined as

$$m = \frac{1}{2N} \sum_{i=1}^N (1 + s_i). \quad (11)$$

Three patterns (and their corresponding antipatterns) are involved here which consist of a string of 1s, a string with the first 50% positions set to 1 and the rest to -1 , and a string with only the first 20% positions set to 1, respectively. In this Monte Carlo experiment, the activity remains wandering around one of the patterns for any $\rho < \rho_c$. The choice of pattern depends on the initial condition (top graphs in the Fig. 4). For larger values of ρ within a chaotic window (middle graphs and left-bottom graph in Fig. 4), the system tends to visit the other patterns as well. In particular, the middle-left graph in the figure ($\rho = 0.384$) shows visits to the three patterns, and a trajectory which is structured, namely, there are many jumps between the pairs of more correlated patterns, and only a few between the most distant ones. Moreover, the number of jumps between the less correlated patterns tends to grow as ρ is further increased within the chaotic window. The figure shows that, for $\rho = 0.39$ and 0.40 , even the antipatterns are visited; note that we have that $\xi^2 = -\xi^2$. Increasing ρ further, e.g., for $\rho = 0.6$ in this specific experiment, the network surpasses equiprobability of patterns and, eventually, abandons

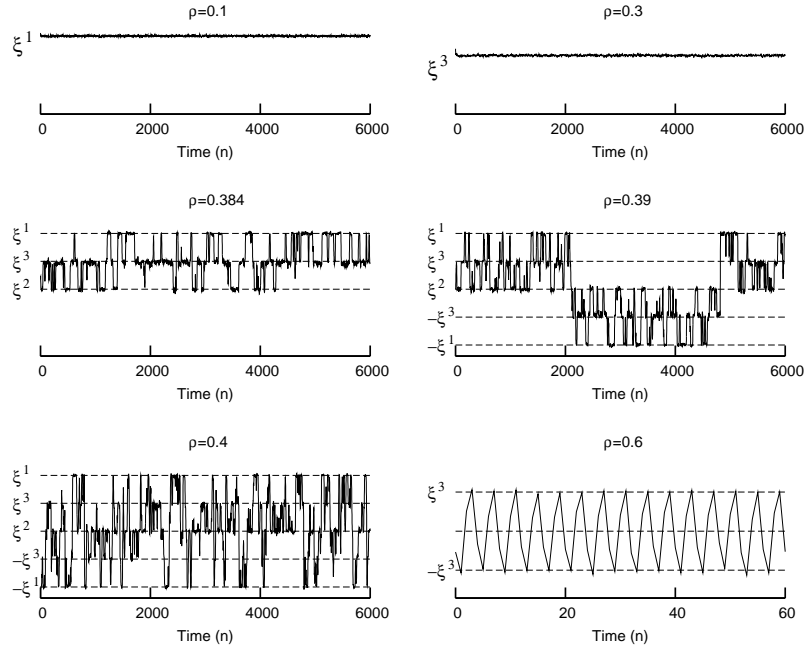


Figure 4: Monte Carlo runs that one may interpret as *states of attention* in the network, which illustrates the possible role of chaos. This shows time-series of the mean firing rate for $N = 1600$, $\beta = 167$, $\Phi = -\frac{1}{2}$, and different values of the parameter $\rho = 0.1, 0.3, 0.384, 0.39$ and 0.4 . Here, $\rho_c = 0.38$, and the system stores three patterns, ξ^μ , $\mu = 1, 2$ and 3 , as described in the main text. The figure shows how the number of visited attractors increases with ρ after ρ_c . Note that although there are three stored patterns ξ^μ , the antipatterns $-\xi^\mu$ are also attractors of the network's dynamics.

the chaotic regime to fall into a limit cycle (bottom-right graph), where it periodically oscillates between a pattern and its antipattern.

This interesting behaviour is made more explicit in Fig. 5, where we plotted the distribution probability for the mean firing rate, $\mathcal{P}(m, \rho) = kN(m)$, with k a normalization constant and $N(m)$ the number of occurrences that m has a value between m and $m + dm$ during a large temporal window Δt . This tells us how often the activity of the network is around a particular memory pattern, and how this is affected when one varies ρ . The figure shows that for ρ small $\mathcal{P}(m, \rho)$ is centered around the mean activity of one of the stored patterns. As ρ increases the variance of the distribution also increases, and for $\rho > \rho_c$ $\mathcal{P}(m, \rho)$ becomes multimodal with several peaks centered around

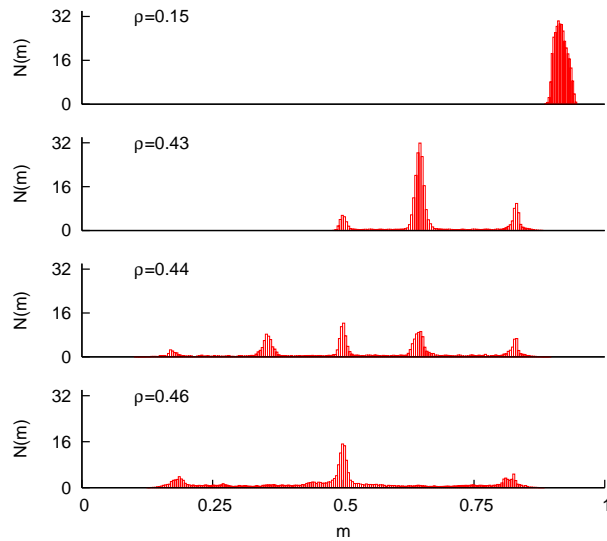


Figure 5: Monte Carlo histograms showing qualitative changes in the distribution of the mean firing rate m , which is a measure of the time the system is around a particular pattern or antipattern. This is for time series with patterns defined as in Fig. 4, $N = 1600$, $\beta = 167$ and $\Phi = 0.05$, and it follows that now $\rho_c \simeq 0.43$.

the mean-activity associated to all stored patterns. Note that the two first cases in this figure are asymmetric (it can be centered in the pattern or in its antipattern) while the other two are symmetric around $m = 0$, due to the chaotic itineracy among all patterns and the particular set of patterns we used.

In order to deepen further on the nature of the chaotic switching, we have computed the normalized power spectra $p(\omega)$ of the time series for the mean firing rate m . If one computes the associated entropy [36], namely, $S = -\sum_{\omega} p(\omega) \log p(\omega)$, it ensues a sharp minimum at $S \simeq 0.37$ for $\Phi = -0.048$ (data not shown). The series corresponding to this minimum and, for comparison purposes, a different one for a much larger entropy are presented in Fig. 6 (left). The power spectra for these two series is presented in Fig. 6(right). This reveals a qualitative change of behaviour, namely, that (only) the series describing a more efficient chaotic mechanism exhibit a power law distribution. We are presently analyzing in more detail this interesting phenomenon.

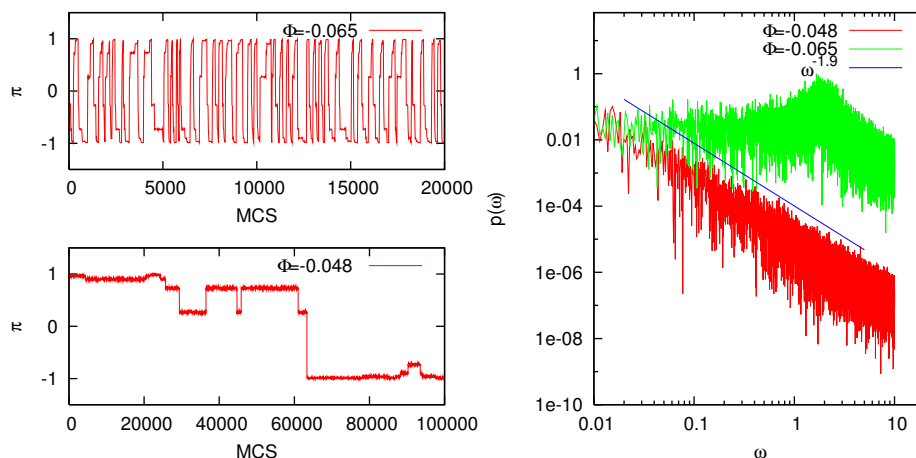


Figure 6: Left: Time series for the overlap π in the case $\rho = 0.632$, $M = 1$, $\beta = \infty$ (zero temperature), $N = 3600$, and $\Phi = -0.048$ (top) and -0.065 (bottom) showing chaotic transitions between the associated pattern and its antipattern. This series correspond to entropies $S \simeq 0.37$ and 0.9 , respectively. Left: The power spectra corresponding to the two series in the left panels. The straight line here has slope 1.9 .

4. Discussion

We have described in this paper details concerning a model network in which connections are heterogeneously weighted and time-dependent, namely, correlated to the global activity. As documented above, these two conditions occur in many natural networks. Furthermore, only a fraction ρ of nodes are active at each time, so that the rest maintain the previous state. This would occur in an excitable media, for instance.

A main conclusion is that, although the synchronization parameter ρ is generally irrelevant, varying ρ may greatly modify the system behaviour under certain conditions. The necessary condition is a kind of susceptibility or sensitivity to external stimuli which greatly favours dynamic instabilities. It may be achieved in our example by appropriate tuning of two parameters, Φ and the inverse of the temperature β . The former induces either enhancement ($\Phi > 1$) or lowering ($\Phi < 1$) for positive Φ , or even change of sign for negative Φ , of the intensities of connections. This process is a very fast one —as compared with the nodes changes—, and it occurs more likely the larger the current degree of order is.

Within the most interesting range for its parameters, our model exhibits heteroclinic trajectories which imply, in particular, a kind of *dynamic association*. That is, the network activity either goes to one attractor for $\rho < \rho_c$, or else, for larger ρ , is capable of an intriguing programme of visits to possible attractors. This dynamic may abruptly become chaotic, which seems the most relevant regime. Besides synchronization of a minimum of nodes, this requires careful tuning of ρ , β and Φ . That is, as suggested by Fig. 2, there is a complex parameter space which makes it difficult to predict the ensuing behaviour for slight changes of parameter values.

The most interesting behaviour of the network consists of *switching* among attractors, that can be regular for $\rho < \rho_c$, or to involves chaos which makes such process much more efficient. More specifically, we observe a highly-structured chaotic itinerancy process in which, as illustrated in Fig. 4, modifying ρ within a chaotic window—which requires also tuning β and Φ —one may control the subset of visited attractors. That is, increasing ρ within the relevant regime makes the system to visit *more distant* (less correlated) attractors. In this way the system may perform, for instance, family discrimination and classification by tuning ρ [37]. On the other hand, the complexity of the parameter space for $\rho > \rho_c$ suggest that one could devise a method to control chaos in these cases, and also that one should pay attention to these facts when determining efficient computational strategies in artificial machines. Similar switching phenomena, in which the activity describes a heteroclinic path among saddle states, has already been incorporated in models which thus simulate experiments on animal olfactory systems [38, 39, 40, 41]. Comparable oscillatory activity has been reported to occur in cultured neural networks [13] and ecology models and food webs [42, 43, 44], and it is believed it could account for other natural phenomena as well [38].

Finally, an important feature of the model chaotic itinerancy is illustrated in Fig. 6. This reveals the existence of power-law distributions within the regimes in which the network exhibits its most interesting behaviour. This is the case for the power spectra of time series and for the time spent in the neighbourhood of each attractor for appropriate values of ρ . This fact suggests that a *critical condition* which has been called for to explain some of the brain exceptional behaviour [45, 46, 47] could perhaps consists, as in our model here, of a highly susceptible, unstable and chaotic condition similar to the one we have described for the model.

Acknowledgements

We acknowledge financial support from FEDER-MEC project FIS2005-00791, JA project P06-FQM-01505, and EPSRC-COLAMN project EP/CO 10841/1.

References

- [1] A.L. Barabási, *Rev. Mod. Phys.* **74**, 47 (2002)
- [2] S. Boccaletti, V. Latora, Y. Moreno, M. Chavez, and D.U. Hwang, *Phys. Rep.* **424**, 175 (2006)
- [3] A. Barrat, M. Barthélemy, and A. Vespignani, *Phys. Rev. E* **70**, 066149 (2004); *ibid* , *J. Stat. Mech.* P05003 (2005)
- [4] M.A. Serrano, M. Boguñá, and R. Pastor-Satorras, *Phys. Rev. E* **74**, 055101R (2006)
- [5] C. Zhou, A.E. Motter, and J. Kurths, *Phys. Rev. Lett.* **96**, 034101 (2006)
- [6] R. Salvador, J. Suckling, M.R. Coleman, J.D. Pickard, D. Menon, and E. Bullmore, *Cereb. Cortex* **15**,1332 (2005)
- [7] L.F. Abbott and W.G. Regehr, *Nature* **431**, 796 (2004)
- [8] J.H.E. Cartwright, *Phys. Rev. E* **62**, 1149 (2000)
- [9] G. Korniss, M.A. Novotny, H. Guclu, Z. Toroczkai, and P.A. Rikvold, *Science* **299**, 677 (2003)
- [10] P. Tosic and G. Agha, in *Proceedings of the First European Conference on Complex Systems ECCS'05*, European Complex Systems Society, Paris, November 14-18 2005.
- [11] M.R. Evans, *J. Phys. A: Math. Gen.* **30**, 5669 (1997)
- [12] F.E. LeBeau, A. El Manira, and S. Griller, *Trends Neurosci.* **28**, 552 (2005)
- [13] D.A. Wagenaar, Z. Nadasdy, and S.M. Potter, *Phys. Rev. E* **73**, 051907 (2006)
- [14] R. Azouz and C.M. Gray, *Proc. Natl. Acad. Sci. USA* **97**, 8110 (2000)
- [15] B.A. Olshausen and D.J. Field, *Curr. Opin. Neurobiol.* **14**, 481 (2004)

- [16] S. Shoham, D.H. O'Connor, and R. Segev, *J. Compar. Physiol. A* **192**, 777 (2006)
- [17] J.M. Cortes, J.J. Torres, J. Marro, P.L. Garrido, and H.J. Kappen, *Neural Comp.* **18**, 614 (2006)
- [18] O. Kinouchi and M. Copelli, *Nat. Phys.* **2**, 348 (2006)
- [19] J.J. Torres, J. M. Cortes, J. Marro, and H.J. Kappen, *Neural Comp.* **19**(10), in press (2007)
- [20] A.V.M. Herz and C.M. Marcus, *Phys. Rev. E* **47**, 2155 (1993)
- [21] K. Park, Y. Lai, and N. Ye, *Phys. Rev. E* **70**, 026109 (2004)
- [22] J. Marro and R. Dickman, "Nonequilibrium Phase Transitions in Lattice Models", Cambridge Univ. Press, Cambridge 1999.
- [23] J.J. Hopfield, *PNAS* **79**, 2554 (1982)
- [24] D.J. Amit, "Modeling Brain Function: Attractor Neural Networks", Cambridge Univ. Press, Cambridge 1989.
- [25] G. Grinstein, C. Jayaprakash, and Y. He, *Phys. Rev. Lett.* **55**, 2527 (1985)
- [26] G. Ódor, *Rev. Mod. Phys.* **76**, 663 (2004)
- [27] D. Ferster, *Science* **273**, 1812 (1996)
- [28] A. Reyes, R. Luján, A. Rozov, N. Burnashev, P. Somogyi, and B. Sakmann, *Nat. Neurosci.* **1**, 279 (1998)
- [29] Y. Wang, H. Markram, P.H. Goodman, T.K. Berger, J. Ma, and P.S. Goldman-Rakic, *Nat. Neurosci.* **9**, 534 (2006)
- [30] A.M. Thomson and J. Deuchars, *Trend. Neurosci.* **17**, 119 (1994)
- [31] L.F. Abbott, J.A. Varela, K. Sen, and S.B. Nelson, *Science* **275**, 220 (1997)
- [32] D. Bibitchkov, J. M. Herrmann, and T. Geisel, *Network: Comp. Neural Syst.* **13**, 115 (2002)
- [33] L. Pantic, J.J. Torres, H.J. Kappen, and S.C.A.M. Gielen, *Neural Comp.* **14**, 2903 (2002)
- [34] S. Romani, D.J. Amit, and G. Mongillo, *J. Comp. Neurosci.* **20**, 201 (2006)

- [35] J. Marro, J.J. Torres, and J.M. Cortés, *Neural Net.*, in press (2007)
- [36] J.M. Cortés, J.J. Torres, and J. Marro, *Biosystems* **87**, 186 (2007)
- [37] J.M. Cortés *et al.*, “Algorithms for identification and categorization”, *AIP Conf. Proc.* **779**, 178 (2005)
- [38] P. Ashwin and M. Timme, *Nature* **436**, 36 (2005)
- [39] M. Rabinovich, A. Volkovskii, P. Lecanda, R. Huerta, H. Abarbanel, and G. Laurent, *Phys. Rev. Lett.* **87**, 68102 (2001)
- [40] O. Mazor and G. Laurent, *Neuron* **48**, 661 (2005)
- [41] R. Huerta and M. Rabinovich, *Phys. Rev. Lett.* **93**, 238104 (2004)
- [42] J. Hofbauer and K. Sigmund, *J. Math. Biol.* **27**, 537 (1989)
- [43] J. Vandermeer, *The Am. Naturalist* **163**, 857 (2004)
- [44] J. Vandermeer, H. Liere, and B. Lin, *Theor. Popul. Biol.*, in press (2007)
- [45] C.W. Eurich, J.M. Herrmann, and U.A. Ernst, *Phys. Rev. E* **66**, 066137 (2002)
- [46] C. Haldeman and J.M. Beggs, *Phys. Rev. Lett.* **94**, 058101 (2005)
- [47] D.R. Chialvo, *Nature Phys.* **2**, 301 (2006)

The Structure of Collective Behavior in Complex Topologies

Y. Moreno¹

¹*Institute for Biocomputation and Physics of Complex Systems, BIFI, University of Zaragoza, Zaragoza, 50009 Spain.*

Abstract

Modern network theory has produced a number of relevant results in the last few years. However, there are still many relevant questions open, particularly, when it comes to comprehend the relation between the structure and function (dynamics) of networked systems. In this contribution, we briefly address some of the most recent advances on the emergence of collective behavior in complex networks focusing on two generic phenomena that support our findings: the synchronization of phase oscillators and the emergence of cooperation through game modeling. The results show that there are some regularities that unveil universal principles, pointing to new organizing relationships in the interplay between the structure and function of complex networks that might provide new insights into why the class of scale-free networks are so ubiquitous in Nature. We round off the discussion by highlighting the current trends in this exciting and emerging field of research.

Keywords: complex networks, synchronization phenomena, evolutionary game theory

MSC 2000: 91D30, 4C15, 91A43

1. Introduction

Complex networks are becoming manifest in all fields of contemporary science. As part of a broader movement towards research in complex systems, scientists have recently found a striking degree of self-organization that emerges again and again in otherwise seemingly diverse systems [1, 2]. The network approach is particularly suitable to explore several aspects of complexity. It

emails: yamir@unizar.es

has to do with the unraveling of the structure of interactions as well as the emergent behavior of many non-identical objects coupled with the underlying structure. The massive and comparative analysis of networks from different fields has produced a series of unexpected results and has shown that previous models proposed in mathematical graph theory are very far from the real needs [1, 2]. The first issue that has been faced is certainly structural and consists of identifying a series of unifying principles and statistical properties common to most of real networks. Another important body of works has dealt with spreading and percolation-like processes on top of networks, addressing a variety of phenomena ranging from disease spreading to information flow and resilience to random failures and attacks. Finally, a third and promising branch of research has arisen in the last few years spurred by the new insights gained through network modeling. It consists of studying the dynamical behavior of large assemblies of dynamical systems interacting via complex topologies. Phenomena such as synchronization, the emergence of cooperation in social and biological systems, as well as signaling and gene regulatory dynamics and other biochemical processes could be now tackled with a fresh viewpoint by considering both sources of entangled complexity: the structure and the dynamics of the system's constituents.

In this contribution, we briefly revise some recent results on two distinct phenomena: the synchronization of Kuramoto phase oscillators and the Prisoner's Dilemma on top of complex topologies. Although these processes are quite different, we will see that the dynamical organization of the system's constituents share a number of features, therefore pointing to new regularities in the emergence of collective behavior and the role played by the underlying topology.

2. Synchronization of Kuramoto oscillators

Studies on synchronization in complex topologies where each node is considered as a Kuramoto oscillator, were first reported for Watts-Strogatz (WS) networks [3, 4] and Barabási-Albert (BA) scale-free graphs [5, 6]. The Kuramoto model (KM) on top of complex topologies is described by the equations of motion

$$\frac{d\theta_i}{dt} = \omega_i + \sum_j \sigma_{ij} A_{ij} \sin(\theta_j - \theta_i) \quad (i = 1, \dots, N), \quad (1)$$

where σ_{ij} is the coupling strength between pairs of connected oscillators and A_{ij} are the elements of the connectivity matrix ($A_{ij} = 1$ if i is linked to j and 0 otherwise). The original Kuramoto model is recovered by letting

$A_{ij} = 1, \forall i \neq j$ (all-to-all) and $\sigma_{ij} = K/N, \forall i, j$. The intrinsic or natural frequencies ω_i are distributed according to some distribution $g(\omega)$, that is usually assumed to be unimodal and symmetric about its mean frequency Ω .

The global dynamics of the system Eq. (1) turns out to be qualitatively the same as for the original Kuramoto model for the case in which we are interested, namely, for networks whose degree distribution follows a power law $P(k) \sim k^{-\gamma}$, with $2 < \gamma < 3$. The coherence of the set of N oscillators can be characterized by the order parameter $0 < r(t) \exp(i\phi(t)) = \frac{1}{N} \sum_{j=1}^N \exp(i\theta_j(t)) < 1$. For small values of the coupling ($\sigma_{ij} = \sigma \forall i$), the strength of the interactions is not enough to break the incoherence produced by the individual dynamics of the oscillators. This behavior persists until a certain critical value σ_c is attained, where some elements lock their relative phase and a cluster of synchronized nodes comes up. When $\sigma > \sigma_c$, the population of oscillators splits into a partially synchronized state made up of oscillators locked in phase that adds to r and a group of nodes whose natural frequencies are too spread as to be part of the coherent pack. Finally, for large enough values of σ , almost all nodes get entrained around the mean phase ϕ and the system settles into a completely synchronized state where $r \approx 1$.

The very existence of a critical point for the Kuramoto model on top of SF networks is surprising, as most of previous studies on dynamical processes taking place on top of these networks revealed the lack of critical points when $\gamma \leq 3$ [1, 2]. This is the case, for instance, of the spreading of a disease, which always pervades the system no matter the value of the epidemic spreading rate [1, 2]. On the other hand, the KM on top of homogeneous like networks such as a random graph shows a critical point greater than that obtained in SF nets. As the equations of motion are functionally the same and only the second term on the right hand of Eq. (1) contains the topology of both kinds of networks, the differences in the collective behavior should come from the microscopic organization of the groups of coherent oscillators. Therefore, the dynamical organization of these groups (driven by the underlying substrate) is at the very root of the mechanisms behind the differences observed. Recently, Refs [7, 8] proposed a new local parameter that captures and quantifies the way in which clusters of locked oscillators emerge. The main difference with respect to r is that one measures the degree of synchronization of nodes (r) with respect to the average phase ϕ and the other (r_{link}) the degree of synchronization between every pair of connected nodes.

This new parameter, r_{link} , gives the fraction of all possible links that are

synchronized in the network and is defined as

$$r_{link} = \frac{1}{2N_l} \sum_i \sum_{j \in \Gamma_i} \left| \lim_{\Delta t \rightarrow \infty} \frac{1}{\Delta t} \int_{t_r}^{t_r + \Delta t} e^{i[\theta_i(t) - \theta_j(t)]} dt \right|, \quad (2)$$

being Γ_i the set of neighbors of node i , t_r the time the system needs to settle into the stationary state, and Δt a large averaging time. By computing the extend to which pairs of connected oscillators are synchronized in terms of a symmetric matrix whose entries corresponds to every possible pair of links, the clusters of synchrony for any value of σ can be identified [7, 8]. From the microscopic analysis, it turns out that for homogeneous topologies (Erdős-Rényi graphs (ER)), many small clusters of synchronized pairs of oscillators are spread over the graph and merge together to form a giant synchronized cluster (GC) when the effective coupling is increased. On the contrary, in heterogeneous graphs, a central core containing the hubs first comes up driving the evolution of synchronization patterns by absorbing small clusters. Moreover, the evolution of r_{link} as σ grows explains why the transition is sharper for ER networks: nodes are added first to the GC and latter on the links among these nodes that were missing in the original clusters of synchrony, while in SF graphs oscillators are added to the largest synchronized component together with most of their links, resulting in a much slower growth of r_{link} . Finally, the probability that a node with degree k belongs to the largest synchronized cluster is an increasing function of k for every σ , namely, the more connected a node is, the more likely it takes part in the cluster of synchronized links. Moreover, the highly connected nodes are also more robust to perturbations once the fully synchronized state is attained, that is, the average time $\langle \tau \rangle$ a node needs to get back into the fully synchronized state is inversely proportional to its degree, i.e., $\langle \tau \rangle \sim k^{-1}$.

The observed differences in the behavior at a local scale are rooted in the growth of the *GC*. That is, in one case (ER-like networks), almost all the nodes of the network takes part of the giant component from the beginning and latter on, when σ is increased, what is added to the *GC* are the links among these nodes that were missing in the original cluster of synchronized nodes. For SF-like networks, the mechanism is the opposite. Nodes are added to the *GC together* with most of their links, resulting in a growth of r_{link} much slower than for the homogeneous topologies. This study about the patterns of self-organization towards synchronization reveals that the quantitative difference about the macroscopic behavior, shown by the computation of the evolution of the global coherence r for ER and SF networks, has its roots on a qualitatively different route at the microscopic level of description. The use of the new parameter r_{link} which involves the computation of the degree of coherence

between each pair of linked nodes is a useful tool for describing such differences. Moreover, the results suggest that the degree of heterogeneity of the network is the key ingredient to explain the two different routes observed.

More important for what concerns to the present communication, is the fact that structural differences appear when the control parameter σ grows. Imagine that one measure the topological properties of a network by measuring the degree of local synchrony in the system. Therefore, the structure of the network will be given by the emerging topology of oscillators beating at the same pace. In other words, even if the underlying network is of size N , unless the system is completely synchronized, the observer would only detect the topology resulting from the emerging collective behavior, the rest of the nodes being invisible for the measuring system. Strikingly, if the substrate network is a SF graph, one would be able to distinguish it from the homogeneous case. A clear evidence of this effect is given by the synchronization of networks with community structure. It has been shown that the community structure is progressively unveiled when the coupling σ drives the system's dynamics towards the coherent state. In particular, the nodes belonging to the first community level are the first to get synchronized, subsequently the second level nodes achieve the frequency entrainment and finally the whole system shows global synchronization. Thus, one can conclude that the inner the link is the faster it gets synchronized and that different values of σ would reveal different levels and correspondingly distinct topological features. The above dynamical organization and the key role of hubs is not exclusive of synchronization phenomena. As we shall see in the next section, the same qualitative picture for the emergence of collective behavior also holds for a quite different phenomenon, namely, the evolution of cooperation in the prisoner's dilemma when played on top of scale-free networks.

3. Prisoner's Dilemma on complex networks

To understand the observed survival of cooperation among unrelated individuals in social communities when selfish actions provide a higher benefit, a lot of attention is being paid to the analysis of evolutionary dynamics of simple two-players games like the Prisoner's Dilemma. In this game individuals adopt one of the two available strategies, cooperation or defection; both receive R under mutual cooperation and P under mutual defection, while a cooperator receives S when confronted to a defector, which in turn receives T , where $T > R > P > S$. Under these conditions it is better to defect, regardless of the opponent strategy, and assuming that strategies are allowed to spread within the population according to their payoffs (replicator dynamics [9, 10]), the

proportion of cooperators asymptotically vanishes in a well-mixed population (*i.e.* when each agent interacts with all other agents).

The Prisoner's Dilemma game is defined in its more general form by the payoff matrix:

$$\begin{pmatrix} R & S \\ T & P \end{pmatrix} \quad (3)$$

where the element a_{ij} is the payoff received by an i -strategist when playing against a j -strategist, with $i = 1$ meaning cooperator, and $i = 2$ defector. The payoff ordering is given by $T > R > P > S$. Other payoff orderings have received other names, *e.g.* $T > R > S > P$ corresponds to the so-called Snowdrift (or Hawks and Doves, or Chicken) game. Following several studies [11, 12], the PD payoffs are set to $R = 1$ (so the reward for cooperating fixes the payoff scale), $T = b > 1$, $P = 0$ (no benefit under mutual defection), and $P - S = \epsilon = 0$. This last choice places us in the very frontier of PD game. It has the effect of not favoring any strategy when playing against defectors (while being advantageous to play defection against cooperators). Small positive values of the parameter $\epsilon \ll 1$ leads to no qualitative differences in the results [11], so the limit $\epsilon \rightarrow 0^+$ is agreed to be continuous.

The dynamic rule is specified as follows: each time step is thought of as one generation of the discrete evolutionary time, where every node i of the system plays with its nearest neighbors and accumulates the payoffs obtained during the round, say P_i . Then, individuals are allowed to synchronously change their strategies by comparing the payoffs they accumulated in the previous generation with that of a neighbor j chosen at random. If $P_i > P_j$, player i keeps the same strategy for the next time step, when it will play again with all of its neighborhood. On the contrary, whenever $P_j > P_i$, i adopts the strategy of j with probability $\Pi_{i \rightarrow j} = \beta(P_j - P_i)$, where $\beta^{-1} = \max\{k_i, k_j\}b$. Note that this dynamic rule, though stochastic, does not allow the adoption of irrational strategy, *i.e.* $\Pi_{i \rightarrow j} = 0$ whenever $P_j \leq P_i$.

The dynamics of the PD game on top of complex networks turns out to be very rich, which a wide region of the parameter b where cooperation survives at variance with the well mixed population. However, the average cooperation level strongly depends on the underlying topology. One novel feature of this game on complex topologies is the existence of three different asymptotic states for the strategies of the nodes. The first set is made up of nodes that always cooperate, henceforth called pure cooperators. The elements of a second set, where defection is fixed, will be called pure defectors. Finally, there is also a set in which nodes are neither pure cooperators nor pure defectors, but they are forced to fluctuate between the two strategies, sometimes playing as cooperators and sometimes playing as defectors [12].

The detailed characterization of the clusters made up by pure cooperators CC (pure defectors, DC) reveals an striking dynamical organization of the strategists in the population. It follows, for instance, that for irrational values of b , pure cooperators can not be in contact with pure defector. Therefore, they are surrounded by the fluctuating individuals that keep them safe from the fixation of defection on the whole system until cooperation is extremely expensive (very large values of b). Another noticeable result concerns the number of cooperator cores. While for random graphs the number of cooperator clusters, N_{cc} , is equal to 1 only for a small range of b values, and later increases up to a maximum, for the BA network the number of such cores is always 1, no matter how many pure cooperators are in the system. That is to say, in one topology (ER), there is a wide region of b where there are several cooperator cores, whereas pure cooperators in SF networks always form a single core. On its turns, the cooperator core in SF networks contains the hubs, which are the ones that stick together all pure cooperators, that would otherwise be disconnected [12].

Interestingly, the path followed by pure defectors until they invade the whole population and cooperation is extinguished (which happens as b is increased), is radically different in homogeneous and heterogeneous networks and is rooted in the local organization of pure defectors. In ER networks, pure defectors first appear distributed in several clusters that later coalesce to form a single core before the whole system is invaded by defectors [12]. Conversely, defectors are always organized in several clusters for SF networks (except when they occupy the whole system). This latter behavior results from the role hubs play. As they are the most robust against defector's invasion, highly connected individuals survive as pure cooperators until the fraction of them vanishes, thus keeping around them a highly robust cooperator core that loses more and more elements of its outer layer when the density of pure defectors tends to 1, until cooperation is finally defeated by defection.

In summary, for the PD in complex topologies, two different paths characterize the emergence (or breakdown) of cooperation. Starting at $b = 1$ all individuals in both topologies are playing as pure cooperators. However, for $b > 1$, the pure cooperative level in SF networks drops below 1 and the population is constituted by pure cooperators forming a single CC , as well as by a cloud of fluctuating individuals. As b is further increased, the size of the cooperation core decreases and some of the fluctuating nodes turn into pure defectors. These defectors are grouped in several clusters around the fluctuating layer. For even larger payoffs, the cooperator core is reduced to a small loop tying together a few individuals, among which is highly likely to find the hubs, while the cores of pure defectors gain in size. Finally, pure and fluctuat-

ing elements are invaded by defectors and a single N -defector core is formed. On the contrary, the original N -cooperator core survives longer for ER graph. However, when b grows, this cluster splits into several cooperator cores that are in a flood of fluctuating elements. Larger payoffs first gives rise to several defector cores that by coalescence form an outer layer that is separated from a single central core of cooperators by individuals of fluctuating strategies. Finally, an N -defector core comes out when b is further increased.

4. Conclusions

As we have seen, the same qualitative picture for the dynamical organization in two kinds of collective behaviors, namely the emergence and evolution of cooperation and the formation of clusters of synchrony in synchronization phenomena, manifest when the dynamics takes place on homogenous or heterogeneous networks. These works adds to other findings about the topology emerging from dynamical processes. The evidences that are being accumulated point to a dynamical organization, both at the local and global scales, that is driven by the underlying topology. Whether or not this intriguing regularity has something to do with the ubiquity of complex heterogeneous networks in Nature is not clear yet. More works in this direction are needed, but we think that they may ultimately lead to uncover important universal relations between the structure and function of complex natural systems that form networks.

As for current trends in the modeling of complex networks, there are still many fundamental questions that remain open in this emerging field of research which will be tackled in the future. For instance, despite many efforts, we have seen that the question of why scale-free networks are so ubiquitous in Nature is still unanswered on firm grounds. Other open questions include: What universal organizing principles drive the growth and evolution of networked systems? How local interactions scale up to and are modulated by global dynamics at network levels, and how are they integrated into the emergent behavior associated with the system states?, and what common patterns can be identified not only in the topology but also in the dynamical organization of the systems constituents? These questions have only been partially addressed and the results point out that seemingly diverse phenomena can share dynamical patterns when they take place on complex topologies. Future works should thoroughly study the emergence of collective behaviors in biological, social and technological systems with the aim of unveiling universal principles and uncovering new structural and dynamical organizing relationships in the interplay between the structure and function of networked systems.

Finally, we would like to mention another promising line of research that is receiving more and more attention from the scientific community. Due to adaptive and dynamical wirings, networks are themselves dynamical entities, whose topology evolves and adapts in time, driven by some external action, or by the action of the internal elements, or following specific predetermined evolving rules. This kind of networks is very important from a practical point of view and are found in many natural and manmade systems. Prototypical examples of these networked systems are brain and wireless networks. To understand how the structure of adaptive networks correlates with their functions is not a simple task. However, the expectancy is that the network approach will surely provide the tools to tackle the problem, with the added value that any progress in this line will result in new applications in technology or to a better cottoning of the dynamical and functional behavior of neurological processes.

Acknowledgements

I am grateful to my collaborators on the subjects discussed here and would also like to thank A. Arenas, S. Boccaletti, A. Díaz-Guilera, L.M. Floria, J. Gómez-Gardeñes for many helpful discussions on complex networks during the last several years. The author is supported by MEC through the Ramón y Cajal Program. This work has been partially supported by the Spanish DGI-CYT Projects FIS2006-12781-C02-01 and FIS2005-00337 and by the European NEST Pathfinder project GABA under contract 043309.

References

- [1] M. E. J. NEWMAN, "The structure and function of complex networks" *SIAM Review* **45**, (2003) 167-256.
- [2] S. BOCCALETTI, V. LATORA, Y. MORENO, M. CHAVEZ, AND D.-U. HWANG, "Complex networks: Structure and dynamics" *Phys. Rep.* **424** (2006) 175-308.
- [3] D. J. WATTS, *Small Worlds: The Dynamics of Networks between Order and Randomness* Princeton University Press, Princeton, New Jersey, 1999.
- [4] H. HONG, M. Y. CHOI, AND B. J. KIM, "Synchronization on small-world networks" *Phys. Rev. E* **65**, (2002) 026139.

- [5] Y. MORENO, A. F. PACHECO, "Synchronization of Kuramoto oscillators in scale-free networks" *Europhys. Lett.* **68**, (2004) 603–609.
- [6] Y. MORENO, M. VÁZQUEZ-PRADA, AND A. F. PACHECO, "Fitness for synchronization of network motifs" *Physica A* **343** (2004) 279–287.
- [7] J. GÓMEZ-GARDEÑES, Y. MORENO, AND A. ARENAS, "Paths to Synchronization on Complex Networks" *Phys. Rev. Lett.* **98**, (2007) 034101.
- [8] J. GÓMEZ-GARDEÑES, Y. MORENO, AND A. ARENAS, "Synchronizability determined by coupling strengths and topology on Complex Networks" *Phys. Rev. E* **75**, (2007) 066106.
- [9] J. HOFBAUER AND K. SIGMUND, *Evolutionary Games and Population dynamics* Cambridge University Press, Cambridge, UK, 1998.
- [10] H. GINTIS, *Game Theory Evolving* Princeton University Press, Princeton, NJ, 2000.
- [11] F.C. SANTOS, J. M. PACHECO, AND T. LENAERTS, " Evolutionary dynamics of social dilemmas in structured heterogeneous populations" *Proc. Nat. Acad. Sci.* **103**, (2006) 3490-3494.
- [12] J. GÓMEZ-GARDEÑES, M. CAMPILLO, L. M. FLORÍA AND Y. MORENO, "Dynamical Organization of Cooperation in Complex Topologies" *Phys. Rev. Lett* **98**, (2007) 108103.

Graph Reconstruction using Spectral Energy

S.Strunkov¹ and S.Sánchez²

¹*Dept.of Higher Mathematics , Higher School of Economics*

²*Dept. of Applied Mathematics, University Rey Juan Carlos*

Abstract

In this paper we show that any set of pairwise non isomorphic pseudographs whose spectral energy is bounded is finite.

Keywords: Energy of graph; Spectra of graph; Line graphs; Iterated line graphs

MSC 2000: 05C50, 05C35; 05C50; 05C90

1. Introduction

There are various important problems in the spectral graph theory. One of them is the problem of establishing in what measure the information on the properties of the different parameters relating to the spectra of graph allows us its reconstruction. Note that even knowing the characteristic polynomial of the adjacency matrix of graph, the graph is recovered in a non unique way [3]. One of the important parameters in the characterization of a graph is its *graph energy* [5],[6],[7],[8]. Therefore it is essential to determine the role this parameter play in the problem of determination of a graph[10].

2. Finiteness of pseudographs with bounded energy

In this paper the finite pseudographs or pseudoorgraphs are analyzed[2], in other words a nondirected and directed finite graphs in which both loops and multiple lines are permitted. Let $G = (V, E)$ be a pseudograph with

emails: root@ssp.mccme.ru, sergio.sanchez@urjc.es

$m = |V|$ vertices and the adjacency matrix M . Let $\lambda_1 \geq \lambda_2 \geq \dots \geq \lambda_k$ be the eigenvalues of M . The spectral graph energy $E(G)$ is by definition [5],[6]

$$E(G) = \sum_{i=1}^k |\lambda_i|. \quad (1)$$

Theorem 21 *Let E_0 be any non negative real number. Then the set, of pairwise non isomorphic pseudographs whose energy is bounded by E_0 , is finite.*

Proof:

Suppose that for some number E_0 the set Σ of pairwise non isomorphic connected pseudographs whose spectral energy is bounded by E_0 is infinite. Let G be a pseudograph ($G \in \Sigma$) and $P_G(\lambda)$ a characteristic polynomial of the adjacency matrix $M(G) = (a_{ij})$. Then we can represent $P_G(\lambda)$ in the form $P_G(\lambda) = \lambda^s P(\lambda)$ where s is an integer and $P(\lambda)$ a polynomial with rational coefficients, whose leading coefficient is equal to 1 and $P(\lambda) \neq 0$. Let $P(\lambda)$ have the form $P(\lambda) = \lambda^n + \alpha_1 \lambda^{n-1} + \dots + \alpha_n$ where $\lambda_1, \lambda_2, \dots, \lambda_n$ are the roots of a polynomial $P(\lambda)$. Suppose that $|\lambda_1| \geq \lambda_2 \geq \dots \geq |\lambda_n|$ then $1 \leq |\lambda_1| \leq E_0$ because $|\lambda_1 \lambda_2 \dots \lambda_n| = |\alpha_n|$ and α_n is an integer. Let m be the number of vertex of a pseudograph G ($G \in \Sigma$) then $m = s + n$. Let $\lambda_1 > \lambda_2 > \dots > \lambda_k$ be a set of distinct eigenvalues of adjacency matrix $M_G = (a_{ij})$ of some connected finite pseudograph G with $m > 1$ vertices. Then all matrix entries are nonnegative so by Frobenius theorem [1] $\lambda_1 > 0$ and $|\lambda_\nu| \leq \lambda_1 \leq E_0$ for all $\nu = 2, \dots, k$.

We claim that for all $i = 1, \dots, m$ the degree of a vertex V_i of pseudographs G is less or equal to $E_0^2 + E_0$. Clearly $a_{ii} \leq E_0$. First we show that the following inequality holds for all $i = 1, \dots, m$

$$\sigma_i = \sqrt{\sum_{\substack{j=1 \\ j \neq i}}^m a_{ij}^2} \leq E_0 \quad (2)$$

For this purpose we analyze the quadratic form $q(x)$ in some m -dimensional Euclidean space E , whose matrix in some orthonormal basis e_1, e_2, \dots, e_m coincide with the matrix M_G . Therefore, the restriction of the quadratic form $q(x)$ a over 2-dimensional space E' which is expanding over orthonormal vectors

$$e_1, e'_i = \frac{a_{i1}}{\sigma_i} e_1 + \dots + \frac{a_{ii-1}}{\sigma_i} e_{i-1} + \frac{a_{ii+1}}{\sigma_i} e_{i+1} + \dots + \frac{a_{im}}{\sigma_i} e_m \quad (3)$$

will have in this basis the matrix of the form

$$M' = \begin{pmatrix} a_{ii} & \sigma_i \\ \sigma_i & b \end{pmatrix} \quad (4)$$

where $b = q(e'_i)$. It can be easy to prove that the difference between the eigenvalues $\lambda'_1 > \lambda'_2$ of matrix M' satisfies an inequality

$$\lambda'_1 - \lambda'_2 = \sqrt{(a_{ii} - b)^2 + 4\sigma_i^2} \geq 2\sigma_i \quad (5)$$

Note that

$$\det(M' - \lambda E) = \begin{vmatrix} a_{ii} - \lambda & \sigma_i \\ \sigma_i & b - \lambda \end{vmatrix} = \lambda^2 - (a_{ii} + b)\lambda + a_{ii}b - \sigma_i^2 \quad (6)$$

where $\lambda'_1 \geq \lambda'_2$ are its roots. By the Vietta theorem we have

$$\lambda'_1 + \lambda'_2 = a_{ii} + b$$

$$2\lambda'_1\lambda'_2 = 2a_{ii}b - 2\sigma_i^2$$

$$(\lambda'_1 + \lambda'_2)^2 = a_{ii}^2 + 2a_{ii}b + b^2$$

$$(\lambda'_1 + \lambda'_2)^2 = \lambda_1'^2 + 2\lambda'_1\lambda'_2 + \lambda_2'^2$$

$$0 < (\lambda'_1 - \lambda'_2)^2 = a_{ii}^2 + 2a_{ii}b + b^2 - 4a_{ii}b - 4\sigma_i^2 = a_{ii}^2 - 2a_{ii}b + b^2 + 4\sigma_i^2$$

$$\lambda'_1 - \lambda'_2 = \sqrt{(a_{ii} - b)^2 + 4\sigma_i^2}$$

$$(a_{ii} - b)^2 \geq 0$$

so

$$\sqrt{(a_{ii} - b)^2 + 4\sigma_i^2} \geq 2\sigma_i$$

Since the values of a quadratic form over the unit sphere are between it maximum and minimum values of their adjacency matrix in a certain orthonormal basis, we obtain

$$2\sigma_i \leq \lambda'_1 - \lambda'_2 \leq 2E$$

Therefore for

$$V_i = \sum_{j=1}^m a_{ij} \leq a_{ii} + \sigma_i^2 \leq E_0^2 + E_0$$

Since G is a connected graph its adjacency matrix M_G is symmetrical and is indecomposable, hence all its entries are nonnegative. Therefore for any pair of distinct indexes $i, j \in \{1, 2, \dots, m\}$ there exists a natural number δ such that (i, j) -th entry of M_G^δ does not vanish. The minimal of these numbers for a given pair i, j we shall denote by $\delta^{(ij)}$. Let d be the maximum of all $\delta^{(ij)}$.

It is easy to see that for any natural number l the sum of entries of each row of matrix M_G^l is less or equal to $(E_0^2 + E_0)^m$. Therefore

$$1 + (E_0^2 + E_0) + (E_0^2 + E_0)^2 + \dots + (E_0^2 + E_0)^d \geq m \quad (7)$$

by and

$$m \leq \frac{(E_0^2 + E_0)^{d+1} - 1}{E_0^2 + E_0 - 1} \quad (8)$$

Let $P(t) = t^k + \alpha_1 t^{k-1} + \dots + \alpha_k$ -be the minimal polynomial of the matrix M_G . Its degree k is equal to the number of distinct eigenvalues of M_G . If $d \geq k$ then

$$\begin{aligned} M_G^{d-k} P(M_G) &= M_G^{d-k} (M_G^k + \alpha_1 M_G^{k-1} + \dots + \alpha_k E) = \\ &= M_G^d + \alpha_1 M_G^{d-1} + \alpha_k M_G^{d-k} = 0 \end{aligned} \quad (9)$$

The last equality is impossible since the entry (ij) in the left side is nonzero provided by $d = \delta^{(ij)}$. Therefore $d < k$ and

$$m \leq \frac{(E_0^2 + E_0)^{d+1} - 1}{E_0^2 + E_0 - 1} \quad (10)$$

So we have

$$0 \leq a_{ii} \leq E_0, \quad 0 \leq a_{ij} \leq \sigma_i \leq E_0, \quad i \neq j \quad (11)$$

From these inequalities for the entries of matrix M_G it follows that the number of vertexes of pseudographs from \sum is bounded. □

If the quantity of degrees of the polynomial $P(\lambda) = \frac{P_G(\lambda)}{\lambda^\sigma}$ for all $G \in \sum$ is bounded, then the number of different roots of polynomials $P_G(\lambda)$ is bounded and the set \sum is finite as it claimed in **Theorem 1**.

Finally it is necessary to examine the case in which for all n there exists a pseudograph G ($G \in \sum$) such that the degree of the polynomial $P(\lambda) = \frac{P_G(\lambda)}{\lambda^\sigma}$ is bigger than n .

Since $|\lambda_1| \geq |\lambda_2| \geq \dots \geq |\lambda_n|$ and $|\lambda_1| + |\lambda_2| + \dots + |\lambda_n| \leq E_0$ then $\lambda_1 < 1$ for all $n \geq E_0$ and $\lambda_n < \varepsilon$ for all $n \geq \frac{1}{\varepsilon}$.

Take $\varepsilon = \frac{1}{2^{[E_0]^{E_0}}}$ and $P_i(\lambda) = \frac{P_G(\lambda)}{\lambda^\sigma}$ the polynomial of degree $n > [\frac{1}{\varepsilon}] + 1$.

Then

$$|\alpha_l| = |\lambda_1 \dots \lambda_n| = |\lambda_1 \dots \lambda_{[E_0]}| \left| \lambda_{[E_0]+1} \dots \lambda_{[\frac{1}{\varepsilon}]} \right| \left| \lambda_{[\frac{1}{\varepsilon}]+1} \dots \lambda_n \right| < (E_0)^{[E_0]} \frac{1}{2^{(E_0)^{[E_0]}}} = \frac{1}{2} \quad (12)$$

So α_l is a nonzero integer, and the set of degrees of polynomials $P(\lambda)$ for all G ($G \in \Sigma$) is finite. But in this case the set Σ is a finite set as it claimed by **Theorem 1**.

However, for the regular strongly connected graphs the **Theorem 1** does not hold. Takes as an example a line graph $L(G)$ of certain pseudograph G , in other words $L(G)$ is a pseudograph whose vertexes are all the edges of the pseudograph G and their edges are all the possible ordered pairs of the vertexes in $L(G)$ in the form $((u, v)_i, (v, w)_j)$. This construction is similar to the corresponding definition of a line graph for non directed graphs [2],[3], but the spectral properties of directed and non directed line graphs are different.

3. Coenergetic pseudographs

Theorem 3.1 *The set of nonzero eigenvalues of the adjacency matrixes M_G and $M_{L(G)}$ of the pseudographs G and $L(G)$ coincide. Furthermore the multiplicities of each nonzero root in the characteristic equation of the matrixes M_G and $M_{L(G)}$ are the same.*

Proof:

Let v_1, v_2, \dots, v_n be all vertexes and $\varepsilon_1, \varepsilon_2, \dots, \varepsilon_n$ all edges of pseudograph G . Following the definition of the adjacency matrix $M(G) = (a_{ij})$ of the pseudograph G , a coefficient a_{ij} is equal to the number of oriented edges, which come from the vertex i to the vertex j . Define a *outmatrix* S_G a $n \times m$ matrix $S_G = (s_{ik})$, which (ik) -th element s_{ik} is equal to 1 if the edge ε_k of pseudograph G leaves from the vertex v_i and equal 0 otherwise. In the some way define a *inmatrix* F_G a $m \times n$ matrix $F_G = (f_{kj})$, which (kj) -th element f_{kj} is equal to 1 if the end of the edge ε_k stay in the vertex v_j and equal 0 otherwise. Let $\Sigma(G)$ be a pseudograph of *subdivision* of pseudograph G , which is defined in the natural way as a pseudograph with a set

$u_1, u_2, \dots, u_n, u_{1+n}, \dots, u_{m+n}$ as vertexes and which directed edges are the following ordered pairs of his vertex for the corresponded indexes i, j, k

$$(u_i, u_{k+n}), (u_{k+n}, u_j), \quad i, j \in \{1, 2, \dots, n\}, \quad k \in \{1, 2, \dots, m\} \quad (13)$$

in which a directed edge ε_k goes out from the vertex v_i and go in the vertex v_j . It is easy to check that

$$M_{\Sigma(G)} = \begin{pmatrix} 0 & S_G \\ F_G & 0 \end{pmatrix}, \quad (14)$$

$$M_{\Sigma(G)} = \begin{pmatrix} M_G & 0 \\ 0 & M_{L(G)} \end{pmatrix} \quad (15)$$

So we obtain that

$$M_G = S_G F_G, \quad M_{L(G)} = F_G S_G \quad (16)$$

Therefore the conclusion of the theorem is obtained from the properties of the characteristic polynomials of matrix AB and BA , where A and B are an arbitrary matrices $n \times m$ and $m \times n$ respectively [4].

□

Conclusion 1 *Pseudographs G and $L(G)$ have same spectral energy*

$$E(G) = E(L(G)) \quad (17)$$

4. Sample pseudograph

Example 1 *Example of a set of pseudographs with same energy.*

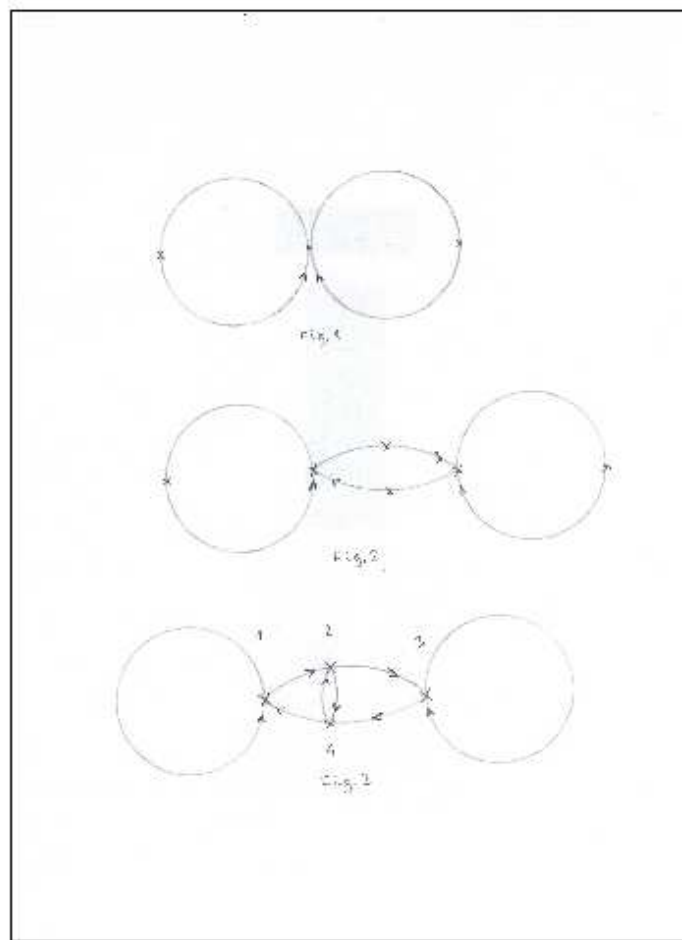
Fig.1 Pseudograph G , $M_G = (2)$, $\lambda_1 = 2$, $E(G) = 2$

Fig.2 Line graph $L(G)$, $M_{L(G)} = \begin{pmatrix} 1 & 1 \\ 1 & 1 \end{pmatrix}$, $\lambda_1 = 2, \lambda_2 = 0$, $E(L(G)) = 2$

Fig.3 Line graph $L^2(G) = L(L(G))$,

$$M_{L^2(G)} = \begin{pmatrix} 1 & 1 & 0 & 0 \\ 0 & 0 & 1 & 1 \\ 0 & 0 & 1 & 1 \\ 1 & 1 & 0 & 0 \end{pmatrix},$$

$$\lambda_1 = 2, \lambda_{2,3,4} = 0, E(L(L(G))) = 2$$



Acknowledgements

This work has been partially supported by RFBR (grant # 05-01-01018) and SU-HSE (grant # 06-01-0107)

References

- [1] FR Gantmacher, The Theory of Matrices, Vol. 1, Chelsea, New York, 1990.
- [2] F.Harary, Graph theory, Perseus Books Publishing, 1969
- [3] Cvetkovic, Doob, Sachs, Spectra of Graphs: Theory and Applications, Verlag, 1995

- [4] Marcus M., Minc H., A Survey of Matrix Theory and Matrix Inequalities. Allyn and Bacon, Boston, 1964.
- [5] Gutman, The energy of a graph, Ber. Math. Statist. Sect. Forschungszentrum Graz 103 (1978), pp. 1–22.
- [6] H.B. Walikar, H.S. Ramane and P.R. Hampiholi, On the energy of a graph. In: R. Balakrishnan, H.M. Mulder and A. Vijayakumar, Editors, Graph Connections, Allied Publishers, New Delhi (1999), pp. 120–123.
- [7] Koolen and V. Moulton, Maximal energy graphs, Adv. Appl. Math. 26 (2001), pp. 47–52.
- [8] H.B. Walikar, I. Gutman, P.R. Hampiholi and H.S. Ramane, Non-hyperenergetic graphs, Graph Theory Notes N. Y. 51 (2001), pp. 14–16.
- [9] Y. Hou, Bicyclic graphs with minimum energy, Lin. Multilin. Algebra 49 (2002), pp. 347–354
- [10] S.Strunkov,S.Sanchez, Energy spectral specification for the graph reconstruction. Communications in Algebra, (2008),(to appear).

Prediction of claims and risk factor selection in automobile insurance using Support Vector Machines and Genetic Algorithms

P. Tolmos Rodríguez-Piñero¹ and R. S. Mozos²

¹*Dep. Financial Economy and Accountability II, Rey Juan Carlos University of
Madrid*

²*Dep. Signal Theory and Communications, Carlos III University of Madrid*

Abstract

In this paper we propose an approach to predict if an insured in a given automobile portfolio is going to report a claim or not during a year. The algorithm we suggest is based on the application of a standard Support Vector Machines (SVMs), hybridized with a global search heuristics, a Genetic Algorithm (GA). The SVM is used to classify insures as failed (reported a claim) or not failed, whereas the GA is used to perform on-line feature selection in the risk factors space of the SVM, in order to improve its performance. This is also an important issue for the insurer company, because it allows them to select the "best" risk factors (the ones that retain the most amount of information).

We used with this purpose given risk factors included in the data base of the insurance company MAPFRE. In the simulations section, we compare the performance of the SVM and of a classical statistical method, the Discriminant Analysis. The results obtained shown that the learning techniques, and SVM in particular, can be useful tools for researchers interested in evaluating claim frequency of insures of automobile insurance firms.

Keywords: Claim risk, Risk Factors, Support Vector Machines, Genetic Algorithms, Discriminant Analysis

MSC 2000:

1. Introduction

Claim frequency, as well as claim size, is an important issue to determine the prime an insured has to pay. Is essential for an insurance company to classify insured as homogeneous as possible attending claim risk, in a way that insured belonging to a same class pay the same prime. To achieve this goal, statistics techniques are used, selecting what we know as risk factors, insured's features correlated with claim rate that explain a big amount of its variance.

Our goal is to give the better insured classification attending claim risk in one year, using innovative techniques, that of Learning Machines. This kind of algorithms has been successfully employed specially in engineering tasks. In the financial or economic field, we can find them mainly in problems about bankruptcy prediction (see [6] for further information). In these cases, the algorithms used are Neural Networks, Genetic Algorithms, Classification Trees, but just in a few cases, SVMs. Nevertheless, there are no applications to the actuarial problems (except that related with business failure) of any of these methods.

SVM has been proven to be a powerful method for classification problems, with very good properties of versatility [2]. These properties, and the fact that SVM is a novelty technique in this area, are the reasons why we have selected it to solve the task of insured's classification.

The feature selection process, implemented through the GA heuristics, eliminates irrelevant or redundant risk factors, for, in a first stage, improving the SVM performance. Nevertheless, the risk factor selection is an important issue by its own, because is related with the accident rate.

We will show that the obtained results are very encouraging, and we expect that this will aimed further investigations relating Learning Machines and Insurance problems.

2. Problem Definition

The problem we want to study can be considered as a particular example of the so called *multi-attribute classification problem*. This problem consists in the assignment of an object, described by values of *attributes*, to a predefined class.

Mathematically a multi-attribute classification problem can be stated as follows [Schölkopf 1999]:

We want to estimate a (decision) function $f : \mathbb{R}^n \rightarrow \{\pm 1\}$ using data (observations or objects) from the set of observations we will employ to *train* what we know as “classification machine” (Neural Network, Genetic Algorithm,). So, Let $\{x_i\}$, $x_i \in \mathbb{R}^n$, $i \in \{1, \dots, \ell\}$ be a set of observations (objects) drawn from some unknown probability distribution $P(x, y)$, and $y_i \in \{-1, 1\}$ (categories), a set of associated true labels.

Then, the considered data set would be

$$(x_1, y_1), \dots, (x_\ell, y_\ell) \in \mathbb{R}^n \times \{\pm 1\}, \quad (1)$$

and our goal is function f to rightly classify the new and unseen examples (x, y) , i.e. $f(x) = y$ for examples (x, y) that where generated from the same underlying probability distribution $P(x, y)$ as the trained data.

Concept of function f can be extended to that of *classification machine*, defined as a set of possible mappings $x \rightarrow f(x, \alpha)$ where a particular choice of parameters α generates what is called a “trained machine”. The machine is supposed to be deterministic, i.e. for each given x , and one α the output of $f(x, \alpha)$ is always the same. We can consider α corresponds with the “free” parameters determining a particular machine; in a general neural network with fixed architecture, α corresponds to the weights and biases of the neural network, in the case of Classification Trees α is the number of nodes, branches and functions in nodes of the final tree.

The training error (or empirical risk) can be set as:

$$R_{emp}[\alpha] = \frac{1}{\ell} \sum_{i=1}^{\ell} |f(x_i, \alpha) - y_i|. \quad (2)$$

The expected test error (called *risk*), averaged over test examples drawn from the underlying distribution $P(x, y)$, is

$$R[\alpha] = \int \frac{1}{2} |f(x, \alpha) - y| dP(x, y) \quad (3)$$

$\frac{1}{2} |f(x_i, \alpha) - y_i|$ is known as *loss*.

It can be noted that $R_{emp}[\alpha]$ don't depends of the probability distribution, is fixed for each α and each trained set $\{x_i, y_i\}$. Hence, only minimizing the training error does not imply a small risk. Statistical learning theory (Vapnik y Chervonenkis, 1974; Vapnik, 1979) or VC (Vapnik-Chervonenkis) theory,

shows that is imperative to restrict the class of functions that f is chosen from to one which has a *capacity* that is suitable for the amount of available training data. VC theory provides bounds on the test error. The minimization of these bounds, which depend on both the empirical risk and the capacity of the function class, leads to the principle of structural risk minimization (Vapnik, 1979) [Segovia-Vargas et al (2004)].

In the general case, the multi-attribute classification problem consists in finding the machine which learns the mapping $x_i \rightarrow y_i$ with the highest generalization ability possible. According with the statistical learning theory, the generalization error of a learning machine can be analyzed considering the machine's capacity and it's empirical risk [Bishop 1995]. The capacity factor represents the machine's complexity, whereas the empirical risk factor measures its quality. To ensure high generalization ability, the trade-off between these two factors should be addressed [Segovia-Vargas et al (2004)].

2.1. Prediction of claims

The multi-attribute classification problem is applicable in a straight forward manner to our problem, with $\{x_i\}$, $i \in \{1, \dots, \ell\}$ being the insured described by a set of risk factors (every component $x_{i,j}$) and $y_i \in \{-1, 1\}$ a label which describes the class, -1 the one without claims, and 1 the one with claims.

3. The employed algorithm

3.1. Brief introduction to SVM

The use of classification machines, mainly neural networks, in the financial field, is not a new trend. What is an innovation is the application in the actuarial area. We have chose SVMs because they are a competitive and robust approach in classification tasks, and they have obtained greatest results in a similar problem, the prediction of insolvency in non-life insurance companies [8].

Consider a set of insured represented by the value of their risk factors $\{x_i\}$, $i \in \{1, \dots, \ell\}$, and a set of associated labels $y_i \in \{-1, 1\}$ which describe the insured as presented a claim (*failed*) or don't. First imagine that this training set can be separated by a linear hyperplane. Briefly speaking (see [Borges(1998)] to a more complete analysis as well as further results about SVMs), the linear SVM for separable sets solves the following problem:

“Find $w \in \mathbb{R}^n$ and $b \in \mathbb{R}$ to minimize $\tau(w) = \frac{1}{2}\|w\|^2$, subject to:

$$y_i (w^t \cdot x_i + b) \geq 1 \quad \forall i = 1, \dots, \ell.” \quad (4)$$

Once such w and b are found, our classification rule for insured is given by $sign(w^t \cdot x_i + b)$, and the associated error to this classification is $R_{emp}(w, \alpha)$.

The points who verify the equality in restriction (4), are what we call *Support Vectors*. Those vectors lies on one of the two optimal separation hyperplane, $w^t \cdot x_i + b = 1$ or $w^t \cdot x_i + b = -1$.

Consider now the case when the points in the training set are no linearly separable; then the constraint (4) cannot be satisfied. One possibility is to introduce some nonnegative slack variables ξ 's in order to overcome this difficulty. The new formulation for the SVM results:

“Find $w \in \mathbb{R}^n$, $b \in \mathbb{R}$ and $i = 1, \dots, \ell$ to minimize

$$\tau(w) = \frac{1}{2}\|w\|^2 + C \sum_{i=1}^{\ell} \xi_i \quad (5)$$

subject to $y_i (w^t \cdot x_i + b) \geq 1 - \xi_i$ and $\xi_i > 0 \forall i = 1, \dots, \ell$ ”, where C is a parameter of the classifier to be estimated.

The nonlinear SVM maps the input variable into a high dimensional (often infinite dimensional) feature space, and applies the linear SVM in this feature space. Computationally, this can be achieved by the application of a kernel function.

The nonlinear SVM is able to classify any set of insured in failed or not failed with a probability of error given by $R_{emp}(w, \alpha)$.

3.2. The feature selection problem

In its more general form, FSP for a learning problem from samples can be addressed in the following way: given a set of labelled data points $(x_1, y_1), \dots, (x_\ell, y_\ell)$ with $x_i \in \mathbb{R}^n$ and $y_i \in \{-1, 1\}$, and choose a subset of m features ($m < n$), that achieves the lowest classification error, see [Weston et al. (2000)] for details.

The general FSP can be particularized for our problem by considering that the components of vectors $\{x_i\}$, $i \in \{1, \dots, \ell\}$ are the risk factors which describe the insured, and vector σ defines the best set of factors to be used by

the SVM. Feature selection eliminates irrelevant and redundant risk factors of every customer, what improves the performance of the SVM (besides the “extra” interest related to the claim rate earlier mentioned). The remaining risk factors are used by the SVM for the classification process.

In this paper we propose solving the FSP by means of a Genetic Algorithm.

3.3. A Generic Algorithm for FSP

Genetic Algorithms (GAs) are a class of robust problem solving techniques based on a population of solutions (binary strings), called *individuals*, which evolves through successive generations by means of the application of the so called genetic operators: selection, crossover and mutation, see [Goldberg (1989)].

Selection is the process by which individuals in the population are randomly sampled with probabilities proportional to their fitness values. An elitist strategy, consisting in passing the highest fitness string to the next generation, is applied in order to preserve the best solution encountered so far in the evolution.

The selected set, of the same size of the initial population, is subjected to the crossover operation. Firstly, the binary strings are coupled at random. Second, for each pair of strings, an integer position along the string is selected uniformly at random. Two new strings are composed by swapping all bits between the selected position and the end of the string. This operation is applied to the couples with probability P_c less than one.

The population of the GA for the FSP is formed by a number ξ of binary strings σ in $\{0, 1\}$, which evolves by the iterative procedure of the genetic operators described above. A component $\sigma_i = 1$ means that the correspondent risk factor i has to be taken into account for the SVM (so will be for the company), and if the component $\sigma_i = 0$ means that the correspondent ratio i has to be removed from the set of risk factors.

Note that every individual of the GA population (a binary vector σ) stands for a different set of risk factors to be used by the SVM. The fitness function associated the each individual is the classification error obtained classifying ℓ training points $(x \star s, y)$, that can be estimated as $Remp(w, b, \sigma)$. Due to GAs maximizes the fitness function, and the objective function in the FSP is minimizing the error probability, a modified fitness function is introduced:

$$F = 100(1 - Remp(w, b, \sigma)). \quad (6)$$

4. Results and comparative

4.1. Classification using all the risk factors

We consider a sample of 58238 clients taken from the data base provided by MAPFRE with the insured and claims of 2003. They are described by 13 risk factors (Driving license date, birth date, Kind of driving license, Sex, Civil State , Profession, Vehicle Fabrication date, Vehicle Use, Circulation zone, Power rating, Vehicle Value, Vehicle Marc), which we had to split to categorize the variables (Civil State was split in Single, Married, Divorced and Widowed, and in a similar way in the other cases) so we finally had 40 risk factors.

To do the simulation, we have employed standard software, LibSVM (Chih–Chung Chang and Chih–Jen Lin, LIBSVM a library for support vector machines, 2001 Software at <http://www.csie.ntu.edu.tw/~cjlin/libsvm>). In the process of experimenting with the arguments, we used the built-in support for validation of svmtrain “ n -fold cross validation”. This consists of splitting the input data in n sets ($n = 5$ in our case), and then train the model with $n-1$ of the n sets, and validating the results with the remaining set. This process is repeated for each of the possible n elections of the set which is omitted from the training process.

We used LibSVM with a Radial Basis Function kernel, and 5-fold cross-validation, and we obtained an **accuracy rate of 77.72%**.

We have compared these results with those obtained by *Discriminant Analysis*, the classical technique used in this kind of studies. Discriminant Analysis is a technique that works with quantitative variables and where the groups are characterized by a categorical variable, in our case this categorical variable is going to be the claim variable that has two values: -1 and 1. Because of the qualitative nature of our variables, it has been necessary to previously transform the set of variables in a quantitative/continuous one. To do that we have proceed as follows:

1. We have done a Multiple Factor Analysis (with the SPAD software) over the complete set of variables.
2. We have selected a reduced number of factors that explain the 100% of the variance (the first 59 factors).
3. We have done a Discriminant Analysis with this 59 factors (using the SPSS software).

The result was a **70,5% of well classified cases**.

As we can observe, the SVM improve the results obtained with the usual technique of Discriminant Analysis, and so its use is well justified.

4.2. Classification with the selected risk factors

In order to select the risk factors retaining the big amount of information for the claim rate, a GA was programmed. We used “one point crossover” and mutation with “one bit”. Our goal was to choose the 30 best risk factors. The fitness function was the prediction capacity estimated with a SVM.

The selected factors were:

‘ANTIGÜEDAD CARNET’

‘EDAD CONDUCTOR’

‘ANTIGÜEDAD VEHÍCULO’

‘MADRID’

‘BARCELONA’

‘VALOR’

‘POTENCIA’

‘CASTILLA Y LEÓN’

‘GALICIA’

‘PROF12’ (sin código)

‘PROF41’ (FUNCIONARIOS Y ADMINISTRATIVOS (desplazamiento profesional habitual urbano))

‘CASADO’

‘HOMBRES’

‘USO110’ (TURISMO DE USO PARTICULAR)

‘ANDALUCÍA (-Sevilla)’

‘PROF56’ (SIN PROFESION)

‘MURCIA’
 ‘ARAGÓN’
 ‘SOLTERO’
 ‘SEVILLA’
 ‘PROF20’ (“*Industriales, Comerciantes, Profesiones liberales*”)
 ‘BALEARES’
 ‘PROF 0’ (sin código)
 ‘VALENCIA’
 ‘CATALUÑA (- Barna)’
 ‘CASTILLA-LA MANCHA’
 ‘COMUNIDAD VALENCIANA (- Valencia)’
 ‘USO168’ (TODO TERRENO +5 HASTA 9 PLAZAS -)
 ‘ASTURIAS’
 ‘PROF55’ (OBREROS MANUALES)

We run again the SVM, now with just the selected risk factors. The results was

Classification	30 selected variables	All the variables
SVM	77.66%	77.72%

5. Concluding remarks and further studies

In this work, an insured classification attending their claims with a SVM, has been presented. This technique had never been employed in this area, and we have obtained good results with it.

We classify the insured again, selecting first the relevant risk factors (because this is an interesting issue in insurance, and because it improves the performance of the SVM), and hybridizing so the SVM with a Genetic Algorithm. We also obtain interesting results.

Nevertheless, we think that the more important contribution of our work is the opening of the actuarial field to the application of learning machines in solving this kind of problems.

Acknowledgements

This work had never been done without the support of Fundación MAPFRE Estudios and its “Beca de Riesgos y Seguros 2006”.

References

- [1] Brockett, P.L., Xiaohua Xia and Derring, R. A. “Using Kohonen’s Self-Organizing Feature Map to Uncover Automobile Bodily Injury Claims Fraud”. *Journal of Risk and Insurance*, Vol. 65, No 2, (1998) 245.
- [2] Burges, C. J.: “A tutorial on Support Vector Machines for pattern recognition”, *Knowledge Discovery and Data Mining*, 2(2) (1998):121-167
- [3] Salcedo-Sanz, S., Fernández-Villacañas, J. L., Segovia-Vargas, M. J. and Bousoño-Calzón, C. “Genetic programming for the prediction of insolvency in non-life insurance companies”, *Comp. & Op. Research*. 2002.
- [4] Sanchis, A., Gil, J. A., and Heras, A.: “El análisis discriminante en la previsión de la insolvencia en la empresa de seguros no-vida”, *Revista Española de Financiación y Contabilidad* (2003) 115.
- [5] Scholkopf B, Smola A. *Learning with kernels*. Cambridge, MA: MIT Press; 2002.
- [6] Shapiro, A. *Soft Computing Applications in Actuarial Science*. ARCH. 2001. <http://www.soa.org:80/library/arch/2000-09/arch01v113.pdf>
- [7] Shapiro, A. The merging of Neural Networks, fuzzy logic and genetic algorithms. 2002, *Insurance: Mathematics and Economics* 31 (2002) 115-131
- [8] Segovia-Vargas MJ, Salcedo-Sanz S, Bousoño-Calzón C. Prediction of insolvency in non-life insurance companies using Support Vector Machines and genetic algorithms. In: *Proceedings of X SIGEF Congress in Emergent Solutions for the Information and Knowledge Economy*, León, 2003
- [9] Tolmos, P. Molero J.J., Sevillano F. J. The use of a Neural Network in the prediction of the IBEX-35 stock index. *Proceedings of the 5th International Meeting on Artificial Intelligence And Emerging Technologies in Accounting, Finance and Taxation*. Huelva, 2000.
- [10] Vapnick, V., Cortes, C. Support-Vector Networks.. *Machine Learning*, 20, (1995) 273-297

Complete Synchronization between Hyperchaotic Space-Time Attractors

G. Vidal¹ and H. Mancini¹

¹*Instituto de Física and Departamento de Física y Mat. Aplicada, Universidad de Navarra. Irunlarrea s/n, E-31080, Pamplona. Spain*

Abstract

Many dynamical processes that occur in nature or in experiments are space-time bifurcations in systems with symmetries. One of the most outstanding examples is the Takens-Bogdanov bifurcation [1] that has been used to model Codimension-two bifurcations with double zero eigenvalues and square symmetries, that exhibit chaotic behavior [2], [3]. In particular, the dynamics of thermo-convective experiments in square cells with a small aspect ratio have been modeled with the groups of symmetry Z_2 [4] and D_4 [5].

In the first part of this work we describe the dynamic behavior appearing in the equation system with the group of symmetry D_4 proposed in [2], as a function of the different parameters. The space of parameters is analyzed in order to identify those variables that could be useful to synchronize, in space and time, two identical systems of this kind. In the second part we describe the first results obtained to synchronize two identical systems.

Keywords: NonLinear Dynamics, Benard-Marangoni Convection.

MSC 2000:

1. Introduction

Bifurcations, in presence of symmetries appearing in extended systems with patterns formed by more or less periodic structures, have a symmetry group directly related to the lattice symmetry of the periodic structure. Under this conditions, solutions in bifurcations are normally very complex and has been solved in detail only in some particular situations. But in strongly confined

emails: gvidal@alumni.unav.es, hmancini@fisica.unav.es

systems where natural structures are imposed by boundary conditions with less symmetries, some typical situations of this kind of bifurcations can be analyzed more easily. There is a classical situation that appear in Benard-Marangoni convection [6] when the aspect ratio Γ (the ratio between the medium horizontal dimension D divided by depth of the fluid d ($\Gamma = D/d$) is low enough as to put the system near a Codimension-2 point. A Codimension 2 point in a convective system let us analyse experimentally this kind of bifurcation in high detail and to compare it with theoretical and numerical solutions [1].

Codimension two points in small aspect ratio convective systems are related to the simultaneous instability of two convective modes. Unfortunately, only in a few cases, this kind of bifurcations have been studied experimentally [4], [5], [7]. The systems cited in these references (considering square and cylindrical symmetries) has been studied experimentally and also modeled by solving the Navier Stokes equations and using adequate lateral boundaries conditions. This works consider resonances between the lowest order modes (1:1, 1:2), [8], [9]. Numerical simulations reproduce qualitatively the complex dynamical results obtained experimentally as a function of the control parameter.

But in [4], it was shown that the dynamic behavior can be modeled by a Takens-Bogdanov bifurcation reproducing all the sequence of bifurcations without reference to the physical variables (the velocity and temperature fields). In this work, the vector dynamics of the system was represented by a scalar (geometrical) variable, easily observed and measured in the planform of the system. By means of this variable, the complex dynamics of the experimental system could be analyzed by a scalar variable simplifying the analysis of the fluid dynamics. The system of equations used here have been studied numerically by different authors [2], [10].

We can see the stationary states obtained when the control parameter (temperature) is increased and it is possible relate it to the bifurcations in the system of equations. It can be observed how the system, firstly in the zero double point, breaks the spatial symmetry going then to one of the two possibilities that keep a part of the symmetry (the diagonal). Each possibility of symmetry represent an spatial attractor.

After the spatial break of symmetry the sequence of bifurcations follows with a time-dependent regime. A further increase in the control parameter brings the system throughout a Hopf bifurcation to a limit cycle and then, to a chaotic attractor in presence of the symmetries of the square partially broken. A further increase in the control parameter brings the symmetric attractors to collide with the (0,0) point, opening the possibility to an hete-

roclinic conection. This heteroclinic connection produces a chaotic oscillation with a very rich dynamic between both attractors, each of them representing one of the preserved symmetries in the system.

In this work we present a detailed numerical analysis of the system of equations, identifying the influence of the different parameters on the dynamics. The aim is to detect the influence of those that could be used to control or synchronize the system in the chaotic attractor. After it, we present some results of simulations obtained when two identical experiments of this type are synchronized. To detect the different synchronization regimes we used the Lyapunov exponents calculated by the Runge-Kutta method for each variable. The system is hyperchaotic having more than one Lyapunov exponent positive. When two identical systems are coupled, we obtain a system of 8 dimensions instead of two of 4 and the space of phases can change as a function of the coupling parameters values.

As an interesting result we obtained generalized synchronization in windows as it has recently been shown in reference [11], but as a difference with this work, the chaotic behavior is not suppressed. When synchronization takes place the system remains chaotic, but the order of chaos is lowered. This paper describes first the different dynamic states of the system and then the results on synchronization of two identical systems with symmetric coupling.

2. Bifurcations in systems with square symmetry

One of the simplest models to represent a real experiment in square symmetry can be found in [4]. However the set of equations used in this work is over-simplified because only the symmetries that define the sub-space Z_2 are considered, and consequently, the experimental results can only be partially reproduced.

In order to recover all the details of this experiment the same authors [5] introduce a system of equations that reproduce all the group of symmetries D_4 , the symmetries of the square. The bifurcation problem is now D_4 equivariant as long as non additional symmetries are generated by the boundary conditions of the box (hidden symmetries). D_4 represent the group of reflections (m) and rotations (ρ) of the square and the following equations system include all the elements of symmetry. Hidden symmetries have been used in [8] to reproduce the dynamics.

In our simulations we use the system of equations introduced in [2]:

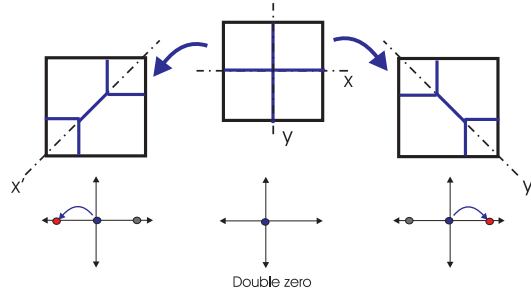


Figure 1: Spatial Bifurcations in the experiment and in the model. Symmetry breaks preserving the diagonal elements.

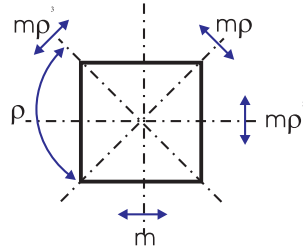


Figure 2: Generators of D_4 , the symmetry group of the square.

$$x' = y + \varepsilon^2 fz(z y - w x) \quad (1)$$

$$y' = \mu x + x(a(x^2 + z^2) + bz^2) + \varepsilon(\nu y + y(c(x^2 + z^2) + ez^2 + dx(xy + zw))) + \varepsilon^2 fw(z y - w x) \quad (2)$$

$$z' = w - \varepsilon^2 fx(z y - w x) \quad (3)$$

$$w' = \mu z + z(a(x^2 + z^2) + bx^2) + \varepsilon(\nu w + w(c(x^2 + z^2) + ex^2 + dz(xy + zw))) - \varepsilon^2 fy(z y - w x) \quad (4)$$

where (x, y, z, w) are the variables and $(a, b, c, d, e, f, \mu, \nu, \varepsilon)$ are parameters that must be adjusted to fit the experiment. In order to solve this system a 4th order Runge-Kutta method has been used and the solutions obtained were controlled by comparing to well known situations obtained by other authors that use the same equations (when available). In order to check our simulations we reproduce here the results obtained in [4] for the sequence of bifurcations appearing when the control parameter is increased. It can be seen in Figure 3.

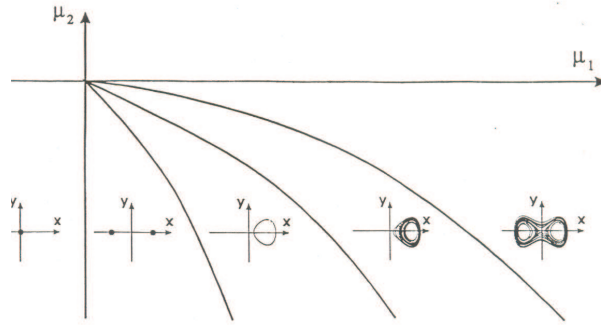


Figure 3: Bifurcations in the parameter space. The control parameter in the experiment is the heath flow, associated with μ_1 (Used to check the simulations against reference [5]).

When the control parameter is sufficiently high to have the heteroclinic connection, the system is equivalent to four coupled oscillators. The phase space of this oscillators seem two pair of eyes distributed in the planes (x, y) and (z, w) . Each pair of oscillators are winded by the heteroclinic conection trajectories that never close. In Figure 4 (a), we present temporal signals obtained for each variable; and the plane of phases $y(t)$ vs. $x(t)$ and $w(t)$ vs. $z(t)$ are shown in Fig. 5 b). The similitude between both planes is easily seen.

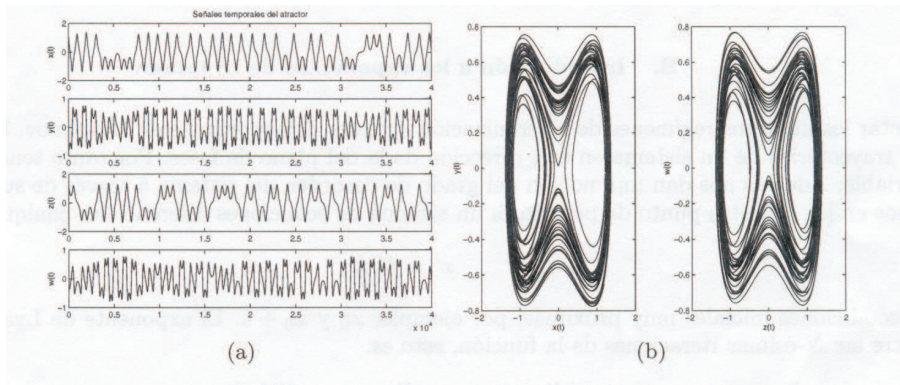


Figure 4: (a) Temporal data signals for each variable and attractors in the planes (x, y) and (z, w) .

It is important to remark that in the model ε is a critical parameter. If we look for solutions representing the experiment, we need the ε value near zero because the equations system becomes unstable [2]. We adjusted the parameters in the model in order to fit during a certain time the temporal series obtained from the experiment.

3. Attempts to synchronize two identical systems

In order to analyze the synchronization possibilities two sets of equations like Eq. (1-4) has been coupled. We used a coupling scheme that can be symmetric or asymmetric and the coupling is a direct function of the error between both systems (acting as a feedback loop).

The equations for the coupled system can be seen in the set of Eq. (6-12) where variables are named by the subscripts (1,2) corresponding to each original system. The parameter θ change the strength of the coupling between the variables and $\theta \in [1, -1]$ controls the coupling symmetry. From the perfect symmetric coupling ($\theta = 0$), to the master-slave condition obtained when $\theta = (1, -1)$.

$$x'_1 = y_1 + \varepsilon_x/2(1 + \theta_x)(x_2 - x_1) \quad (5)$$

$$y'_1 = \mu x_1 + x_1(a(x_1^2 + z_1^2) + bz_1^2) + \varepsilon_x/2(1 + \theta_y)(y_2 - y_1) \quad (6)$$

$$z'_1 = w_1 + \varepsilon_z/2(1 + \theta_z)(z_2 - z_1) \quad (7)$$

$$w'_1 = \mu z_1 + z_1(a(x_1^2 + z_1^2) + bx_1^2) + \varepsilon_w/2(1 + \theta_w)(w_2 - w_1) \quad (8)$$

$$x'_2 = y_2 + \varepsilon_x/2(1 + \theta_x)(x_1 - x_2) \quad (9)$$

$$y'_2 = \mu x_2 + x_2(a(x_2^2 + z_2^2) + bz_2^2) + \varepsilon_y/2(1 + \theta_y)(y_1 - y_2) \quad (10)$$

$$z'_2 = w_2 + \varepsilon_z/2(1 + \theta_z)(z_1 - z_2) \quad (11)$$

$$w'_2 = \mu z_2 + z_2(a(x_2^2 + z_2^2) + bx_2^2) + \varepsilon_w/2(1 + \theta_w)(w_1 - w_2) \quad (12)$$

In order to detect synchronization windows we calculated the Lyapunov exponents when the systems are coupled on the variables x (with a coupling strength ε_x) and making $\varepsilon_y = \varepsilon_z = \varepsilon_w = 0$. To obtain a symmetric coupling the value of θ_x must be fixed to zero ($\theta_x = 0$). The system has now four positive Lyapunov exponents and the results against the coupling strength are shown in Figure 5.

In reference [11] the coupling of several chaotic 3-Dimensional systems have been analyzed (Rossler, Lorenz, etc.), and they found windows to synchronization observing the Lyapunov exponents behavior. Also in our system

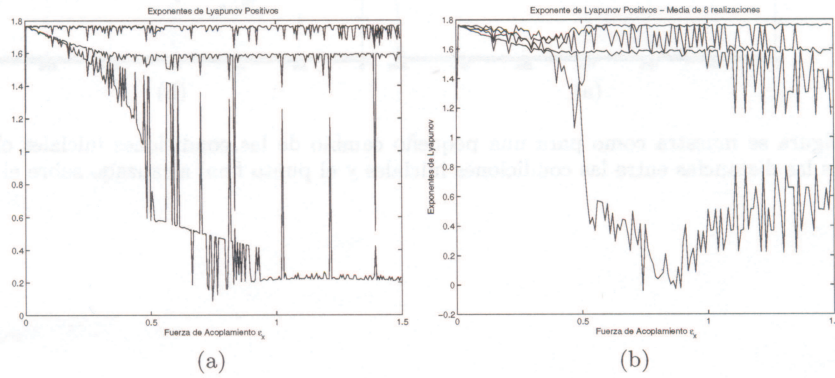


Figure 5: Lyapunov exponent for the coupled systems.

we found different windows where the coupled systems could be synchronized, but as a strong difference, here the chaos is not suppressed and variables are completely synchronized [13].

4. Conclusions

The Takens-Bogdanov bifurcation equations can be used to analyze the space-time synchronization between two systems with square symmetry (like the experiment in reference [4]). Complete synchronization is achieved without chaos suppression. But some remarks about the relation between simulations and the experiment must be added. In the experiment represented by the equations considered here, the pattern obtained after the spatial bifurcations becomes time dependent. Under these conditions, the convective fluid layer receives a stationary flow of heat from a heater below and transfers it to the air in the upper side of the layer, but transformed into a time-dependent heat flow. Physically considered, this means that the system must store during a certain time a part of the total flow. Continuity requires to conserve the mean flow at the output equal to the stationary flow at the input. That is, the fluid layer needs to transfer the heat flow modulating it in amplitude by the heat stored in the system. This produces, in consequence, a time-dependent convective pattern following these modulations. In our experiment, the flow mean value was modulated 10% in amplitude (approx.) with quasiperiodic chaotic fluctuations.

Our model focuses on the time-dependent variable around the mean flow

(the instantaneous value less the mean value). A scheme to clarify this can be seen in Figure 6. In the pattern, the projection of the diagonal length: ($x = d \cos \alpha$), follows the evolution of temperature in a wide range of the control parameter, as was demonstrated in [12]. The mean flow is a stationary quantity that can easily be calculated by the normal heat transfer equations.

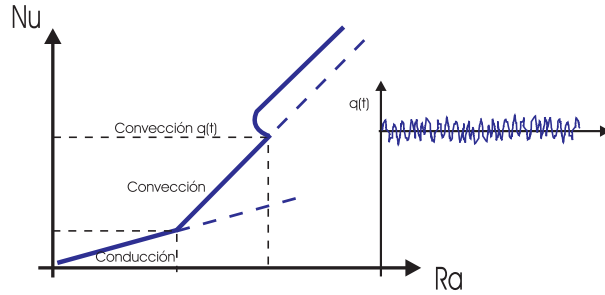


Figure 6: Scheme to clarify the time dependent flow magnitude against its mean value. Nu is the Nusselt number, a measure of the effective heat flow and Ra is Rayleigh number, the non-dimensional control parameter [12].

Another mathematical restriction must be remarked. The system of equations considered here is very useful to represent the bifurcation process in a space with symmetry D_4 . However it has some limitations if we need too long temporal series because the solution becomes unstable. In this case the model is not valid, unless we make $\varepsilon = f(x, y, z, w, t)$, which is not possible. As we have noted, variables (x, y, z, w) have a physical meaning, they define the size of the diagonals in the square, that is, a magnitude independent proportional to the instantaneous heat flow.

It is important to remember that the model is constructed not with the physical variables (velocity and temperature fields), but with a scalar projection of them defined on the pattern, that can be measured more easily. In short, the model represents the dynamic observed on the pattern and synchronization was achieved in the simulations, in the variables describing the movements of the pattern.

Acknowledgements

We acknowledge to G. Mindlin for fruitful discussions and to D. Ambruster for their answers about the solutions of system of equations used. One of us (G.V.) also acknowledges a fellowship from the Asociación de Amigos, University of

Navarra. This work has been partially supported by Spanish Government through project number FIS2007-66004 and by Univ. de Navarra (PIUNA project).

References

- [1] R. HOYLE, *Pattern Formation*, Cambridge Univ. Press (2006).
- [2] D. ARMBRUSTER, “Codimension 2 bifurcation in binary convection with square symmetry”, pp.385-398, in *Non-linear Evolution of Spatio-Temporal Structures in Dissipative continuous Systems F. Busse and L. Kramer, Ed. Plenum Press, N. York (1990)*.
- [3] J. GUCKENHEIMER AND P. HOLMES, *Non-linear Oscillations, Dynamical Systems and bifurcation of Vector Fields*, Springer-Verlag (1983).
- [4] ONDARÇUHU, T. MINDLIN, G., MANCINI, H., PÉREZ GARCÍA, C., “Dynamical patterns in Bénard-Marangoni convection in a square container”, pp.385-398, in *Non-linear Evolution of Spatio-Temporal Structures Phys. Rev. Lett. 70, 3892 (1993)*.
- [5] G.B. MINDLIN, T. ONDARÇUHU, H. L. MANCINI, C. PÉREZ GARCÍA, A. GARCIMARTIN, “Comparison of data from Bénard-Marangoni convection in a square container with a model based on symmetry arguments”, pp.385-398, in *Non-linear Evolution of Spatio-Temporal Structures Int. J. Bifurcation Chaos 4, 1121-1133 (1994)*.
- [6] P. COLINET.J.C. LEGROS, M. G. VELARDE, *Nonlinear Dynamics of Surface-Tension Driven Instabilities*, Wyley-VCH Berlin (2001).
- [7] D. JOHNSON AND R. NARAYANAN, “Experimental observation of dynamic mode switching in interfacial-tension-driven convection near a codimension-two point”, *Phys. Rev. E* 54, 3102-3104 (1996).
- [8] D. KRMPOTIC, G. B. MINDLIN AND C. PÉREZ-GARCÍA “Bénard-Marangoni convection in square containers”, *Phys. Rev. E*, v.54, 3609-3613, (1996).
- [9] B. ECHEBARRIA, D. KRMPÓTIC, C. PÉREZ-GARCÍA “Resonant interactions in Benard-Marangoni convection in cylindrical containers”, *Physica D* 99 487-502 (1997).
- [10] GOLUBITSKY, M., STEWART, I., SCHAEFFER D.G., *Singularities and Groups in Bifurcation Theory*, v.II, Springer-Verlag, N.York (1988).

- [11] J. BRAGARD, G. VIDAL, H. MANCINI, C. MENDOZA, S. BOCCALETTI
“Chaos suppression through asymmetric coupling”, (*submitted*) *Chaos*,
Jun. 2007.
- [12] H. MANCINI, D. MAZA “Benard-Marangoni Thermal Oscillators: An
experimental study”, *Phys. Rev. E* 55, pp. 2757-2768 (1997).
- [13] S. BOCCALETTI, J. KURTHS, G. OSIPOV, D. VALLADARES, C. ZHOU
“The synchronization of chaotic systems”, *Phys. Reports* 366, pp. 1-101
(2002).

Preferential attachment, aging and weights in recommendation systems

M. Zanin¹, P. Cano¹ and J.M. Buldú²

¹*Music Technology Group, Universitat Pompeu Fabra*

²*Nonlinear Dynamics and Chaos Group, Departamento de Física, Universidad
Rey Juan Carlos*

Abstract

In the current work, *preferential-attachment* algorithms are applied to *Recommendation Systems* in order to improve their quality of prediction from a sparse dataset. We show how some networks are grown under the influence of trendiness forces, and how this can be used to enhance the results of a recommendation system, i.e. increase their percentage of right predictions. After defining a base algorithm, we create recommendation networks which are based on an histogram of user ratings. We show the influence of data aging in the prediction of user habits and how the exact moment of the prediction influences the recommendation. Finally, we design weighted networks that take into account the age of the information used to generate the links. In this way, we obtain a better approximation to evaluate the users' tastes.

Keywords: Recommendation systems, preferential attachment, network evolution

MSC 2000: AMS codes

1. Introduction

Since the experiment of Milgram in 1967 [1], the study of (social) networks have attracted the interest of many scientists from completely different fields. Boosted by the seminal paper of Watts and Strogatz [2], complex networks theory has become a strong utility to analyze different kinds of data structures. The application of complex networks to social problems has generated special

emails: massimiliano.zanin@hotmail.com, pedro@bmat.com, javier.buldu@urjc.es

interest, and it has given fruitful results in different subjects, ranging from sexual disease control [3, 4] to music community identification [6, 7]. Another field where complex networks have been successfully implemented is in Recommendation Systems. In the last years, developments in computer and information technologies have created new channels of commerce, mainly electronic, where millions of customers are served each day, generating an enormous quantity of information about their habits. On the other hand, this innovation has created the need for personalization in customer cares, and this has supposed a great interest in generating algorithms that recommend items to users that enter an “e-store”.

In the search for better recommendation algorithms using complex networks theory, properties of the system like Clustering Coefficient [13] or Jaccard’s Coefficient [12] have been explored, obtaining different results. When the growth of the recommendation system is considered, the *Preferential Attachment* strategy, has been recently proposed [12], but without much consideration within the community working on recommendation algorithms.

In this paper, we want to go deeper in the idea of applying preferential attachment to a recommendation system: after defining a base algorithm, we study the effect of time in the network evolution, and find a better approximation to evaluate the users’ tastes.

2. Preparing the ground

The item-based strategy [8, 11] is one of the most popular in recommendation systems: it presents interesting advantages, like short computation time and low sensitivity to network sparsity. Since it is the most extended way of generate a recommendation matrix, we take this algorithm as the ground to compare with any other results.

The basic idea behind an item-based strategy is to look into the set of items related with the target user, to compute the similarity of these items with the others in the network, and select the most similar (see [8] for details). For this purpose, a *cosine-based similarity* is commonly used. For each item, a vector of length N is created, being N the total number of users. The vector accounts for the relation between items thanks to user ratings: for example, if the n^{th} element of the vector has a value of 1, it means that the user number n has selected that item. Then, the similarity between two items i and j is defined as:

$$sim(i, j) = \cos(\vec{i}, \vec{j}) = \frac{\vec{i} \cdot \vec{j}}{|\vec{i}| \cdot |\vec{j}|}. \quad (1)$$

In our experimental study we have used two datasets, each one with different characteristics, to observe results in different backgrounds.

The first dataset is the collection of ratings of NetFlix [9], a web page of movie renting where users can also evaluate movies (from 1 to 5). In order to work with a network of simple (unweighted) connections, we filter ratings different from 5 (the highest mark), so that we only keep users connected with their top-rated movies. The result is a set of 17770 items (movies), 2.6 millions users and more than 23 millions of operations (links).

The second dataset, is from *Art Of The Mix* [10]. In this network, we have 90000 users, 472000 items (songs, in this case) and 1.3 millions of links. The Art Of The Mix is a project started at the end of 1997 and consists of a web site where users upload and interchange playlists of their favorite music. The songs, somehow, fit in those lists, even though they do not need to belong to the same country, decade or musical genre. In this way, a certain connection results between songs of the list, whose origin is based on the musical taste of the playlist' author.

Once networks are defined, it is worth noting that the size of the present datasets is much higher than previous results in other networks, like [12], where 10000 items and 2000 users were considered, or [13] with a dataset close to 40000 items.

3. Preferential attachment

The initial step to improve a recommendation algorithm taking advantage of complex networks theory is to use the concept of preferential attachment; first introduced by Barabási and Albert in [16]. The preferential attachment has become a paradigmatic growing algorithm in order to explain the structures and evolution of social networks.

The main idea in [16] is that nodes with higher degrees (i.e., with more links) acquire new links at higher rates than low-degree nodes; the probability that a link will connect a new node j with another existing node i is linearly proportional to the actual degree of i :

$$p(j \rightarrow i) = \frac{k_i}{\sum_{j=1}^N k_j}, \quad (2)$$

where k_i is the degree of node i and N is the total number of nodes. When defining a recommendation algorithm, this is equivalent to suppose that a given user has a higher probability of selecting a *popular* item than an unknown one. Intuitively, it may be clear that in some cases it will be right: every time the

algorithm is applied to a selling system, where goods being sold depend on trendiness, items that are well-known will have a higher probability of being bought. Nevertheless, there can be cases where popularity of an item, or the existence of a certain fashion, do not affect the creation of new links, and users make their choices only following personal criteria.

As we will see, both considerations should be taken into account and some kind of balance between them should also be included. Another interesting point is that the initial dataset consist on a bipartite network [14] with two different kind of nodes, users or items (movies/songs). The bipartite network could be projected in two different networks; one with users being the fundamental nodes and other with movies/songs being the nodes. Nevertheless, both projected networks disregard part of the information when they are considered independently and we must define a way of accounting for all the information within the dataset.

At this point, let us explain the way of implementing a preferential attachment strategy in our recommendation algorithm, i.e., an algorithm that favors the recommendation of the most connected items. The procedure can be summarized in four steps:

- First, we define a distance between a target user and any other user. As in the case of items, a vector is created for each user, accounting for his/her selected items. The vector has length M which corresponds to the total number of items, and it will have a value of 1 at position m if the m item has been chosen by the user. Next, the *cosine-distance* $dis(j)$ with respect to the target user is calculated, and values are stored in a linear array:

$$dis(j) = \cos(\vec{i}, \vec{j}) = \frac{\vec{i} \cdot \vec{j}}{|\vec{i}| \cdot |\vec{j}|} \quad (3)$$

where i is the target user, and j is other user of the network.

- For each item l of the network, a *compatibility* value $comp(l)$ is calculated as the sum of the *closeness* of users related with that item; *closeness* is defined as $1 - dis$:

$$comp(l) = \sum_j (1 - dis(j)) \quad (4)$$

where l is the item, and j accounts for users that have connections with l .

- Finally, items are ordered according to their *compatibility*, in descending order. Items in the beginning of the list are the more compatible, i.e. the more suitable for recommendation. In this way, items in the top of the list are the best for the target user, and should be submitted to his/her attention.

Two important features of this approach need to be explained in detail.

First of all, this scheme has a very small calculation time; the most expensive operation, i.e. the calculation of distance between users, is executed only one time. On the contrary, for the basic item-based scheme, the algorithm should calculate the compatibility between an item and each one of the items connected to the target user. This is equivalent to carry out this calculation u times, where u is the number of items related with the target user. As a result, the computational cost of the basic algorithm is many times worse, and this can be an important feature when working with large datasets.

Second, unlike the basic algorithm, now we see that the global *score* (the measure of the quality of the recommendation) of an item depends on how many users have a connection with it: for each one of this connections, its compatibility value (i.e. the compatibility between the selected and the target user) is summed up, and the result of the sum is the global compatibility of that item. This means that an item with many links will have a higher compatibility value than another item with only a few links (because of the higher quantity of values summed up); this is the basis of preferential attachment: the more connections, the more the probability of being chosen by another user. On the other side, not only the number of links is considered: the compatibility is calculated, like in the basic algorithm, to be a representation of the user tastes; if an item is well-known, but is far from the tastes of the target user, its total compatibility value will be small, and that item will not be recommended.

4. Aging effect

4.1. Trendiness in real networks

As explained before, preferential attachment can improve the quality of recommendations when the underlying network has a strong trendiness component, where the trendiness component is the presence of some kind of preferential attachment in its grown: in the case of buyers datasets, as the two being studied in this paper, the more an item is known, the more is likely for that item to be chosen by the target user. Up to now, all data previous to prediction date has been considered. This is the traditional approach, since it is a generalized

opinion that the more data is used in calculation, the better the result will be. Nevertheless, trendiness of an item greatly depends on time: one item can have a high popularity on a time t_0 , but it can lose all interest after a certain time t_1 .

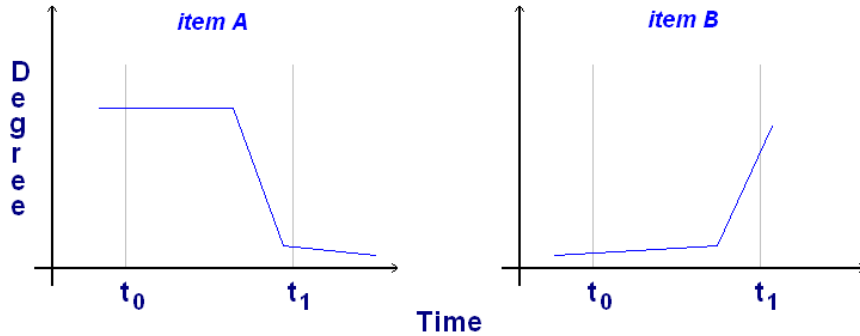


Figure 1: Example of degree evolution for two items; item on the left has a higher global degree, while item B has a higher degree in time t_1 .

This fact can be observed in Fig. 1. The left plot shows an hypothetical evolution of the number of new links for an item A (i.e., the derivative of its degree): in time t_0 this item has a great instantaneous degree (i.e. a great popularity in a given moment, with many new users connecting to this item), while close to t_1 its number of new links decreases. On the other side, item B has an overall lower degree, with a greater degree close to time t_1 . It is important to note, that item A has a greater number of connections if we consider the global data, while B wins in instantaneous degree after time t_1 . A simple recommendation algorithm, like the one exposed before, would consider all data of the network, resulting in a greater probability for item A ; nevertheless, if we want a *real-time* suggestion, e.g. just after t_1 , the recommendation algorithm should advantage B .

The example above explains the importance of the link aging: when the global network is used in calculations, many data that are not strictly necessary are included; sometimes, that unwanted data can lead to mistakes, and in addition they always increase the calculation time.

In Fig. 2 we represent how the instantaneous degree of the items evolves in time. The instantaneous degree takes into account the number of new links per day. We can see in the inset of Fig. 2-(a) an example of the instantaneous degree evolution for a given item. In order to account for all items, we add the instantaneous degree of all items, but aligned at their absolute maxima.

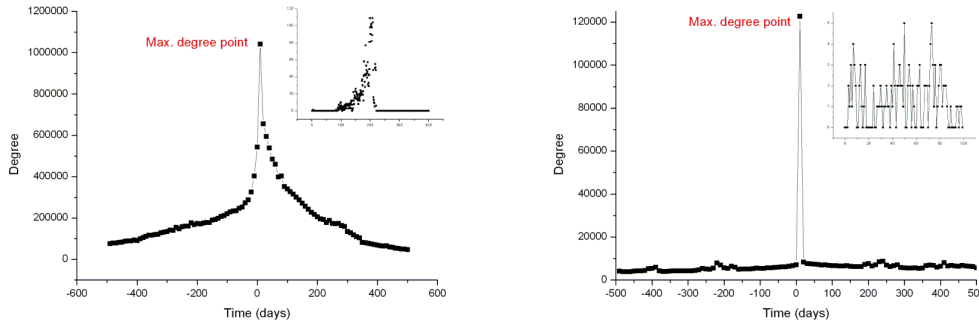


Figure 2: Global degree evolution for NetFlix (a) and Art Of The Mix (b) networks: the central point represents the moment of greatest degree of every item. In the insets, are represented the degree evolution of an example item for each network; note as for (b), the degree shows no clear peak: the mean degree evolution for that network is therefore flat.

We can see in Fig. 2 that we obtain different results for both networks. For the NetFlix dataset, a great peak is observed, with the degree value increasing and decreasing continuously around the central point: from the aging point of view, that means that, first, there is a certain correlation time in the process of achieving the highest popularity. Second, popularity depends on time, and therefore, we must take it into account at the moment of recommending an item.

The opposite case is Art Of The Mix, where the instantaneous degree level of the whole dataset is quite constant, with only a central delta-shaped peak. In fact, the central peak is an artifice, since we align all items at their absolute maxima, we will always have the highest value at time zero. Nevertheless, the flat spectrum of the rest of the series indicates that fluctuations of the instantaneous degree are filtered when adding all items. The absence of correlation in the degree evolution indicates that relations between users and items do not depend on time, and that trendiness is not important to explain network growth: aging should not help in improving results.

4.2. The cut-off time

Starting from the above considerations, we define an improvement of the basic preferential attachment algorithm: before calculating the result, the network is filtered to include only data (i.e. links) enclosed in a time window. We assign a cut-off time d to the window, and for a given time t_1 and a target

item, only links within the window t_1 and t_{1-d} are considered.

Results of applying aging-based filtering to both networks are shown in Fig. 3 (NetFlix) and Fig. 4 (ArtOfTheMix). In order to evaluate the recommendation algorithm we compute the *score* of the predictions, which will be explained in detail in the next section. For the time being, the score must be taken as an indicator of the quality of the recommendation. As expected, thanks to the strong trendiness in the NetFlix dataset, the cut-off dimension of the window results in an improved score. Obviously, when the window is too small, there is not enough information to perform a good recommendation and the score decreases. When applying an aging filtering to Art Of The Mix network we do not obtain an improvement of the score (see Fig. 4): as degree evolution is not important in this kind of network, reducing the dimension of the window excludes important data from the analysis, and therefore the score decreases.

When network growth is based on rules that are equivalent to preferential attachment, an important improvement in recommendation results can be achieved; as summarized in Table I, we go from the 0.924 of the item-based algorithm, to 0.933 of the preferential attachment algorithm without aging, and finally to 0.939 when link aging is considered. At the same time, calculation time can be optimized: when window size is small, there is less information to be processed and the recommendation speeds up (Table 2).

4.3. Score calculation

In the previous section, we have used a *score* value to compare results coming from different algorithms: it is time to explain how it is calculated, and moreover, why we have used this strategy.

When we evaluate a recommendation system, we randomly choose a target user and a target item already selected by this user: that item should be recommended by the algorithm for the given user, using only data prior to link date and time. No restriction is applied to links position: it can be at the beginning of the dataset (thus, only a few data can be used), or it can be at the end (improving the amount of information available, but also increasing the computational cost). The recommendation algorithm would return a list of items, ordered by compatibility, so that the items on the top of the list should be the best for the target user.

The *Score* value is simply calculated as a function of the position of the target item in that list:

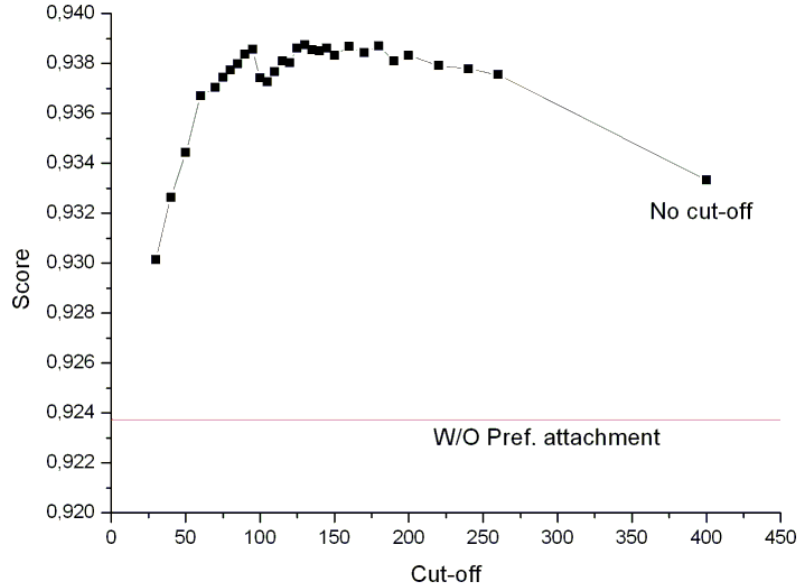


Figure 3: Recommendation score as a function of cut-off window dimension d , for NetFlix dataset. The horizontal line represent the score for the basic item-based algorithm, while the right point, marked with *no cut-off*, is the result of using the preferential attachment algorithm without filtering data (as if $d = \infty$).

$$Score = 1 - \frac{Pos_{item}}{\#items}$$

The more the target item is in the upper part of the recommendation list, the more *score* approximates to 1.

The usual way to check the performance of recommendation algorithms is quite different. As seen in [15], a great part of the dataset is used for training the system, while the last part is the testing period; using data of the first set, the algorithm should generate a ranked list of recommendations for each user, and the quality of the recommendation system is then measured using the number of *hits* and their position in the ranked list.

This method of evaluation is not suitable when preferential attachment is used, and even more when an aging effect is applied, due to the fact that

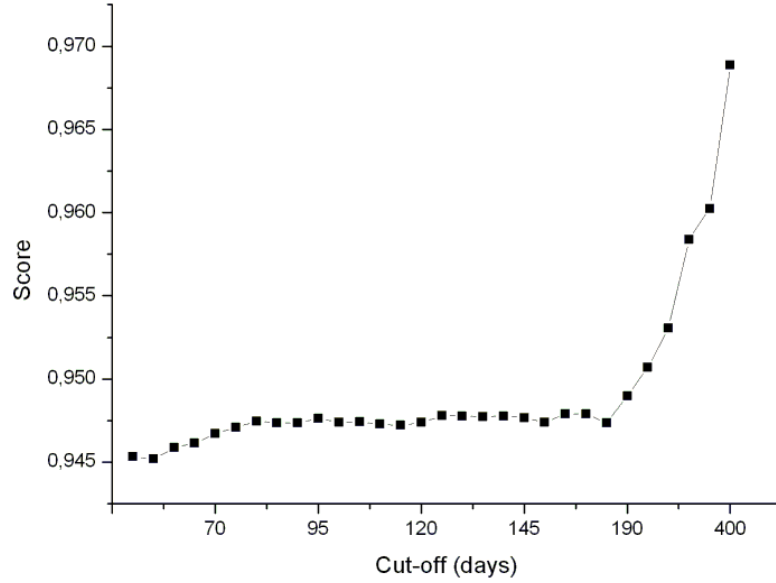


Figure 4: Recommendation score as a function of cut-off window dimension d , for Art Of The Mix dataset.

time has a great influence in calculations. When we choose a time t_0 and a given user for evaluating the recommendation, all data related with item's rank depend on t_0 . If an item i is a *hit* at a distant time t_1 , let us say $t_1 \ll t_0$, we should disregard that result.

5. Links weight

Finally, let us mention some details about the link heterogeneity. When defining recommendation algorithms, links are normally identical, and the network is defined as unweighted. In our case, we have a parameter that can be used to discriminate the importance of each connection: the age of that link.

For a given link, we can assign a weight that is defined as a function W of the number of days passed since its creation. Although any function can be used for this purpose, we have chosen a piecewise linear function, that can be tuned by two parameters α and β :

$$W(i) = \begin{cases} 1, & a_i > \beta \\ 1 + \frac{\beta - a_i}{\beta} \alpha, & a_i \leq \beta \end{cases}$$

where a_i is the age of the link. In this way, we modify the compatibility of a given item l , which now reads:

$$comp(l) = \sum_j (1 - dis(j)) W(j \rightarrow l) \quad (5)$$

where $(j \rightarrow l)$ is the link connecting user j to item l .

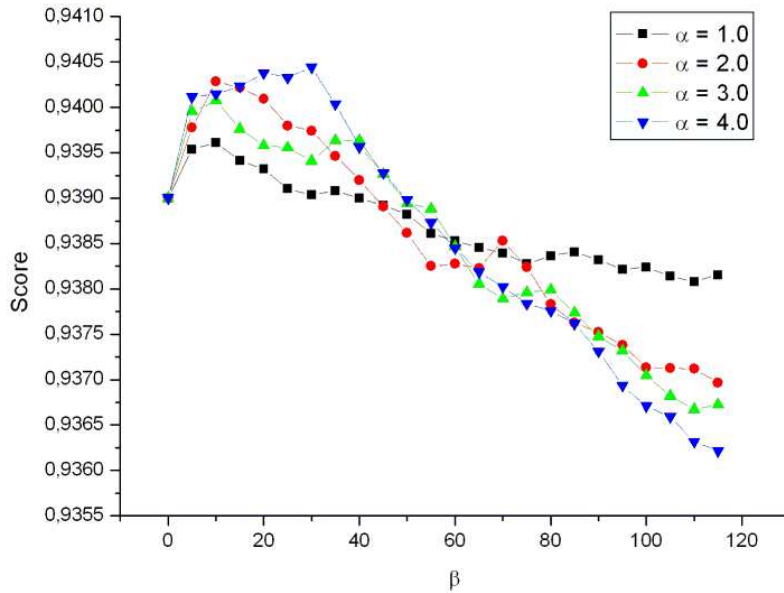


Figure 5: Effect of considering weighted links. Results refer to the Netflix dataset for a window dimension of 120 days.

The obtained *score* for different values of α and β on the Netflix data collection is shown in Fig. 5. A maximum is detected around $\beta = 20$ for different α , while large values of β lead to a reduction of the *score*. This behavior is expected since high values of β are equivalent to increase the importance of old links, a fact that is not favorable for a preferential attachment strategy. On the other side, low values of β are equivalent to include only very young links, excluding a great quantity of information, and making the *score* value to decrease.

6. Some examples

In order to better explain how preferential attachment algorithm works, we report an example of recommendation for the NetFlix dataset. The target user, randomly chosen, is the user number 658088, and the target item is item number 872 (for privacy issues, users and items are encoded with sequential numbers). Target user has links with 24 other items in the moment of the recommendation.

First, we calculate the *score* using the basic algorithm. After making the ranking ordered by compatibility, in firsts positions the followings items are founded, along with their compatibility score:

Item	(1 st) 7843	(2 nd) 5085	(3 rd) 11038	(4 th) 14241
Compatibility	0.16734	0.14864	0.14591	0.14381

Target item is in position 830, with a compatibility of 0.04993: that is, we get a *score* of 0.95329 ($Score = 1 - 830/17770$, where 17770 is the total number of items) for this case.

Next step is executing the preferential attachment algorithm with aging on the same user and item. The dimension of the window d used for data filtering can take different values, and for each value the results obtained (i.e. number of connections of the target user, rankings, *score*) are different.

To show an example, we report what can be obtained with $d = 70$ days. In this case, after filtering the dataset, we have only 2.26 millions operations (about ten time less than original data), and target user has 3 more links to other items. Target item 872 is connected with 198 users in that interval of time, and their compatibility with target user are the following:

User	(1 st) 698478	(2 nd) 2081171	(3 rd) 1558760	...
Compatibility	0.04352	0.06337	0.05803	...

Summing up all 198 values give a total compatibility of 14.69987. In this example, we can see as the compatibility value is greater than the one obtained with the basic algorithm: this is because we are summing up hundreds of values, so the system must work with wider ranges. For this value of d , the ranking obtained starts with the following values:

Item	(1 st) 13728	(2 nd) 14240	(3 rd) 2782	(4 th) 11521
Compatibility	756.14	165.59	160.98	146.96

Target item is at position 357, that represent a *score* of 0.9799: comparing the result of the item-based algorithm, target item climbed 515 positions.

Scores obtained with different values of d are shown below:

d	30	50	100	140	180	∞
<i>Score</i>	0.87530	0.97794	0.97766	0.97535	0.9740	0.97840

7. Conclusions

In recommendation systems, it is a common opinion that the bigger the dataset, the better the result will be. In this paper, we show that in certain case this reasoning is not true. When recommendation systems refer to networks with strong trendiness component, a preferential attachment strategy can improve results, while at the same time, smaller computational cost is required. This fact is due to the aging of the existing information, which can be crucial in certain kind of networks. We demonstrate that, when fashion or trends are present in the evolution of a given network, the age of the links must be taken into account when developing a recommendation algorithm. Moreover, we have seen that weighted links, based on its age, are suitable for discriminating between recent and old information, increasing the quality of the prediction in trendiness networks.

References

- [1] S. MILGRAM, “The small world problem”, *Psychol. Today*, **1** (1967) 61–67.
- [2] D. J. WATTS AND S. H. STROGATZ, “Collective dynamics of small-world networks”, *Nature*, **393** (1998) 440–442.
- [3] R.M. MAY AND A.L.LLOYD, “Infection Dynamics on Scale-free Networks”, *Phys. Rev. E*, **64** (2001) 066112.
- [4] R. PASTOR-SATORRAS AND A. VESPIGNANI, “Epidemic dynamics in finite size scale-free networks”, *Phys. Rev. E* **65** (2002) 035108.
- [5] PETER S. BEARMAN, JAMES MOODY AND KATHERINE STOVEL, “Chain of Affection: The Structure of Adolescent Romantic and Sexual Networks”, *AJS*, **110-1** (2004) 44–91.

- [6] R. LAMBIOTTE AND M. AUSLOOS, “On the genre-fication of music: a percolation approach”, *Eur. Phys. J. B* **50** (2006) 183–188.
- [7] JUYOUNG PARK, OSCAR CELMA, MARKUS KOPPENBERGER, PEDRO CANO AND JAVIER M. BULDÚ, “The Social Network of Contemporary Popular Musicians”, arXiv:physics/0609229v1 (2006).
- [8] BADRUL SARWAR, GEORGE KARYPIS, JOSEPH KONSTAN AND JOHN RIEDL, “Item-based Collaborative Filtering Recommendation Algorithms” *In Proc. of the 10th International World Wide Web Conference (WWW10)* Hong Kong, May (2001).
- [9] <http://www.netflix.com>
- [10] <http://www.artofthemix.org>
- [11] J. WANG, A.P. DE VRIES AND M.J.T. REINDERS “Unifying Userbased and Itembased Collaborative Filtering Approaches by Similarity Fusion” *Proceedings of SIGIR’06* Seattle (2006).
- [12] ZAN HUANG, XIN LI AND HSINCHUN CHEN, “Link Prediction Approach to Collaborative Filtering”, *In Proc. of the 5th ACM/IEEE-CS joint conference on Digital libraries*, 141–142 (2005).
- [13] ZAN HUANG, “Link Prediction Based on Graph Topology: The Predictive Value of the Generalized Clustering Coefficient”, *LinkKDD* (2006).
- [14] M.E.J. NEWMAN, “The structure and function of complex networks”, *SIAM Review*, 45 (2003) 67–256.
- [15] ZAN HUANG, DANIEL D. ZENG AND HSINCHUN CHEN, “Analyzing Consumer-product Graphs: Empirical Findings and Applications in Recommender Systems”, *SSRN September* (2005).
- [16] A.-L. BARABÁSI, R. ALBERT, “Emergence of Scaling in Random Networks”, *Science* **286** (1999).

